Seismic Design Procedure for Steel Moment Resisting Frames with Viscous Dampers

by

Konstantinos Kariniotakis

A thesis submitted in partial fulfillment of the requirements for the degree of

Doctor of Philosophy

in

Engineering

University of Warwick, School of Engineering

November 2017

Table of contents

List of figures

List of tables

Acknowledgements

I would like to acknowledge my supervisor, Professor Theodore Karavasilis. I am grateful for his guidance and support, and for giving me the opportunity to work under his supervision. Also, I would like to thank Dr. Angelos Tzimas for his support. This research was financially supported by the Engineering and Physical Science Research Council (EPSRC) and I would like to express my gratitude for that support.

Declaration

This thesis is submitted to the University of Warwick in support of my application for the degree of Doctor of Philosophy. It has been composed by myself and has not been submitted in any previous application for any degree. The work presented was carried out by the author. Parts of this thesis have been published by the author:

Kariniotakis K., Karavasilis T.L. (2017), "Modified capacity design rule for columns in tall steel MRFs with viscous dampers within the framework of Eurocode 8", *Bulletin of Earthquake Engineering*, in press

Abstract

Modern technologies for seismic hazard mitigation in building structures, such as passive dampers, make it possible to design economically viable buildings that (a) experience significantly less damage than conventional buildings designed according to seismic codes; and (b) return to service within an acceptable short, if not immediate, time after a strong earthquake. The latter is of significant importance as recent strong earthquakes resulted in high socio-economic losses due to long disruption of the use or occupation of a large number of buildings. Among the different types of passive dampers available in the market, fluid viscous dampers are known for their major advantages including large capacity of energy dissipation and peak forces that are out of phase with the peak drifts of elastic or mildly inelastic structures.

Steel moment-resisting frames (MRFs) with viscous dampers are prone to plastic mechanisms that involve hinges in columns because of the large column axial forces due to the large damper forces and have less collapse resistance than conventional steel MRFs designed for the same drift performance under the design earthquake. In this research, a seismic design procedure for steel MRFs with viscous dampers within the framework of Eurocode 8 is developed, addressing the issues of (a) the satisfaction of a sway plastic mechanism with plastic hinges in beams and column bases and (b) collapse resistance of steel MRFs with viscous dampers at least equal with that of conventional steel MRFs. A conservative design rule is proposed for the capacity design of the columns in the force path of viscous dampers. More specifically, the column axial force used to perform the capacity design is the envelope of the axial force from the peak drift state and the axial force from the peak velocity state. The capacity design rule becomes stricter for buildings with more than 10 storeys to address that linear elastic analysis methods for structures with dampers underestimate the peak damper forces in the lower storeys of yielding tall steel MRFs. Appropriate limit values for the storey drift sensitivity coefficient θ are recommended to guarantee for steel MRFs with viscous dampers collapse resistance at least equal with that of conventional steel MRFs.

List of abbreviations

DBE	design based earthquake
IDA	incremental dynamic analysis
IDR	interstorey drift ratio
MCE	maximum considered earthquake
MRF	moment resisting frame
SF	scale factor
SRSS	Square Root Sum of Squares

List of symbols

A	cross-sectional area
B	damping reduction factor
b_{cf}	width of column flange
b_f	width of flange
C	damping coefficient
D_{1D}	roof displacement due to the design earthquake
d	depth of section
d_e	displacement based on the design spectrum
d_r	design interstorey drift
E	modulus of elasticity / seismic actions
F_D	damper force
F_y	yield strength of column and doubler plate
f_y	yield strength
G	dead loads / shear modulus of steel

h storey height / depth of web

I moment of inertia

K_b horizontal stiffness of the bracing system

K_i horizontal storey stiffness

k_{yy} interaction factor

L length

L_b lateral bracing length

M_c capping moment strength

M_{Ed} design bending moment

$M_{Ed,E}$ bending moment due to the design seismic action

$M_{Ed,G}$ bending moment due to non seismic actions in the seismic design combination

$M_{N,Rd}$ plastic moment resistance reduced due to axial force

$M_{N,V,Rd}$ plastic moment resistance reduced due to axial and shear force

$M_{V,Rd}$ plastic moment resistance reduced due to shear force

$M_{pl,Rd}$ plastic moment resistance

M_r residual moment

M_y effective yield moment

$M_{yF,K}$ yield moment of column flange component

$M_{yP,K}$ yield moment of panel component

m_i seismic mass of floor i

N_{Ed} design axial force

$N_{Ed,E}$ axial force due to the design seismic action

$N_{Ed,G}$ axial force due to non seismic actions in the seismic design combination

$N_{pl,Rd}$ plastic axial resistance

P_{tot} total axial forces

Q live loads

q behaviour factor

q_H hysteresis loop adjustment factor

r_y radius of gyration about weak axis

S soil factor

S_{D1} spectral acceleration at period of 1 sec

S_{DS} spectral acceleration at short periods

S_e, S_α spectral acceleration

sgn signum function

T_1 fundamental period of vibration

T_{1D} effective fundamental period

T_B lower limit of the period of the constant spectral acceleration

T_C upper limit of the period of the constant spectral acceleration

T_D period of the constant displacement response

t_{cf} thickness of column flange

t_d thickness of doubler plate

t_f thickness of flange

t_w thickness of web

t_{wc} thickness of column web

V_{Ed} design shear force

$V_{Ed,E}$ shear force due to the design seismic action

$V_{Ed,G}$ shear force due to non seismic actions in the seismic design combination

$V_{pl,Rd}$ plastic shear resistance

V_{tot} total seismic shear

$w_{pl,y}$ plastic section modulus

a velocity exponent

a_g ground acceleration

α_s strain hardening coefficient

β effective damping

β_{HD} hysteretic damping ratio due to post-yield hysteretic behaviour of the building

β_I inherent damping ratio of the building

β_{V1} viscous damping ratio of the fundamental mode of vibration due to viscous dampers

Γ_1 modal participation factor

γ_{ov} material overstrength factor

γ_{M1} partial factor

Δ_{1D} vector of storey drifts

$\delta_{i,1D}$ modal floor deflection of floor i

δ_y effective yield displacement

δ_T target displacement

ε invariant

η damping correction factor

θ storey drift sensitivity coefficient

θ_c capping rotation

θ_p precapping plastic rotation

θ_{pc} postcapping plastic rotation

θ_u ultimate rotation capacity

θ_y yield rotation

$\theta_{yF,K}$ yield rotation of column flange component

$\theta_{yP,K}$ yield rotation of panel component

Λ parameter of reference cumulative plastic rotation

μ_D effective ductility

v velocity

ξ_{eq} equivalent damping ratio

ΣM_{Rb} sum of the plastic moments of resistance of the beams framing the joint

ΣM_{RC} sum of the plastic moments of resistance of the columns framing the joint

τ relaxation time

ϕ_i first modal displacements of floor i

χ_{LT} reduction factor due to lateral torsional buckling

χ_y, χ_z reduction factors due to flexural buckling

ψ_2 load factor

Ω overstrength factor

∇_{1D} vector of storey velocities

CHAPTER 1

INTRODUCTION, SCOPE, RESEARCH NEEDS, RESEARCH OBJECTIVES, AND THESIS STRUCTURE

1.1 Introduction

Modern technologies for seismic hazard mitigation in building structures, such as active and passive control systems, have been extensively studied over the past 20 years and are now considered ready for widespread implementation in seismic-resistant design practice (Christopoulos and Filiatrault 2006). These systems make it possible to design economically viable buildings that (a) experience significantly less damage than conventional buildings designed according to seismic codes; and (b) return to service within an acceptable short, if not immediate, time after a strong earthquake. The latter is of significant importance as recent strong earthquakes resulted in high socio-economic losses due to long disruption of the use or occupation of a large number of buildings (New Zealand Treasury Budget Speech 2013).

Active control systems are designed to monitor the response of the structure and apply a set of control forces to modify its response in a more desirable. Sensors measure the excitation and the response of the structure and based on these data control forces are developed. The structural response's data may be measured at locations different than the location of the active control system. External power source is continuously required by these systems for operation. The dependence on external power source is a significant limitation on the seismic application of these systems.

Passive control systems are designed to absorb a significant amount of the seismic input energy, with result the reduction of the demand on the structural system. These systems may increase the stiffness and the strength of the structure to which they are installed. External power source is not required by these systems for operation and the dissipation of energy is achieved by the relative motion within the passive control devices due to the motion of the structure.

Among the different types of passive control devices available in the market, fluid viscous dampers are known for their major advantages including large capacity of energy dissipation and peak forces that are out of phase with the peak drifts of elastic or mildly inelastic structures (Symans et al. 2008). Viscous dampers consist of a hollow cylinder filled with fluid, the fluid typically being silicone based (Figure 1.1). The damper is attached to the structure within bracing (Figure 1.2, Figure 1.3). As the damper piston rod and piston head are stroked, fluid is forced to flow through orifices either around or through the piston head. The resulting differential in pressure across the piston head, very high pressure on the upstream side and very low pressure on the downstream side, can produce very large forces that resist the relative motion of the damper. These devices are velocity activated, no frequency dependent and when inserted in typical structures, the stiffness of the structure remains essentially unaffected. The behaviour of viscous dampers can be described by the following force-velocity relation (Seleemah and Constantinou 1997):

$$F_{\mathrm{D}} = C \cdot |v|^{\alpha} \cdot \mathrm{sgn}(v) \tag{1.1}$$

where C is the damping coefficient, v is the velocity across the damper, α is the velocity exponent, and sgn is the signum function. For velocity exponent α equal to unit, the viscous damper is described as linear and for less than unit, is described as nonlinear. The hysteretic behaviour of a linear and a nonlinear viscous damper is

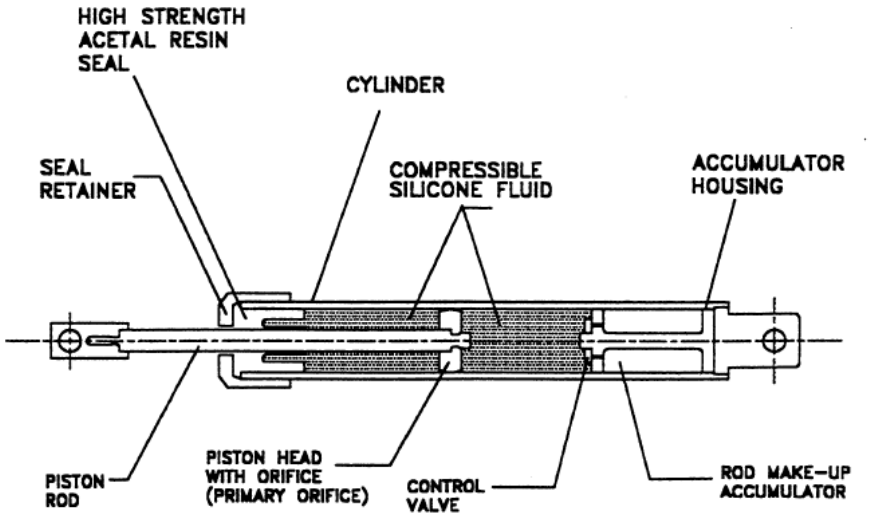

Figure 1.1 Viscous damper (Seleemah and Constantinou 1997)

Figure 1.2 Viscous damper in diagonal configuration (Polat and Constantinou 2017)

Figure 1.3 Viscous damper in horizontal configuration (Taylor Devices)

shown in Figure 1.4. Due to time limitation, this research focuses only on linear viscous dampers.

Other types of passive dampers are the viscoelastic dampers, the metallic dampers and the friction dampers. The viscoelastic dampers dissipate energy through shear deformation of viscoelastic materials such as rubber, copolymers and glassy substances (Lin et al. 1988, Bergman and Hanson 1993, Chang et al. 1993). They are both displacement and velocity activated systems, they are frequency and temperature dependent and they exhibit both damping and stiffness (Figure 1.5).

The metallic dampers dissipate energy through the hysteretic behaviour of metallic materials when deform into their post-elastic range. They are displacement-activated systems and exhibit an elastic-plastic hysteretic behaviour (Figure 1.5). After an earthquake they will be damaged and may need to be replaced. Examples of such dampers include the Added Damping Added Stiffness System (ADAS) (Whittaker et al. 1991), the Triangular Added Damping Added Stiffness System (TADAS) (Tsai et al. 1993), the Lead Extrusion Device (LED) (Robinson and Greenbank 1976) and the Buckling Restrained Brace (BRB) damper (Black et al. 2004).

The friction dampers dissipate energy through the friction that develops at the interface between two solid bodies sliding relative to each other. They are displacement-activated systems and exhibit an elastic perfectly plastic hysteretic

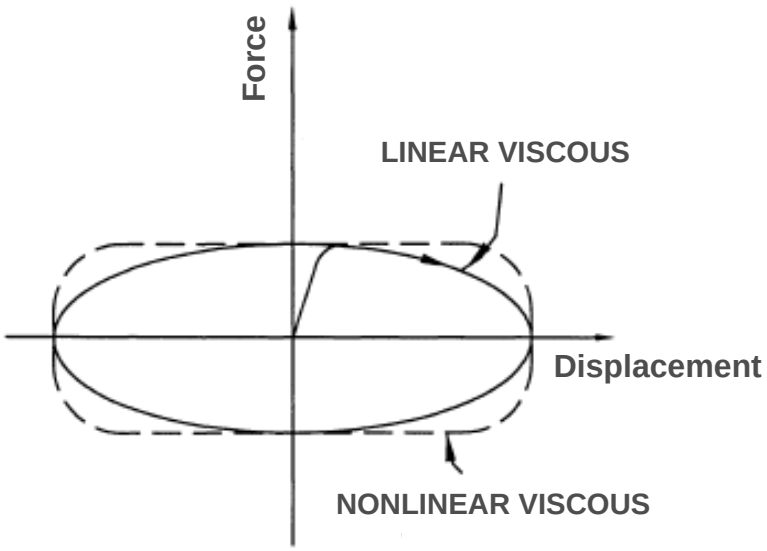

Figure 1.4 Hysteretic behaviour of viscous damper (Ramirez et al. 2000)

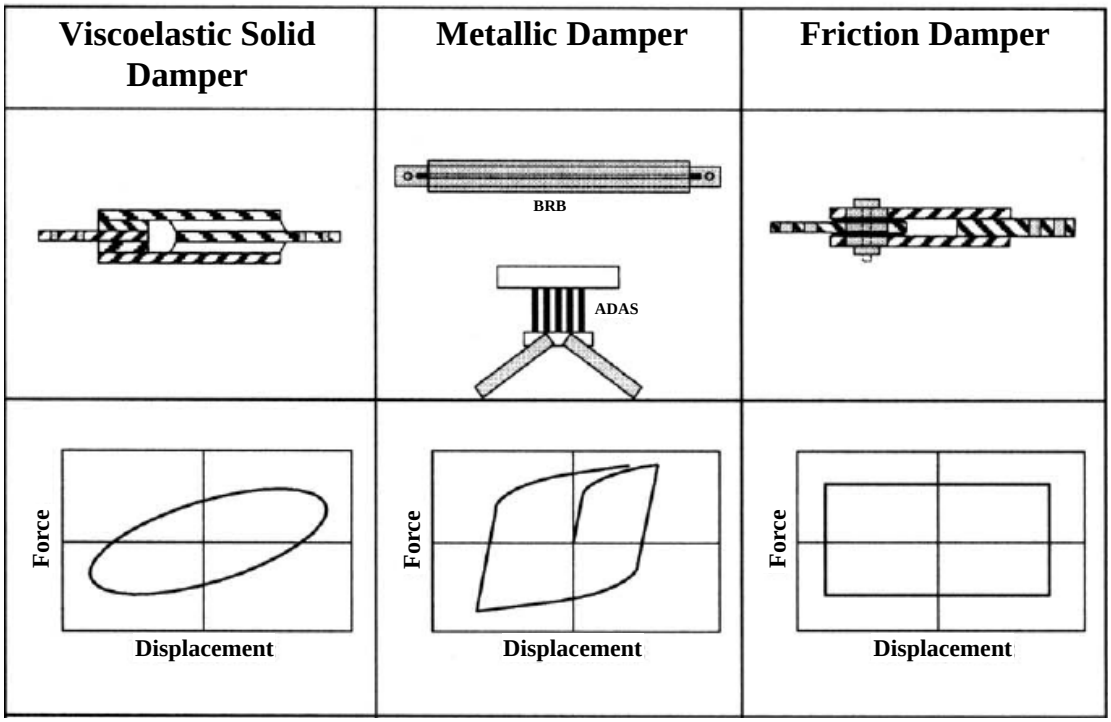

Figure 1.5 Hysteretic behaviour of passive dampers (Symans et al. 2008)

behaviour (Figure 1.5). Examples of such dampers include the slotted-bolted connections (Grigorian et al. 1993), the Sumitomo friction device (Aiken and Kelly 1990) and the Pall friction device (Pall and Marsh 1982).

1.2 Scope

In this research, a seismic design procedure for steel MRFs with viscous dampers within the framework of Eurocode 8 is developed, addressing the issues of (a) the satisfaction of a sway plastic mechanism with plastic hinges in beams and column bases and (b) collapse resistance of steel MRFs with viscous dampers at least equal with that of conventional steel MRFs. A conservative design rule is proposed for the capacity design of the columns in the force path of viscous dampers. Prototype buildings of 5, 10 and 20 storeys are designed using steel MRFs with and without viscous dampers and incremental dynamic analyses are conducted for all steel MRFs. Their global plastic mechanism and their collapse resistance are compared. Appropriate limit values for the storey drift sensitivity coefficient θ are recommended

to guarantee for steel MRFs with viscous dampers collapse resistance at least equal with that of conventional steel MRFs.

1.3 Research needs and research objectives

A fundamental requirement of Eurocode 8 (EC8) (2013) and other current seismic design codes is the formation of a sway plastic mechanism that involves plastic hinges in beams and column bases. However, Seo et al. (2014) and Karavasilis (2016) found that steel MRFs with viscous dampers are prone to plastic mechanisms that involve hinges in columns. Column plastic hinges are formed because of the large column axial forces due to the large damper forces. Note that the peak damper forces may not be completely out of phase with the peak drifts when the steel MRF is well within its inelastic range of response. Therefore, there is an apparent need for further research on capacity design rules for columns in steel MRFs with viscous dampers that will guarantee the formation of a sway global plastic mechanism with plastic hinges in beams and column bases only.

Seo et al. (2014) showed that steel MRFs with viscous dampers and conventional steel MRFs without dampers do not have the same collapse resistance when designed for the same drift performance under the design earthquake. In particular, the lighter steel MRF with dampers may be more prone to P-Delta effects, and thus, have less collapse resistance. Therefore, there is an urgent need to establish design criteria that would guarantee that a steel MRF with viscous dampers has the same collapse resistance with a conventional steel MRF in the case that both frames are designed for the same drift performance. Note that same drift performance essentially means that the steel MRF with viscous dampers has considerably less stiffness and strength than the conventional MRF without dampers since supplemental damping control the seismic induced drifts.

Eurocode 8 does not provide design procedures for steel buildings with viscous dampers, which are a prerequisite for the widespread implementation of dampers in Europe. Therefore, there is a clear need for the development of design procedures for steel buildings with viscous dampers within the framework of EC8. Any attempt to develop a seismic design procedure for steel MRFs with viscous dampers within the

framework of Eurocode 8 shall address the two aforementioned important issues, i.e. (a) the satisfaction of a sway plastic mechanism with plastic hinges in beams and column bases; and (b) collapse resistance of steel MRFs with viscous dampers at least equal with that of conventional steel MRFs.

Having identified the aforementioned gaps in knowledge, the specific measurable objectives of this PhD research are:

1) To propose a seismic design procedure for steel MRFs with viscous dampers within the framework of Eurocode 8 with emphasis on design criteria related to sway plastic mechanism and collapse resistance.
2) To develop nonlinear models for steel MRFs with and without viscous dampers for response history analysis up to collapse.
3) To evaluate the seismic performance of steel MRFs with and without viscous dampers up to collapse.
4) To evaluate the plastic mechanisms of steel MRFs with and without viscous dampers up to collapse.
5) To recommend appropriate limit values for the design criteria of the seismic design procedure that guarantee for steel MRFs with viscous dampers a sway plastic mechanism and collapse resistance similar to those of conventional steel MRFs without dampers.

1.4 Thesis structure

Chapter 2 presents a literature review of experimental research, including shake table tests and hybrid tests, conducted on structures with viscous dampers. Also, analytical studies conducted on structures with viscous dampers are included. The design procedures of American codes and design procedures proposed by other researchers for buildings with viscous dampers are discussed.

Chapter 3 describes the proposed seismic design procedure within the framework of Eurocode 8 for steel MRFs with viscous dampers (objective 1). For the calculation of the damper forces which are needed for the proposed procedure, the response spectrum procedure of ASCE 7-10 is adopted and described in detail.

Chapter 4 presents the design of prototype buildings of 5, 10 and 20 storeys using steel MRFs without viscous dampers. Then, viscous dampers are installed in the steel MRFs by implementing the proposed design procedure described in Chapter 3. The MRFs with viscous dampers are designed to achieve a total viscous damping ratio, ξ_{tot}, at T_1 equal to 20%. Incremental dynamic analyses are conducted for all steel MRFs with and without viscous dampers (objective 2). Their global plastic mechanisms are compared in order to explore whether more conservative capacity design rules are needed for columns in the force path of viscous dampers that will guarantee plastic mechanisms similar to those of steel MRFs without dampers (objective 4). Also, a comparison of the predicted damper forces and the damper forces from analysis is provided.

Chapter 5 provides the design of a number of steel MRFs with viscous dampers, more flexible than the conventional steel MRFs from Chapter 4 and with interstorey drift equal or lower than the conventional steel MRFs, following the proposed seismic design procedure. The upper bound of storey drift sensitivity coefficient θ of the proposed design procedure is neglected. Three groups of MRFs with viscous dampers are designed to achieve a total viscous damping ratio, ξ_{tot}, at T_1 equal to 10%, 15% and 20%, respectively. Incremental dynamic analyses are conducted for steel MRFs with viscous dampers (objective 2) and their collapse resistance is compared with those of steel MRFs without viscous dampers (objective 3). Appropriate limit values for the storey drift sensitivity coefficient θ are recommended to guarantee for steel MRFs with viscous dampers collapse resistance similar to those of steel MRFs without dampers (objective 5).

Chapter 6 presents the conclusions of this research and provides recommendations for future research.

CHAPTER 2

LITERATURE REVIEW

2.1 Introduction

This chapter presents a literature review of experimental research, including shake table tests and hybrid tests, conducted on structures with viscous dampers. Also, analytical studies conducted on structures with viscous dampers are included. The design procedures of American codes and design procedures proposed by other researchers for buildings with viscous dampers are discussed.

2.2 Experimental studies

Constantinou and Symans (1992) conducted a comprehensive program of shake table tests on 1-storey and 3-storey steel structures with and without viscous dampers (Figure 2.1). The numerical results for the earthquake response obtained by using the viscous dampers with the Maxwell model are in good agreement with the experimental results. Below a certain cutoff frequency, the viscous dampers exhibit a pure viscous behaviour and the dampers can be modeled as simple dashpots (Figure 2.2). Usually, structures have dominant frequency below the cutoff frequency and beyond that frequency the dampers exhibit viscoelastic behaviour. The inserted viscous dampers achieved a 30% - 70% reduction in storey drifts and a 40% – 70% reduction in storey shear forces.

Another experimental and analytical study on the behaviour of structural systems with viscous dampers was conducted by Seleemah and Constantinou (1997). Shake table tests were performed on 1-storey and 3-storey steel structures with and without linear and nonlinear viscous dampers. The experimental results were compared with numerical results from response history analysis and from simplified methods largely based on the American Codes and they were in good agreement. The inserted viscous

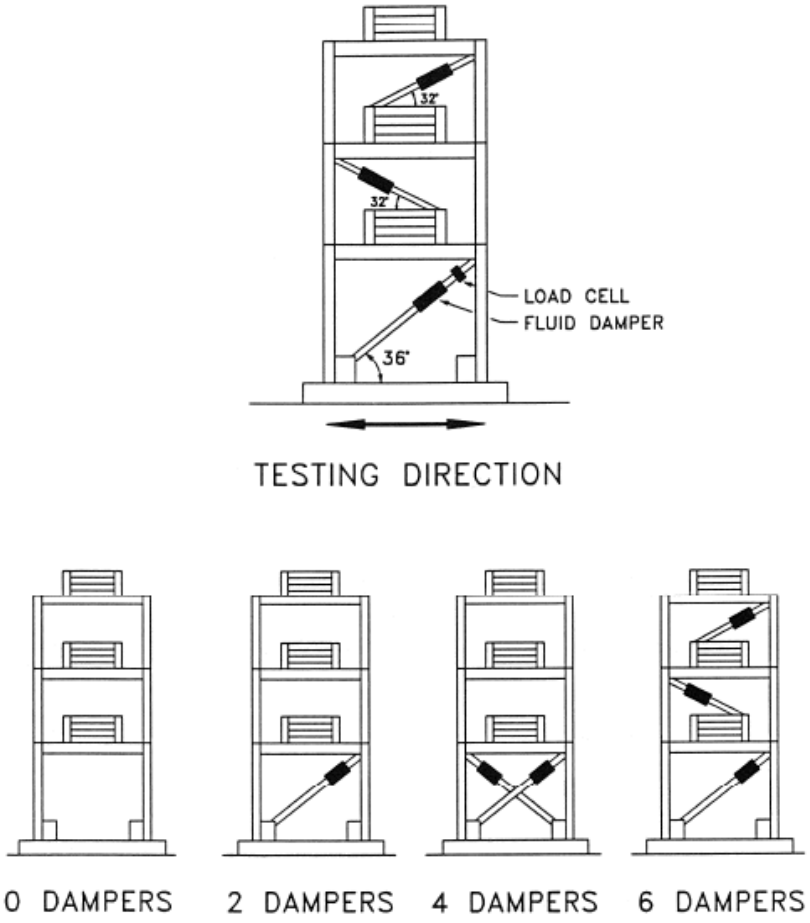

Figure 2.1 Damper configuration for 3-storey structure (Constantinou and Symans 1992)

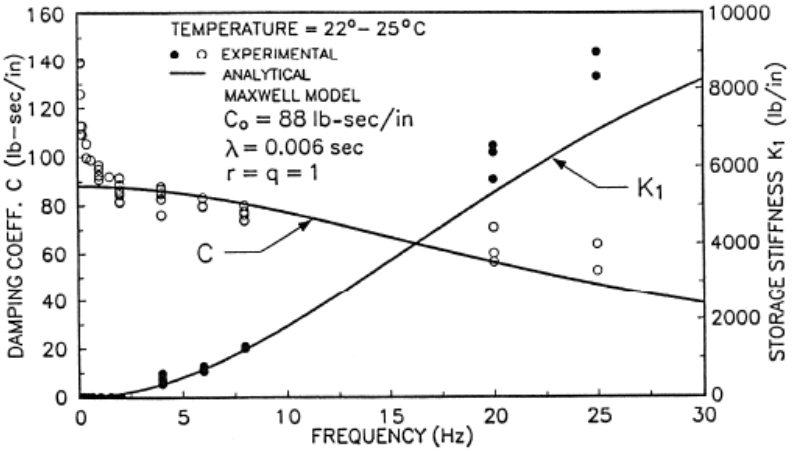

Figure 2.2 Comparison of experimental and analytical values of damping coefficient and storage stiffness (Constantinou and Symans 1992)

dampers resulted in significant reductions in storey drifts and in storey shear forces (Figure 2.3). The reduction in storey drifts was 30% - 90% and in storey shear forces was 20% - 65%. Also, the floor accelerations were reduced. The maximum reduction was achieved when a complete vertical distribution of dampers was used, although an incomplete vertical distribution produced significant reduction.

Kasai et al. (2009) conducted full-scale shaking table tests (Figure 2.4) and Dong et al. (2016) conducted large-scale real-time hybrid simulations of steel structures with viscous dampers (Figure 2.5) and both validated the superior seismic performance of the structures with viscous dampers.

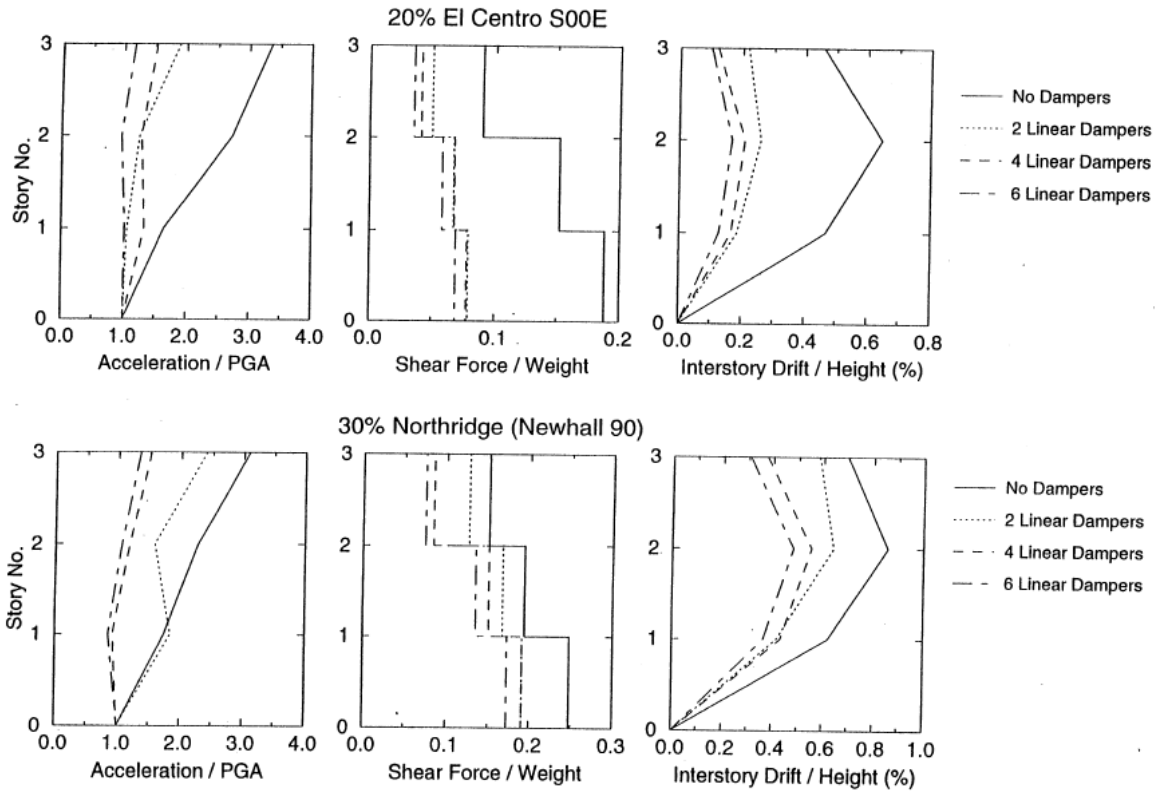

Figure 2.3 Comparison of acceleration, storey shear and interstorey drift profiles of 3-storey structure without dampers and with different dampers configurations subjected to two earthquakes (Seleemah and Constantinou 1997)

Figure 2.4 Exterior views of the building specimen (Kasai et al. 2009)

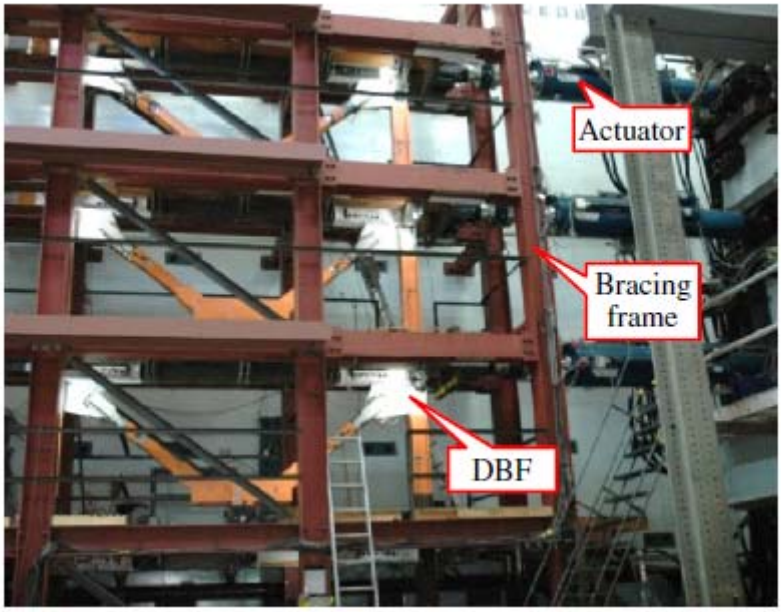

Figure 2.5 Test specimen (Dong et al. 2016)

2.3 Analytical studies

A comparative study of systems with viscous and viscoelastic dampers (Kasai and Fu 1998) describes the mathematical models of these systems and expressions are derived for seismic response prediction. A 10-storey steel moment resisting frame equipped with viscous and viscoelastic dampers is analysed to validate the predicted response. Both viscous and viscoelastic dampers provide added stiffness and damping to the system. Conventionally, a system with supplemental viscoelastic dampers gains both added stiffness and damping, while a system with viscous dampers primarily gains added damping under conditions of low frequency movement. For harmonic excitation, damping effectively reduces the peak displacement response, and thus, reduces the elastic member forces of the frame. With adequate design, the resistance force provided by the viscous damper-brace component can be 90 degrees out-of-phase with the component's deformation (Figure 2.6). However, this does not necessarily cause the column axial force to increase 90 degrees out-of-phase with the column moment. Rather, the global damping of the frame influences the interaction between the column axial force and column moment. In other words, viscoelastic and viscous added components have the same effect on column axial force if they provide the same added damping ratio to the frame. In terms of energy dissipation, viscous

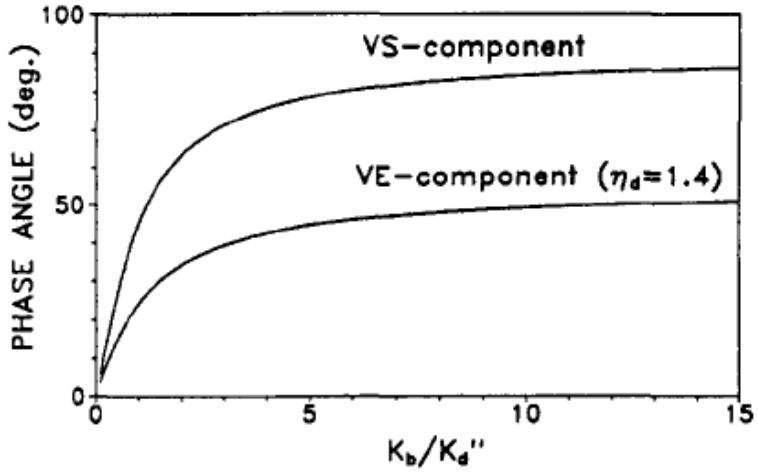

Figure 2.6 Phase angle between force and deformation of the viscous damper-brace component versus the ratio of brace stiffness (K_b) to damper loss stiffness ($K_d'' = \omega \cdot C$) (Kasai and Fu 1998)

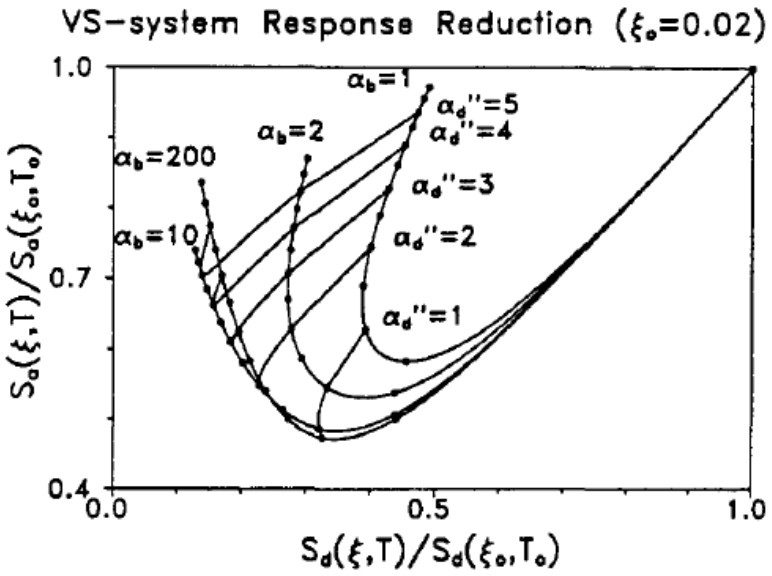

Figure 2.7 Spectral acceleration reduction ratio versus spectral displacement reduction ratio (α_b = ratio of brace stiffness to frame stiffness, α_d'' = ratio of damper loss stiffness to frame stiffness) (Kasai and Fu 1998)

damped systems have slightly higher efficiency than viscoelastic systems, because viscous dampers can deform more than viscoelastic dampers when the added component is subjected to the same deformation. The example design showed that with the same damper loss stiffness, the seismic performances of viscous damped frames were slightly better than those of viscoelastic damped frames, while with the same damping ratio, the performances of viscoelastic frames are better. When using either type of damper, a significant reduction in frame seismic load and deformation can be expected. To achieve the optimal result, a ratio of brace stiffness to frame stiffness equal to 10 and a ratio of damper loss stiffness to frame stiffness equal to 1-1.5 are recommended for either viscous or viscoelastic added components (Figure 2.7). The presented response prediction method works well in the range of structural periods from 0.5 to 2.5 sec.

Another study on viscous dampers has been conducted by Lin and Chopra (2002). In particular, the response of an elastic single degree of freedom system with nonlinear fluid viscous damper is examined under the investigation of the supplemental damping ratio and the nonlinearity parameter. Nonlinear viscous dampers are advantageous because they achieve essentially the same seismic response reduction but with significantly reduced damper force. A design procedure is

presented using the design spectrum. The dynamic characteristics of a nonlinear fluid viscous damper can be described by its energy dissipation capacity represented by the supplemental damping ratio and by its nonlinearity represented by the damping exponent. For systems with same supplemental damping, the influence of damper nonlinearity on harmonic response is very small over the entire range of excitation frequencies for smaller values of damping ratio (Figure 2.8). This influence increases for larger values of damping and for smaller values of the damping exponent because damper nonlinearity shifts the resonant frequency. Damper nonlinearity has more influence on transmissibility than on structural deformation. Damper nonlinearity essentially has no influence on the peak responses, i.e. deformation, relative velocity and total acceleration, of systems in the velocity sensitive spectral region. Differences up to 14% in deformation and velocity were observed in the acceleration region considered. Supplemental damping reduces structural response with greater reduction achieved by increasing the damping. The reduction achieved for a given damping is slightly different in the three spectral regions with the largest being in the acceleration sensitive region (Figure 2.9). The deformation is reduced by up to 25% when the supplemental damping is 5% and up to 60% when the supplemental damping is 30%. Supplemental damping is more effective in reducing structural deformation and hence internal forces, compared to relative velocity or total acceleration. These reductions

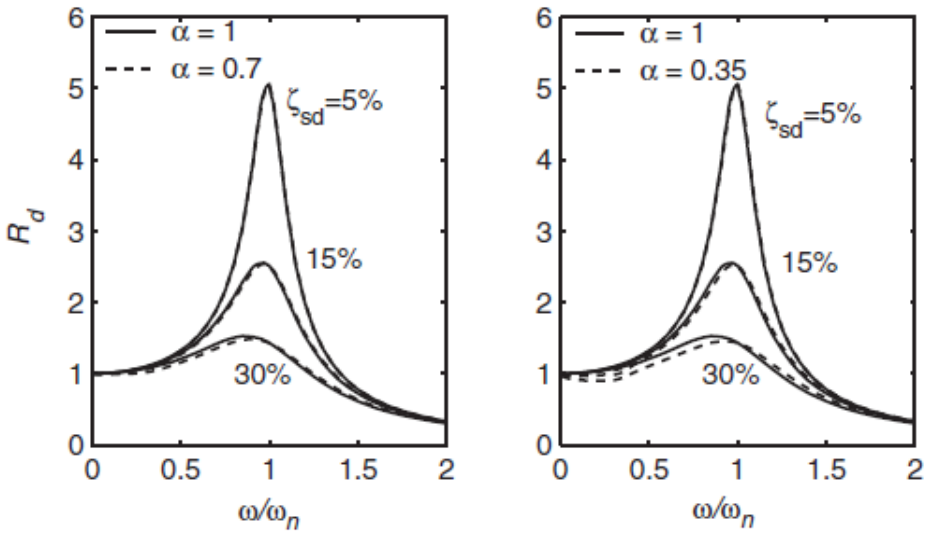

Figure 2.8 Comparison of deformation response factors R_d for systems with linear and nonlinear viscous dampers for three levels of supplemental damping ratio (Lin and Chopra 2002)

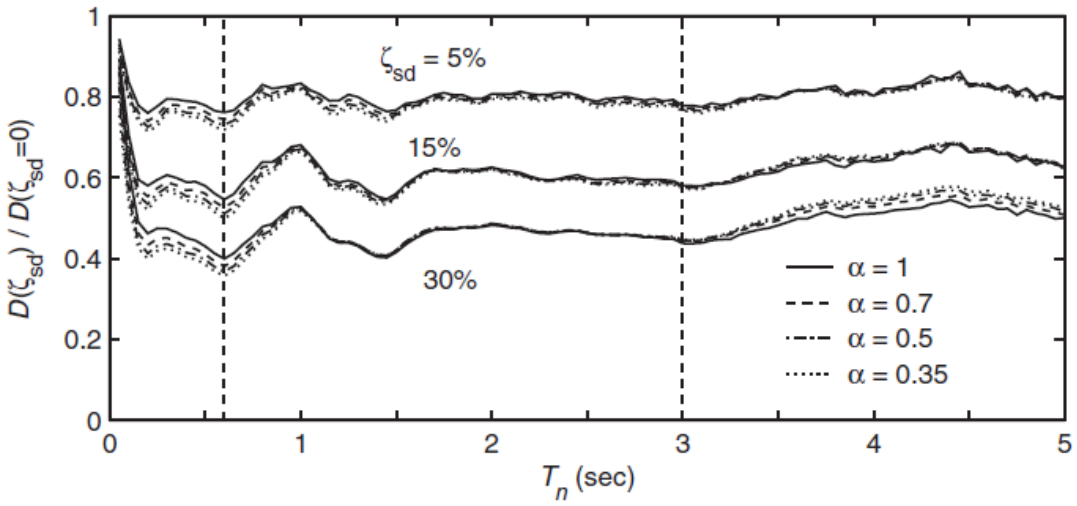

Figure 2.9 Ratios of mean peak deformations with and without supplemental damping (Lin and Chopra 2002)

are essentially unaffected by damper non-linearity in the velocity sensitive region and are only weakly dependent in the acceleration and displacement sensitive regions. The design values of structural deformation and forces for a system with nonlinear dampers can be estimated directly from the design spectrum for the period and the total damping of the system. However the supplemental damping must be determined iteratively as it contains the unknown value of peak deformation. The peak value of earthquake induced force in a nonlinear damper can be estimated with reasonable accuracy from the peak damper force in the corresponding linear system, its peak deformation, and relative velocity. The relative velocity should not be replaced by pseudo-velocity as this approximation introduces large error in the damper force.

Lin and Chopra (2003) studied the response of an elastic single degree of freedom system with nonlinear viscoelastic damper (which consists of a nonlinear fluid viscous damper connected in series to a linear elastic bracing element). Supplemental damping reduced structural response and the response reduction depends on the bracing stiffness. A practical range of the ratio of the brace stiffness to frame stiffness is over 5 that corresponds to ratio of relaxation time to system period less than 2% (relaxation time is the damping coefficient over the brace stiffness). Damper nonlinearity has little influence on harmonic response over the entire range of excitation frequencies when the ratio of the relaxation time to system period is less than 5%. This influence increases slightly for larger values of supplemental damping.

The harmonic responses of the single degree of freedom system with a corresponding linear damper or equivalent linear Kelvin model are essentially identical for small damping. Their difference grows slightly with increase in supplemental damping and bracing flexibility. Damper nonlinearity influences the peak response deformation, the relative velocity and the total acceleration of systems with ratio of relaxation time to system period equal to 2% very little in the velocity sensitive region of the spectrum (Figure 2.10). Differences up to 18% and 12% are observed in the response of these systems in the acceleration and the displacement sensitive regions, respectively, due to damper nonlinearity. Damper nonlinearity influences the system response similarly even if the bracing is more flexible. The response reduction due to supplemental damping depends on the bracing stiffness or the relaxation time over the system period. The response of single degree of freedom system with a nonlinear damper can be estimated with a sufficient degree of accuracy for design applications by analyzing the corresponding linear viscous system (with rigid brace) (Figure 2.11). This simple system is not valid for a ratio of relaxation time to system period more than 5%. The response of a single degree of freedom system with a nonlinear damper and bracing with ratio of relaxation time to system period less than 2%, can be estimated directly from the earthquake design spectrum. However the relative velocity should not be replaced by the readily available pseudo-velocity because this approximation introduced large error in the damper force. The square root of the squared peak values

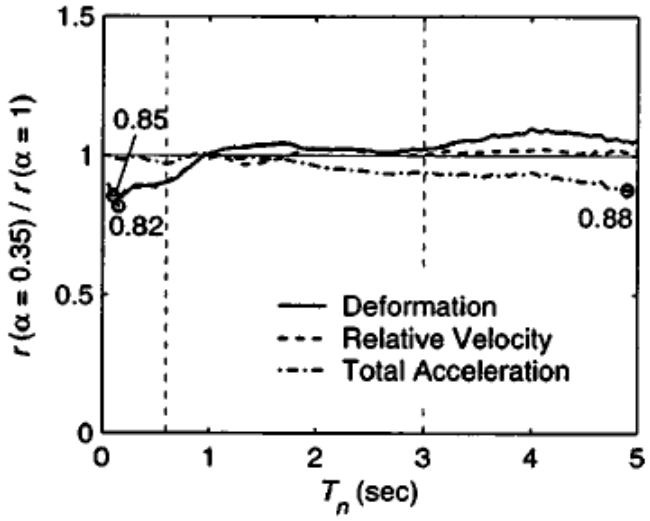

Figure 2.10 Influence of damper nonlinearity (α) on mean peak responses with ratio of relaxation time to system period equal to 2% (Lin and Chopra 2003)

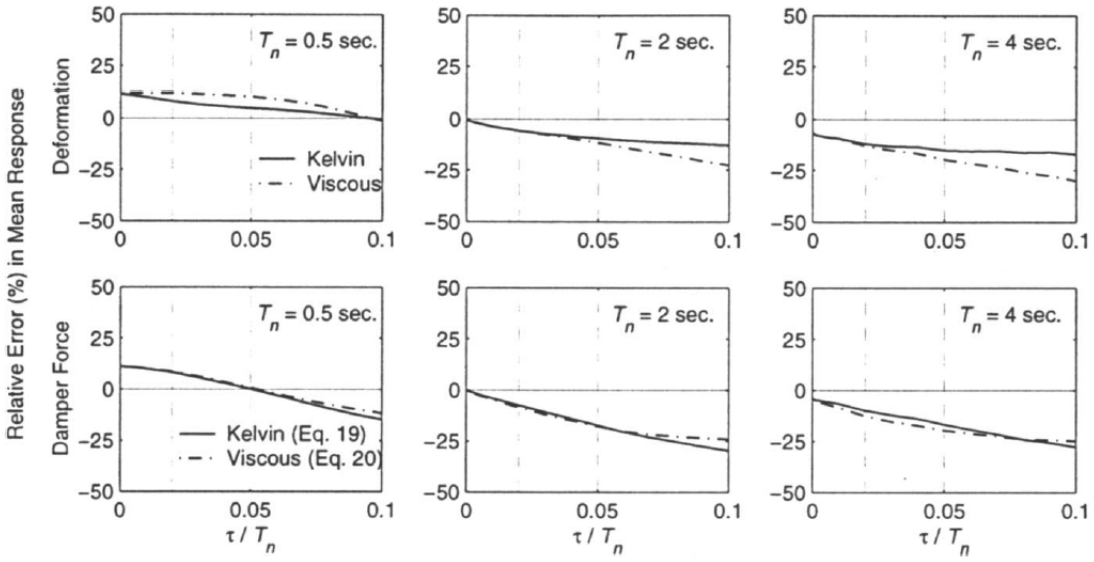

Figure 2.11 Relative errors in mean response of systems with nonlinear viscous dampers estimated from analysis of equivalent linear Kelvin and corresponding linear systems with rigid bracing (Lin and Chopra 2003)

of structural force and damper force estimates the peak value of the shear force transmitted to the foundation.

By adding dampers to a building using diagonal braces, additional axial forces are introduced into the columns which are connected to the braces and dampers. An investigation by Goel (2002) examined the influence of inclined viscous damper on column axial force in a simple one-storey frame. The column axial force consists of two components: the elastic and the damping components. For harmonic loading the damping component is 90 degrees out-of-phase with the elastic component. The maximum axial force in a system with horizontal damper is only due to elastic component and is perfectly in-phase with the displacement response. The maximum force in a system with inclined damper, on the other hand, is due to both elastic and damping components and is not perfectly in-phase with the elastic forces but has a phase lag. The column axial force can be significantly higher in a system with inclined damper compared to a system with horizontal damper, even when the damping ratio in both systems is the same. Also the column axial force in a system with inclined damper increases compared to a system with horizontal damper as the ratio of the forcing frequency to the natural vibration frequency and the damping ratio increase (Figure 2.12). The phase lag increases with increasing values of the ratio of

the forcing frequency to the natural vibration frequency and the damping ratio. The amplification of the column axial forces between a system with inclined damper and horizontal damper is small for very short period systems, less than 0.25 sec (Figure 2.13). The amplification, however, becomes significant for longer period systems. The largest amplification tends to occur for systems with period equal to or about 0.8 sec. Amplification reduces a little for longer periods but begins to increase again as the system period becomes much longer. As noted before, the amplification increases with increasing values of damping.

A series of papers (Ramirez et al. 2002a, 2002b, 2003, Whittaker et al. 2003) is related to a proposed simplified method of analysis of inelastic buildings equipped with linear and nonlinear viscous dampers. The method predicts the seismic response of a damped system by using an equivalent linear elastic, viscously damped single degree of freedom system representing the yielding structure. Further details are presented for the calculation of the properties for the multi degree of freedom system. This method has been incorporated in the American guidelines for new buildings (NEHRP 2000 – FEMA 368). Two types of structural behaviour were considered. The first was smooth perfect bi-linear hysteretic behaviour and the second was a system that lacks the ability to dissipate energy, a bilinear elastic system. The analysed

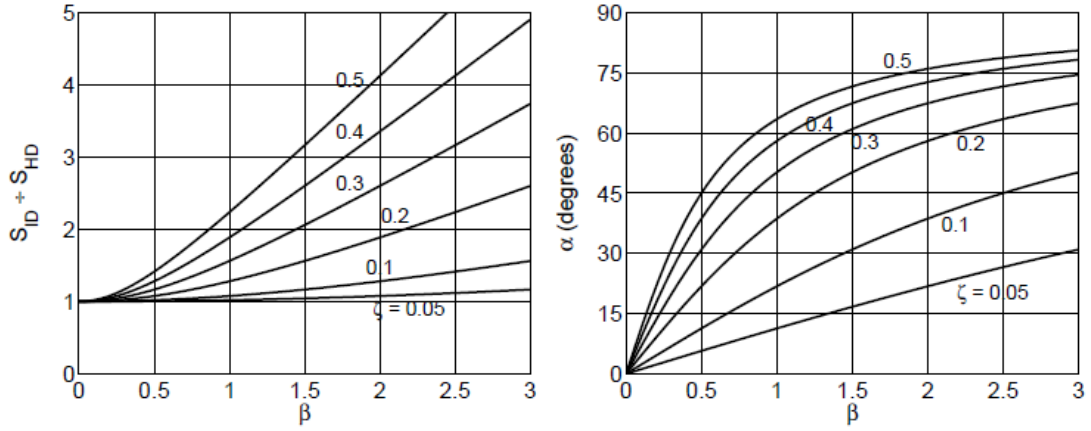

(a) (b)

Figure 2.12 Response of SDOF systems with inclined damper to harmonic loading: (a) amplification of column axial forces and (b) phase lag between axial force and deformation (where β is the ratio of forcing frequency to natural vibration frequency) (Goel 2002)

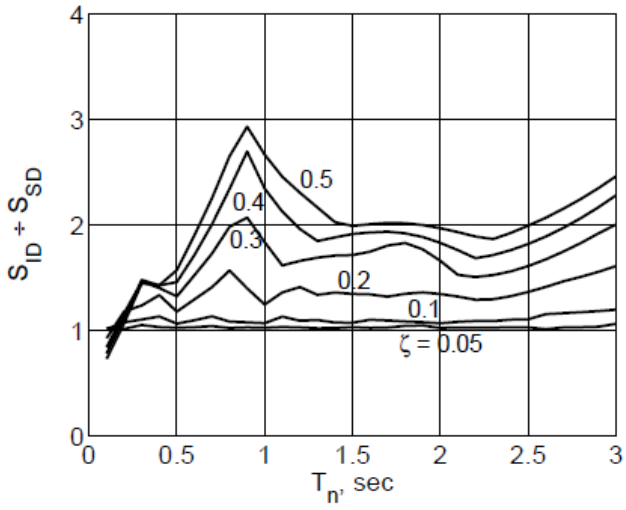

Figure 2.13 Response of SDOF system with inclined damper subjected to an earthquake: amplification of column axial force (Goel 2002)

systems were: the bilinear hysteretic system with linear viscous damping devices, the bilinear hysteretic system with nonlinear viscous damping devices and the bilinear elastic system with linear viscous damping devices (Figure 2.14). The proposed method is iterative based on an assumed value of displacement, calculation of the effective period and the effective damping, calculation of the displacement using the response spectrum after modification for increased damping and comparison of the calculated and assumed values of displacement. In addition, the maximum velocity is needed for the calculation of the peak damping force. A procedure to determine the maximum acceleration is proposed assuming the structure undergoes harmonic vibration. The proposed simplified method produces exact or larger estimates of the peak displacement and the peak acceleration, and within 25% of the correct values of the peak velocities.

Moreover, research efforts evaluated the effectiveness of using viscous dampers to reduce residual displacements as well as damage in velocity-sensitive and acceleration-sensitive non-structural components of buildings (Karavasilis and Seo 2011; Pavlou and Constantinou 2006; Wanitkorkul and Filiatrault 2008).

Recent research efforts focused on the collapse assessment of steel MRFs with viscous dampers under earthquake intensities higher than the MCE (Miyamoto et al. 2010). Seo et al. (2014) showed that 4-storey steel MRFs with viscous dampers develop plastic mechanisms characterised either by the desired combination of plastic

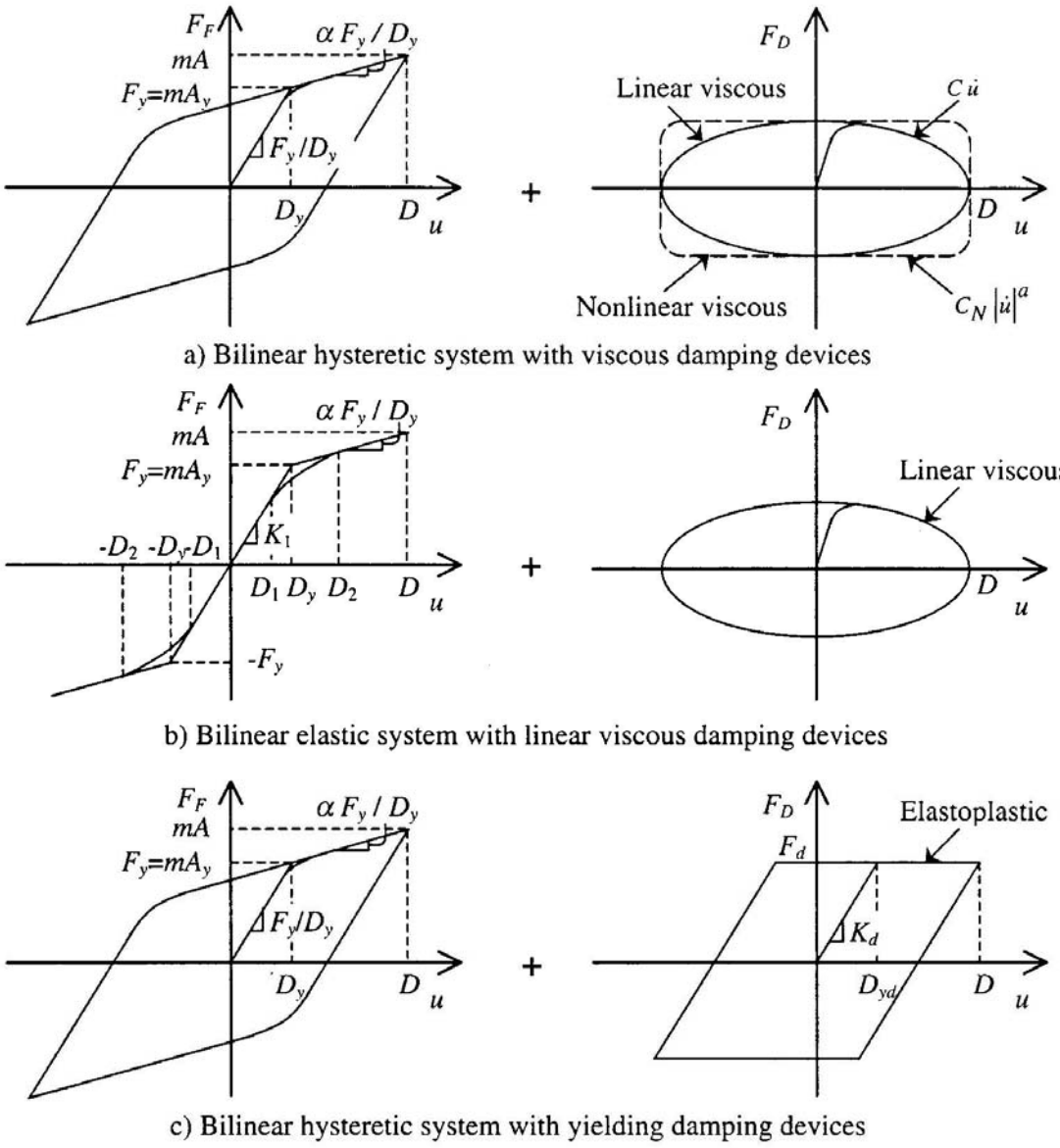

Figure 2.14 Illustration of behaviour of analysed systems (Ramirez et al. 2002a)

hinges in beams and column bases or by plastic hinges in beams and columns of different storeys. For few earthquake ground motions, plastic mechanisms characterised by the formation of a soft storey were also detected (Figure 2.15). The same work provided evidence that the formation of column plastic hinges in steel MRFs with viscous dampers does not necessarily lead to worst collapse resistance. Similar conclusions for the plastic mechanisms have been derived by Karavasilis (2016) for 5-storey, 10-storey and 20-storey steel MRFs. Another important outcome

of the work of Seo et al. (2014) was that steel MRFs with viscous dampers and conventional MRFs without dampers do not have the same collapse resistance when designed for the same drift performance under the design earthquake. In particular, the lighter steel MRF with dampers may be more prone to P-Delta effects, and thus, have less collapse resistance. Seo et al. (2014) did not suggest a solution or formal design recommendation for this issue.

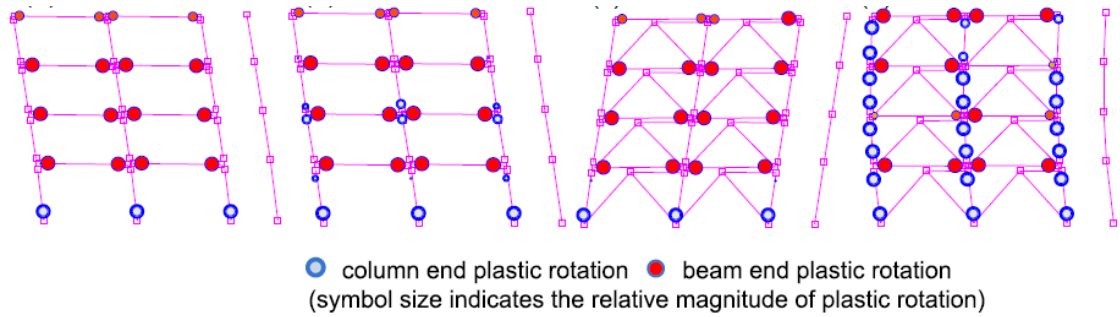

Figure 2.15 Collapse plastic mechanisms for one MRF and one MRF with viscous dampers under two different earthquakes (Seo et al. 2014)

2.4 Existing design procedures

American codes provide design procedures for incorporation of viscous dampers in new and existing buildings since 1997 (FEMA 273, 274, 356) and 2000 (FEMA 368, 369, 450) respectively by using either linear static or linear dynamic procedure. The latest American code ASCE 7-10 (2010) provides design procedures for buildings with viscous dampers, which use a highly damped elastic single degree of freedom system as substitute of the real inelastic multi degree of freedom building. The total damping of the substitute elastic system is the summation of the inherent, supplemental viscous, and hysteretic (due to yielding) damping. The use of the substitute system essentially enables the damping system (i.e. the beams, columns, and connections of the frame that includes the viscous dampers and their supporting braces) to be designed for three different loading conditions, i.e. those associated with the maximum displacement, maximum velocity and maximum acceleration. Structures that contain a damping system are required to have a basic seismic force resisting system in each direction. The seismic force resisting system shall be

designed for not less than 75% of the code seismic base shear. Elements of the damping system shall be designed to remain elastic for design loads. The response spectrum procedure is permitted to be used as long as the damping system has at least two damping devices in each storey and the total effective damping of the fundamental mode is not greater than 35%. The equivalent lateral force procedure is permitted as long as there are at least two damping devices in each storey, the total effective damping is not greater than 35%, the seismic force resisting system does not have any plan or vertical irregularity, floor diaphragms are rigid and the height of the structure above the base does not exceed 30 m. For the equivalent lateral force analysis, response is defined by two modes: 1) the fundamental mode and 2) the residual mode. The residual mode is a new concept used to approximate the combined effects of higher modes. While typically of secondary importance to storey drift, higher modes can be a significant contributor to storey velocity and hence are important for design of velocity dependent damping devices. For response spectrum analysis, higher modes are explicitly evaluated.

Christopoulos and Filiatrault (2006) provided a design procedure to estimate the damping coefficients using a fictitiously braced structure. Another design procedure for buildings with viscous dampers has been proposed by Silvestri et al. (2010) based on shear-type structures with uniform mass and lateral stiffness distribution. It is a simple practical procedure which aims at guiding the professional engineer from the choice of a target reduction in the seismic response of the structural system to the identification of the corresponding damping ratio and the mechanical characteristics of the dampers.

Guo and Christopoulos (2013a) proposed a direct performance-based design method for structures incorporating linear viscous or viscoelastic dampers. This method studies the response of a nonlinear single degree of freedom by using a design tool, called performance-spectra (Guo and Christopoulos 2013b), and a single degree of freedom to multi degree of freedom transformation procedure is also presented. The design tool of performance-spectra estimates the peak response of the single degree of freedom system with damper by using an improved equivalent linearization method. The performance-spectra is a compact graphical design tool that links idealised inelastic single degree of freedom system responses including peak and residual displacement, peak base shear and acceleration to controllable structural and damping properties. The spectra allows for a direct comparison and target of different

damping strategies that achieve a given set of performance goals without completing a full design iteration. For a given base frame the P-Spectra defines the normalised base shear and residual ratio against the normalised displacement for different combinations of damper exponent. P-Spectra can be computed for a set of ground motions using either nonlinear time-history analysis or an equivalent linearization procedure using the design spectrum.

2.5 Summary

This chapter provided a literature review of research on structures equipped with viscous dampers. These studies highlight the benefits of the incorporation of these devices in the structures and they explore the influence of different parameters on the response. Structures with viscous dampers are prone to plastic mechanisms that involve hinges in columns because of the large column axial forces due to the large damper forces.

CHAPTER 3

PROPOSED SEISMIC DESIGN PROCEDURE FOR STEEL MRF WITH VISCOUS DAMPERS

3.1 Introduction

A seismic design procedure for steel MRFs with viscous dampers is developed within the framework of Eurocode 8. For the calculation of the damper forces which are needed for the proposed procedure, the response spectrum procedure of ASCE 7-10 is adopted and described in detail. The presented design procedures will be used in the next chapters.

3.2 Design of steel MRF with viscous dampers

The proposed seismic design procedure for steel MRFs with viscous dampers within the framework of Eurocode 8 is the following:

Step 1

Design the structural elements of the structure, using the elastic spectrum divided by the behaviour factor q and the damping reduction factor B given in Table 3.1 for higher damping ratio than 5%, to satisfy the limitation of interstorey drift ratio (IDR) given in Section 4.4.3.2 of Eurocode 8 (EC8) and the limitation of storey drift sensitivity coefficient θ given in Section 4.4.2.2(2) of EC8. If coefficient θ is less than 0.10, P-Δ effects need not to be accounted. It shall not exceed the value of 0.30 and for values between 0.10-0.20 the P-Δ effects need to be accounted as described in Section 4.4.2.2(2) of EC8. The limits of coefficient θ are re-examined in Section 5.3. The damping reduction factor B is similar to the damping correction factor η of EC8 (Equation 3.6 of EC8). Damping reduction factor B of ASCE 7-10 has been adopted

Table 3.1 Damping reduction factor (B)

[Table 18.6-1 of ASCE 7-10]

Effective damping (β)	Damping reduction factor (B) (for period $\geq T_0$)
≤ 0.02	0.8
0.05	1.0
0.10	1.2
0.20	1.5
0.30	1.8
0.40	2.1
0.50	2.4
0.60	2.7
0.70	3.0
0.80	3.3
0.90	3.6
≥ 1.00	4.0

instead of damping correction factor η of EC8 because EC8 in Section 3.2.2.2(4) describes that for viscous damping ratio different from 5%, value of correction factor η is given in other parts of EC8 and not by Equation 3.6 of EC8.

Step 2 – Step 6

These steps are the same with those that are followed for the design of steel MRFs without dampers and they are provided in Appendix A.

Step 7

For the desired level of viscous damping ratio provided by the viscous dampers, calculate the damping coefficients of the viscous dampers solving the following relation with respect to C_i:

$$\xi_{eq} = \frac{T_1}{4\pi} \frac{\sum_i C_i \cdot (\phi_i - \phi_{i-1})^2}{\sum_i m_i \cdot \phi_i^2} \tag{3.1}$$

where ξ_{eq} : equivalent damping ratio

T_1 : fundamental period of vibration

ϕ_i, ϕ_{i-1} : first modal displacements of floors *i*, *i-1*

m_i : seismic mass of floor *i*

Step 8

Calculate the maximum damper forces under the design seismic action (10% probability of exceedance in 50 years or 475 years return period, hereafter referred to as DBE) following the procedure of ASCE 7-10 which is described in the next section. Impose the damper forces on the braces that support the viscous dampers and apply horizontal restraint forces at each floor such that the horizontal displacement at each level of the structure is zero. Design the supporting braces and the gusset plates for these forces combined with the gravity loads in the seismic design combination, i.e. $G + \psi_2 Q$, (peak velocity state) and such that satisfy the relation (Lin and Chopra 2003):

$$\frac{\tau}{T_1} \leq 0.02 \tag{3.2}$$

where τ is the relaxation time defined as the ratio C/K_b with C the horizontal component of the damping coefficient of viscous damper and K_b the horizontal stiffness of the bracing system.

The viscous dampers and their connections shall be designed to resist forces, displacements and velocities from the peak velocity state but under 150% of the DBE intensity (hereafter referred to as MCE).

Step 9

For the columns in the force path of viscous dampers, repeat Steps 4-6 with design axial force, as given in Step 4, modified as follows:

$$N_{Ed} = N_{Ed,G} + 1.1 \cdot \gamma_{ov} \cdot \Omega \cdot \max\left(N_{Ed,E}, N_{Ed,E,V,SF}\right) \tag{3.3}$$

where $N_{Ed,E,V,SF}$ is the column axial force which is induced by the damper forces multiplied by a scale factor SF and the horizontal restraint forces as described in Step

8. The damper forces and the horizontal restraint forces of each vibration mode are combined through the Square Root Sum of Squares (SRSS) rule. SF is taken equal to 1.0 and its value is re-examined in Section 4.7. Equation (3.3) suggests that the column axial force used to perform the capacity design of columns in the force path of viscous dampers is the envelope of the axial force from the peak drift state (under the design seismic action) and the axial force from the peak velocity state for SF equal to 1.0. For an elastic or mildly inelastic frame, $N_{Ed,E,V,SF}$ is out-of-phase with M_{Ed} and V_{Ed}, and therefore, the modified capacity design rule seems rather conservative. It is though noted that for seismic intensities higher than the DBE, peak damper forces increase beyond their design values under the DBE, while inelasticity of the steel MRF may result in unfavorable combinations of axial forces, shear forces, and bending moments in the columns. Therefore, the proposed conservative design rule is justified with respect to the overall goal of promoting a global sway plastic mechanism in tall steel MRFs with viscous dampers.

3.3 Calculation of damper forces

For the calculation of damper forces under the DBE, the response spectrum procedure in Section 18.4 of ASCE 7-10 will be adopted rather than the derivation of expressions based on theory of structural dynamics due to time limitation. To apply this procedure, first the response spectrum of ASCE 7-10 needs to be correlated with the EC8, both for 5% damping.

Figure 3.1 shows the response spectrum of ASCE 7-10 with the following parameters:

S_α : spectral acceleration

S_{DS} : spectral acceleration at short periods

S_{D1} : spectral acceleration at period of 1 sec

T : fundamental period of the building

$$T_0 = 0.2 \cdot \frac{S_{D1}}{S_{DS}}$$

$$T_S = \frac{S_{D1}}{S_{DS}}$$

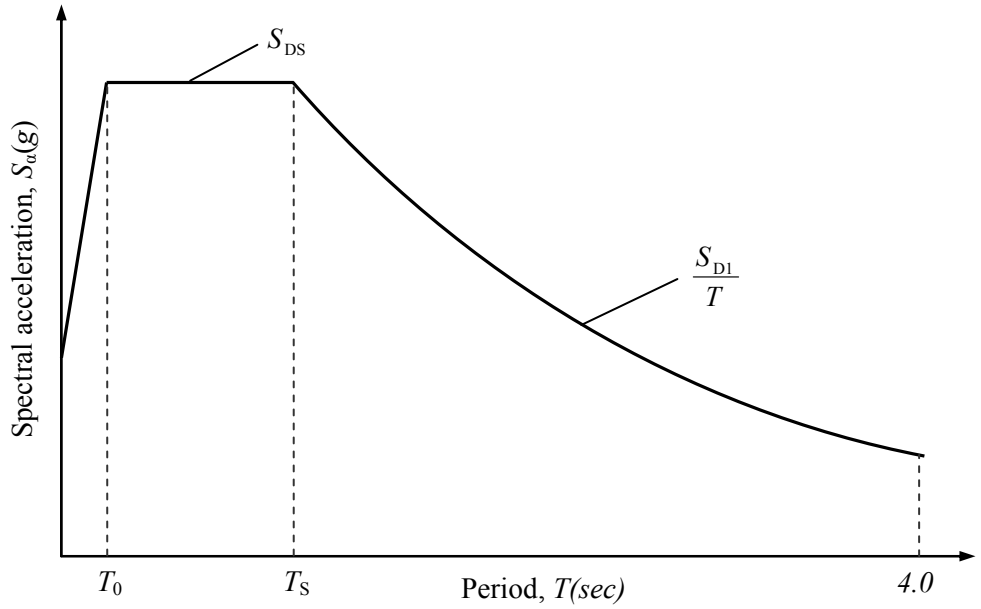

Figure 3.1 Response spectrum for 5% damping of ASCE 7-10

[Figure 11.4-1 of ASCE 7-10]

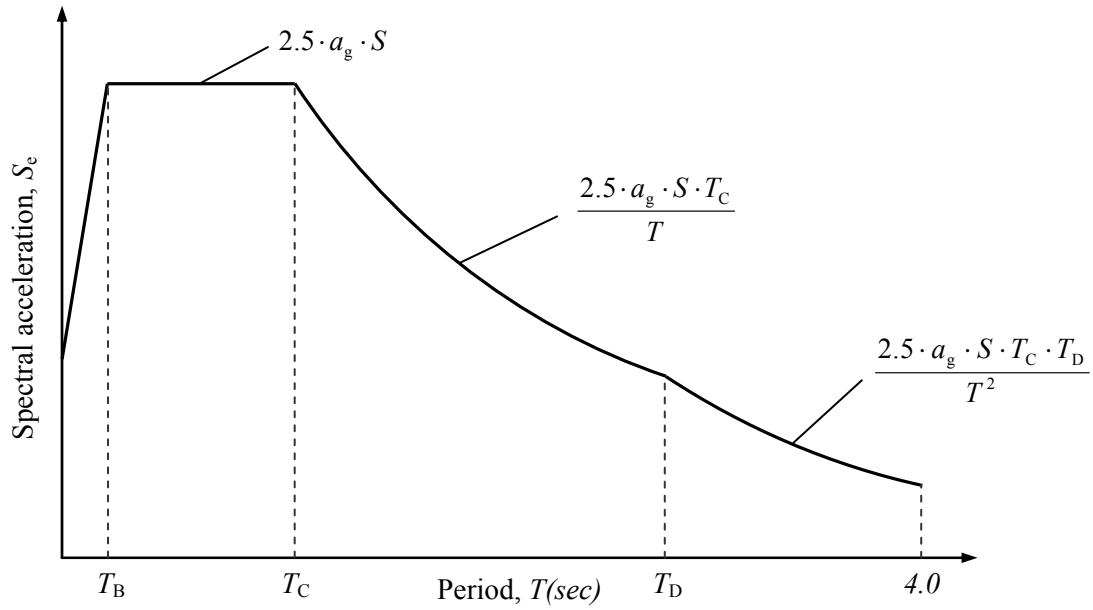

Figure 3.2 Response spectrum for 5% damping of EC8

[Figure 3.1 of EC8]

Figure 3.2 shows the response spectrum of EC8 with the following parameters:

S_e : spectral acceleration

a_g : ground acceleration

S : soil factor (Table 3.2 of EC8)

T : fundamental period of the building

T_B : lower limit of the period of the constant spectral acceleration (Table 3.2 of EC8)

T_C : upper limit of the period of the constant spectral acceleration (Table 3.2 of EC8)

T_D : period of the constant displacement response (Table 3.2 of EC8)

For the constant spectral acceleration branch of ASCE 7-10, the spectral acceleration $S_\alpha = S_{DS} \cdot g$ for periods T_0 - T_S corresponds to $S_e = 2.5 \cdot a_g \cdot S$ of EC8 for periods T_B - T_C and T_S corresponds to T_C.

Therefore,

$$S_{DS} = 2.5 \cdot \frac{a_g}{g} \cdot S \qquad \text{for } T_0 \le T < T_S \qquad (3.4)$$

For periods greater than T_S of ASCE 7-10, the spectral acceleration $S_\alpha = \frac{S_{D1} \cdot g}{T}$ corresponds to $S_e = \frac{2.5 \cdot a_g \cdot S \cdot T_C}{T}$ of EC8 for periods $T_C - T_D$.

Therefore,

$$S_{D1} = 2.5 \cdot \frac{a_g}{g} \cdot S \cdot T_C \qquad \text{for } T_S \le T < T_D \qquad (3.5)$$

For periods greater than T_S of ASCE 7-10, there is only one branch given by $S_\alpha = \frac{S_{D1} \cdot g}{T}$ while EC8 includes two branches, i.e. for periods T_C – T_D with $S_e = \frac{2.5 \cdot a_g \cdot S \cdot T_C}{T}$ and for periods T_D – 4 sec with $S_e = \frac{2.5 \cdot a_g \cdot S \cdot T_C \cdot T_D}{T^2}$. Therefore, an extra branch of spectral acceleration need to be incorporated for periods T_D – 4 sec with $S_\alpha = \frac{S_{D1} \cdot g}{T^2}$. Actually, this branch already exists in ASCE 7-10 but for periods longer than 4 sec.

Therefore,

$$S_{D1} = 2.5 \cdot \frac{a_g}{g} \cdot S \cdot T_C \cdot T_D \quad \text{for } T_D \le T \le 4\,\text{sec} \qquad (3.6)$$

3.3.1 Fundamental mode

The damper forces of horizontal linear viscous dampers are calculated by the following relation:

$$F_D = C \cdot \nabla_{1D} \qquad (3.7)$$

where C : vector of damping coefficients

∇_{1D} : vector of storey velocities

and

$$\nabla_{1D} = 2\pi \frac{\Delta_{1D}}{T_{1D}} \qquad (3.8)$$

$$\Delta_{1D} = \delta_{i,1D} - \delta_{i\text{-}1,1D} \qquad (3.9)$$

$$\delta_{i,1D} = D_{1D} \cdot \phi_{i,1} \qquad (3.10)$$

$$T_{1D} = T_1 \sqrt{\mu_D} \qquad (3.11)$$

where Δ_{1D} : vector of storey drifts

$\delta_{i,1D}$: modal floor deflection of floor i

D_{1D} : roof displacement due to the design earthquake

$\phi_{i,1}$: modal displacement of floor i, normalised to unity at the roof level

T_{1D} : effective fundamental period

T_1 : fundamental period

$\mu_D = \frac{\delta_T}{\delta_y}$: effective ductility (as described in FEMA 450 but using the reduced elastic spectrum accounting for the equivalent damping ratio)

δ_T : target displacement

δ_y : effective yield displacement

The roof displacement D_{1D} is given by:

$$D_{1D} = \frac{g}{4\pi^2} \cdot \Gamma_1 \cdot \frac{S_{DS} \cdot T_{1D}^2}{B_{1D}} \geq \frac{g}{4\pi^2} \cdot \Gamma_1 \cdot \frac{S_{DS} \cdot T_1^2}{B_{1E}} \qquad \text{for } T_{1D} < T_S \quad (3.12)$$

$$D_{1D} = \frac{g}{4\pi^2} \cdot \Gamma_1 \cdot \frac{S_{D1} \cdot T_{1D}}{B_{1D}} \geq \frac{g}{4\pi^2} \cdot \Gamma_1 \cdot \frac{S_{D1} \cdot T_1}{B_{1E}} \qquad \text{for } T_S \leq T_{1D} < T_D \quad (3.13)$$

$$D_{1D} = \frac{g}{4\pi^2} \cdot \Gamma_1 \cdot \frac{S_{D1}}{B_{1D}} \geq \frac{g}{4\pi^2} \cdot \Gamma_1 \cdot \frac{S_{D1}}{B_{1E}} \qquad \text{for } T_{1D} \geq T_D \quad (3.14)$$

with

$$\Gamma_1 = \frac{\sum_{i=1}^{n} m_i \cdot \phi_{i,1}}{\sum_{i=1}^{n} m_i \cdot \phi_{i,1}^2} \quad (3.15)$$

where m_i : seismic mass of floor i

Γ_1 : modal participation factor

B_{1D} : damping reduction factor given in Table 3.1 for effective damping ratio equal to β_{1D}

B_{1E} : damping reduction factor given in Table 3.1 for effective damping ratio equal to β_{1E}

The effective damping ratios of β_{1D} and β_{1E} are given by the following expressions:

$$\beta_{1D} = \beta_I + \beta_{V1}\sqrt{\mu_D} + \beta_{HD} \quad (3.16)$$

$$\beta_{1E} = \beta_I + \beta_{V1} \quad (3.17)$$

where β_I : inherent damping ratio of the building

β_{V1} : viscous damping ratio of the fundamental mode of vibration due to viscous dampers

β_{HD} : hysteretic damping ratio due to post-yield hysteretic behaviour of the building

For horizontal linear viscous dampers, the viscous damping ratio due to viscous dampers β_{V1} is estimated by the following relation:

$$\beta_{V1} = \frac{T_1}{4\pi} \frac{\sum_{i=1}^{n} C_i \cdot (\phi_{i,1} - \phi_{i-1,1})^2}{\sum_{i=1}^{n} m_i \cdot \phi_{i,1}^2} \tag{3.18}$$

And the hysteretic damping ratio β_{HD} is given by:

$$\beta_{HD} = q_H (0.64 - \beta_I) \cdot \left(1 - \frac{1}{\mu_D}\right) \tag{3.19}$$

where $q_H = 0.67 \cdot \frac{T_S}{T_1}$: hysteresis loop adjustment factor ($0.5 \le q_H \le 1.0$)

3.3.2 Higher modes

The damper forces of horizontal linear viscous dampers are calculated by the following relation:

$$F_D = C \cdot \nabla_{mD} \tag{3.20}$$

where C : vector of damping coefficients

∇_{mD} : vector of storey velocities

and

$$\nabla_{mD} = 2\pi \frac{\Delta_{mD}}{T_m} \tag{3.21}$$

$$\Delta_{mD} = \delta_{i,mD} - \delta_{i-1,mD} \tag{3.22}$$

$$\delta_{i,mD} = D_{mD} \cdot \phi_{i,m} \tag{3.23}$$

where Δ_{mD} : vector of storey drifts

$\delta_{i,mD}$: modal floor deflection of floor *i*

D_{mD} : roof displacement due to the design earthquake

$\phi_{i,m}$: modal displacement of floor *i*, normalised to unity at the roof level

T_m : period of m^{th} mode of vibration

The roof displacement D_{mD} is given by:

$$D_{mD} = \frac{g}{4\pi^2} \cdot \Gamma_m \cdot \frac{S_{D1} \cdot T_m}{B_{mD}} \leq \frac{g}{4\pi^2} \cdot \Gamma_m \cdot \frac{S_{DS} \cdot T_m^2}{B_{mD}} \qquad \text{for } T_m < T_D \quad (3.24)$$

$$D_{mD} = \frac{g}{4\pi^2} \cdot \Gamma_m \cdot \frac{S_{D1}}{B_{mD}} \leq \frac{g}{4\pi^2} \cdot \Gamma_m \cdot \frac{S_{DS} \cdot T_m^2}{B_{mD}} \qquad \text{for } T_m \geq T_D \quad (3.25)$$

with

$$\Gamma_m = \frac{\sum_{i=1}^{n} m_i \cdot \phi_{i,m}}{\sum_{i=1}^{n} m_i \cdot \phi_{i,m}^2} \quad (3.26)$$

where m_i : seismic mass of floor i

Γ_m : modal participation factor

B_{mD} : damping reduction factor given in Table 3.1 for effective damping ratio equal to β_{mD}

The effective damping ratio of β_{mD} is given by the following expression:

$$\beta_{mD} = \beta_I + \beta_{Vm} \quad (3.27)$$

where β_I : inherent damping ratio of the building

β_{Vm} : viscous damping ratio of the mth mode of vibration due to viscous dampers

For horizontal linear viscous dampers, the viscous damping ratio due to viscous dampers β_{Vm} is estimated by the following relation:

$$\beta_{Vm} = \frac{T_m}{4\pi} \frac{\sum_{i=1}^{n} C_i \cdot (\phi_{i,m} - \phi_{i-1,m})^2}{\sum_{i=1}^{n} m_i \cdot \phi_{i,m}^2} \quad (3.28)$$

For the case of damper forces under the MCE, the procedure remains the same but the ground acceleration α_g of the elastic spectrum must be multiplied by 1.5. Note that the effective ductility under the MCE is different than that under the DBE.

3.4 Summary

In this chapter, a seismic design procedure for steel MRFs with viscous dampers was developed within the framework of Eurocode 8. A conservative design rule was proposed for the capacity design of the columns in the force path of viscous dampers. More specifically, the column axial force used to perform the capacity design is the envelope of the axial force from the peak drift state and the axial force from the peak velocity state. For the calculation of the damper forces which are needed for the proposed procedure, the response spectrum procedure of ASCE 7-10 was adopted and appropriate relations were derived to correlate the response spectrums of ASCE 7-10 and EC8.

CHAPTER 4

PROPOSED CAPACITY DESIGN RULE

4.1 Introduction

In order to explore whether more conservative capacity design rules are needed for columns in the force path of viscous dampers that will guarantee plastic mechanisms similar to those of steel MRFs without dampers, prototype buildings of 5, 10 and 20 storeys are designed according to EC8 using steel MRFs with and without viscous dampers. The viscous dampers are selected to provide ξ_{eq} equal to 17%. The inherent damping ratio is 3%, and therefore, the MRFs with viscous dampers have total viscous damping ratio, ξ_{tot}, at T_1 equal to 20%. The global plastic mechanisms of the MRFs with and without viscous dampers are compared. A comparison of the predicted damper forces and the damper forces from analysis is also provided.

4.2 Design of 5-storey steel MRF without dampers

Figure 4.1 shows the plan view of a prototype steel office building with storey height of 4 m for the first storey and 3.2 m for the other storeys. The study focuses on one of the perimeter 3-bay MRFs in the longitudinal direction. This frame is designed as a steel MRF according to Eurocode 3 (EC3) and EC8 against the load combinations of $1.35G + 1.5Q$ and $G + \psi_2 Q + E$ where G are the dead loads (Table 4.1), ψ_2 factor equal to 0.3 for offices, Q are the live loads (Table 4.1) and E are the seismic actions. SAP2000 is employed to perform the design. The centerline model used for the design assumes rigid full-strength beam-column and column base connections along with a diaphragm horizontal constraint for the nodes of each floor to account for the in-plane rigidity of the composite slab. The P-Δ effects of the gravity loads acting in the tributary area (i.e. half of the total plan area for one perimeter steel MRF) are simulated with the aid of a leaning column with cross-sectional properties (i.e. area, moment of inertia) equal to the sum of the cross-sectional properties of the gravity

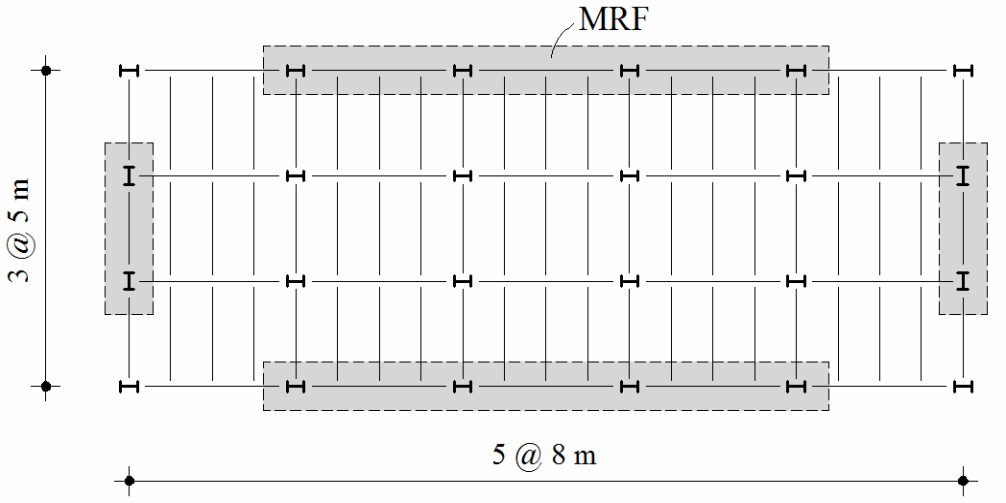

Figure 4.1 Plan view of the prototype building

Table 4.1 Loads

Dead loads (G)	kN/m^2
Selfweight	-
Composite slab (10cm)	2.5
Covering	1.2
Partitions	0.5
Girders	0.3
Mechanical/electrical equipment	0.5
Façade	2.1*
Live loads (Q)	3.0

* Vertical plane

Table 4.2 Cross-sections of gravity columns

Storey	Cross-section of gravity columns (or equivalent to W24)		
	5-storey	10-storey	20-storey
20			HEB220
19			
18			
17			
16			
15			HEB280
14			
13			
12			HEB360
11			
10		HEB220	
9			HEB450
8			
7			
6		HEB280	HEB600
5	HEB220		
4			
3		HEB360	HEB800
2	HEB240		
1			

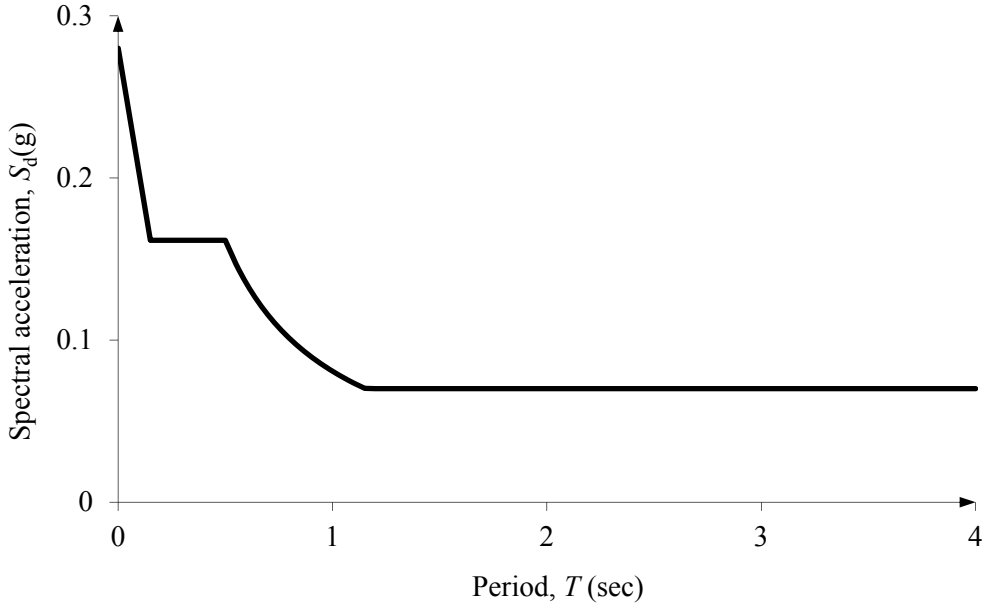

Figure 4.2 Design spectrum

columns (Table 4.2).

A high-ductility class is adopted in the design of the steel MRF according to EC8. The DBE is expressed by the EC8 design spectrum for peak ground acceleration α_g equal to 0.35g (covers regions with the highest seismicity), behaviour factor q equal to 6.5, importance factor II (γ_I=1.0) and soil type B (S=1.2, T_B=0.15, T_C=0.5, T_D=2.0) (Figure 4.2), with these assumptions to be very commonly used. The design spectrum is for 5% damping while the building is assumed to have 3% damping, therefore the appropriate damping factor (B) from Table 3.1 is applied for the conversion. S355 and S275 steel grades are assumed for the columns and beams, respectively.

Figure 4.3 shows the elevation views along with the cross-sections of the beams and columns of the final design of the 5-storey, 10-storey and 20-storey steel MRFs. Table 4.3 lists the steel weight, the fundamental period of vibration (T_1), the IDR_{DBE} and the coefficients θ. The design steps, as described in Appendix A, with sample calculations are provided in Appendix B.

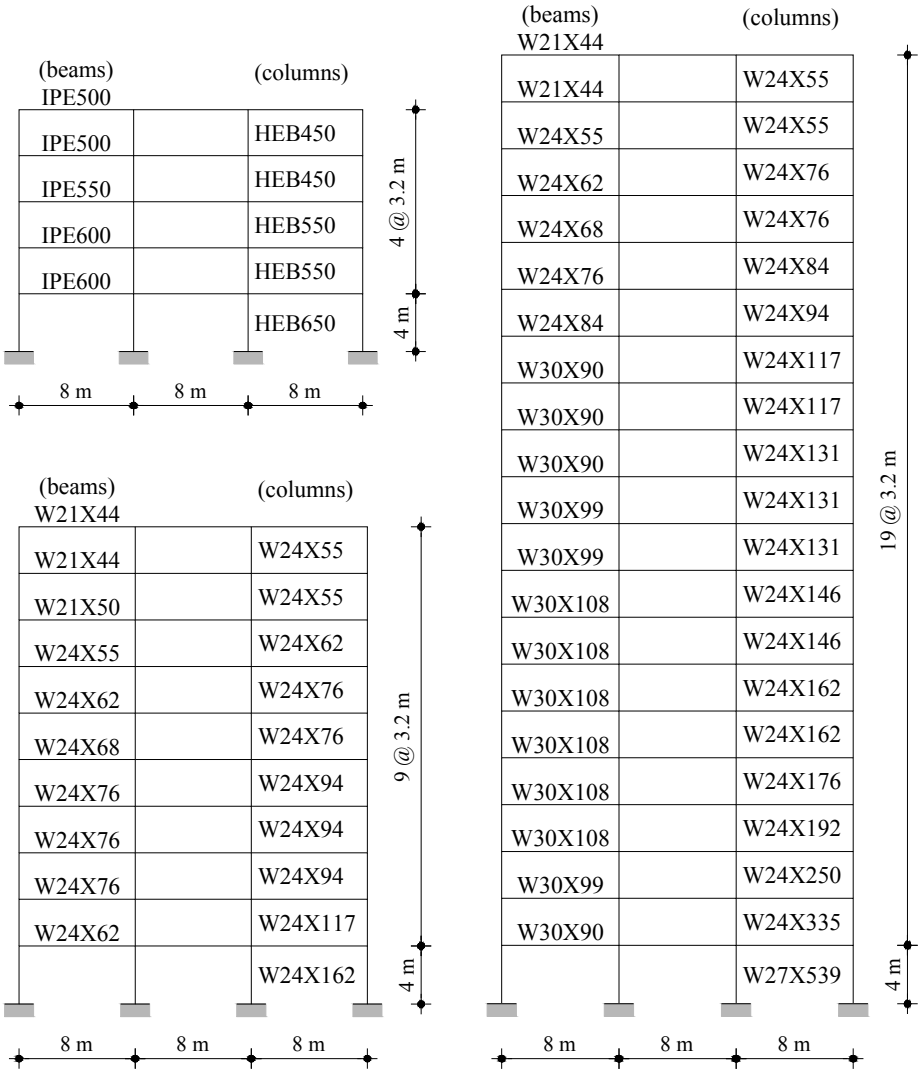

Figure 4.3 Elevation view and beam/column cross-sections of the steel MRFs

Table 4.3 Design details of the steel MRFs

Frame	Steel weight (kN)	θ	T_1 (sec)	ξ_{tot} (%)	IDR_{DBE} (%)
5-storey	254	0.091	1.28		1.79
10-storey	389	0.209	2.68	3	1.57
20-storey	1228	0.134	3.87		0.89

4.3 Design of 5-storey steel MRF with viscous dampers

In the middle bay of the steel MRFs designed in Section 4.2, are installed linear (a=1; see Equation (1.1)) viscous dampers. Inverted V braces support the dampers in a horizontal orientation as shown in Figure 4.5. Steps 1-6 described in Section 3.2 are skipped since the viscous dampers are installed in an existing MRF.

Step 7

For a level of equivalent viscous damping ratio at the fundamental period of vibration provided by the viscous dampers equal to 17%, the damping coefficients of the viscous dampers are calculated by solving Equation (3.1) with respect to C_i. Such level of viscous damping is selected because a considerable peak drift reduction can be achieved and under any level lower than this, viscous dampers will add smaller axial forces into the attached columns (more favourable case). Previous research has shown that distribution of damping coefficients proportional to the horizontal storey stiffness of the steel MRF is effective and practical in comparison with distributions derived from advanced optimization methods (Whittle et al. 2012) and this distribution is adopted in this study.

Thus,

$$C_i = \varepsilon \cdot K_i \tag{4.1}$$

where ε : invariant

K_i : horizontal storey stiffness

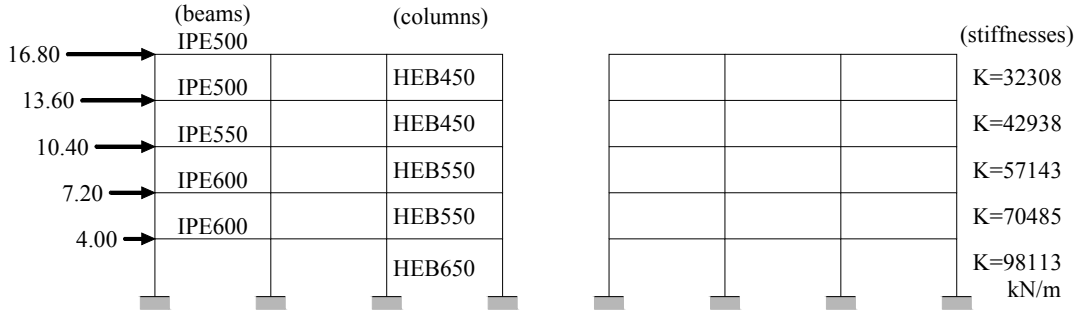

Figure 4.4 Storey stiffnesses

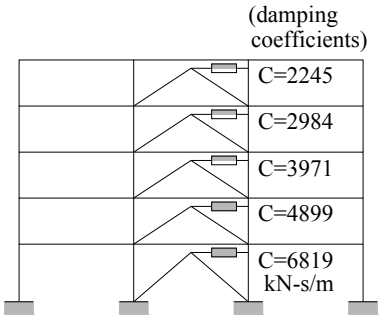

Figure 4.5 Damping coefficients of viscous dampers

The horizontal storey stiffnesses K_i are determined under the horizontal forces shown in Figure 4.4 which are proportional to height. Figure 4.4 also provides the horizontal storey stiffness of each storey. Substituting Equation (4.1) into Equation (3.1) with the horizontal storey stiffnesses given in Figure 4.4 and solving with respect to invariant ε for ξ_{eq} equal to 17%, the invariant ε results in equal to 0.0695. The damping coefficients of viscous dampers are shown in Figure 4.5. The inherent damping ratio is 3%, and therefore, the steel MRF with viscous dampers has a total viscous damping ratio, ξ_{tot}, at T_1 equal to 20%.

Step 8

For the calculation of damper forces under the DBE, the response spectrum procedure in Section 18.4 of ASCE 7-10 will be followed, considering only the lateral mode shapes. The response spectrum for 5% damping of ASCE 7-10 correlated with EC8 can be calculated from Equations (3.4) - (3.6) and it is shown in Figure 4.6.

From Equations (3.4) - (3.6),

$$S_{DS} = 2.5 \cdot \frac{a_g}{g} \cdot S = 2.5 \cdot \frac{0.35g}{g} \cdot 1.2 = 1.05 \qquad \text{for } 0.1 \le T < 0.5 \,\text{sec}$$

$$S_{D1} = 2.5 \cdot \frac{a_g}{g} \cdot S \cdot T_C = 2.5 \cdot \frac{0.35g}{g} \cdot 1.2 \cdot 0.5 = 0.525 \qquad \text{for } 0.5 \le T < 2.0 \,\text{sec}$$

$$S_{D1} = 2.5 \cdot \frac{a_g}{g} \cdot S \cdot T_C \cdot T_D = 2.5 \cdot \frac{0.35g}{g} \cdot 1.2 \cdot 0.5 \cdot 2.0 = 1.05 \qquad \text{for } 2.0 \le T \le 4.0 \,\text{sec}$$

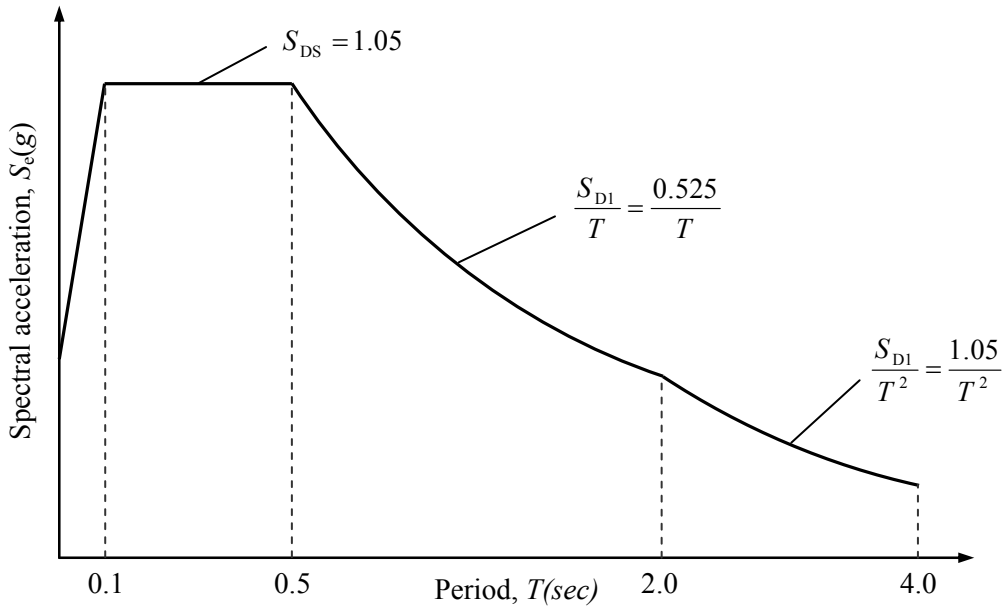

Figure 4.6 Response spectrum for 5% damping of ASCE 7-10 correlated with EC8

Fundamental mode

The damper forces of horizontal linear viscous dampers are calculated as described in Section 0. From FEMA 450 procedure yields:

$$\delta_T = 0.151\,\text{m}$$

$$\delta_y = 0.112\,\text{m}$$

Hence,

$$\mu_D = 1.343$$

and with $T_1 = 1.284$ sec

$$\Rightarrow T_{1D} = T_1\sqrt{\mu_D} = 1.284\sqrt{1.343} = 1.488\,\text{sec}$$

The masses m_i and the modal displacements ϕ_i are given in Table 4.4 and the modal participation factor Γ_1 is:

$$\Gamma_1 = \frac{\sum_{i=1}^{n} m_i \cdot \phi_{i,1}}{\sum_{i=1}^{n} m_i \cdot \phi_{i,1}^2} = \frac{669.09}{499.99} = 1.338$$

For horizontal linear viscous dampers, the viscous damping ratio due to viscous dampers β_{V1} is given by Equation (3.18):

$$\beta_{V1} = \frac{T_1}{4\pi} \frac{\sum_{i=1}^{n} C_i \cdot (\phi_{i,1} - \phi_{i-1,1})^2}{\sum_{i=1}^{n} m_i \cdot \phi_{i,1}^2} = \frac{1.284}{4\pi} \cdot \frac{832}{499.99} = 17\,\%$$

The hysteresis loop adjustment factor is calculated from the following expression:

$$q_H = 0.67 \cdot \frac{T_S}{T_1} = 0.67 \cdot \frac{0.5}{1.284} = 0.261 < 0.5 \qquad \text{with } 0.5 \le q_H \le 1.0$$

$$\Rightarrow q_H = 0.5$$

Then the hysteretic damping ratio β_{HD}, the effective damping ratios of β_{1D} and β_{1E} are calculated:

$$\text{Eq. (3.19)} \Rightarrow \beta_{HD} = q_H (0.64 - \beta_I) \cdot \left(1 - \frac{1}{\mu_D}\right) = 0.5 \cdot (0.64 - 0.03) \cdot \left(1 - \frac{1}{1.343}\right) = 7.8\,\%$$

$$\text{Eq. (3.16)} \Rightarrow \beta_{1D} = \beta_I + \beta_{V1}\sqrt{\mu_D} + \beta_{HD} = 3\,\% + 17\,\%\sqrt{1.343} + 7.8\,\% = 30.5\,\%$$

$$\text{Eq. (3.17)} \Rightarrow \beta_{1E} = \beta_I + \beta_{V1} = 3\,\% + 17\,\% = 20\,\%$$

The damping reduction factors B_{1D} and B_{1E} are obtained from Table 3.1 for effective damping ratios equal to β_{1D} and β_{1E} respectively, and the roof displacement D_{1D} can be calculated from Equation (3.13):

$$D_{1D} = \frac{g}{4\pi^2} \cdot \Gamma_1 \cdot \frac{S_{D1} \cdot T_{1D}}{B_{1D}} = \frac{g}{4\pi^2} \cdot 1.338 \cdot \frac{0.525 \cdot 1.488}{1.815} = 0.143 \qquad \text{for } 0.5 \le T_{1D} < 2\,\text{sec}$$

$$\geq \frac{g}{4\pi^2} \cdot \Gamma_1 \cdot \frac{S_{D1} \cdot T_1}{B_{1E}} = \frac{g}{4\pi^2} \cdot 1.338 \cdot \frac{0.525 \cdot 1.284}{1.50} = 0.149$$

$$\Rightarrow D_{1D} = 0.149 \text{ m}$$

The modal floor deflections δ_i, the storey drifts Δ_{1D}, the storey velocities ∇_{1D} and the damper forces F_D are calculated from Equations (3.7) - (3.10) and are listed in Table 4.4.

The damper forces are imposed on the braces that support the viscous dampers and horizontal restraint forces at each floor are applied such that the horizontal displacement at each level of the structure is zero (Figure 4.8). The resulting axial forces in the interior columns due to damper forces and horizontal restraint forces are shown in Figure 4.9.

Higher mode (m=2)

The damper forces of horizontal linear viscous dampers are calculated as described in Section 3.3.2. The period of the 2nd mode T_2 is equal to 0.426 sec, the masses m_i and the modal displacements ϕ_i are given in Table 4.5 and the modal participation factor Γ_2 is:

$$\Gamma_2 = \frac{\sum_{i=1}^{n} m_i \cdot \phi_{i,2}}{\sum_{i=1}^{n} m_i \cdot \phi_{i,2}^2} = \frac{317.80}{668.12} = 0.476$$

For horizontal linear viscous dampers, the viscous damping ratio due to viscous dampers β_{Vm} is given by Equation (3.28):

$$\beta_{V2} = \frac{T_2}{4\pi} \frac{\sum_{i=1}^{n} C_i \cdot (\phi_{i,2} - \phi_{i-1,2})^2}{\sum_{i=1}^{n} m_i \cdot \phi_{i,2}^2} = \frac{0.426}{4\pi} \cdot \frac{7411.82}{668.12} = 37.6\,\%$$

Then the effective damping ratios of β_{2D} is calculated:

$$\text{Eq. (3.27)} \Rightarrow \beta_{2D} = \beta_I + \beta_{V2} = 3\,\% + 37.6\,\% = 40.6\,\%$$

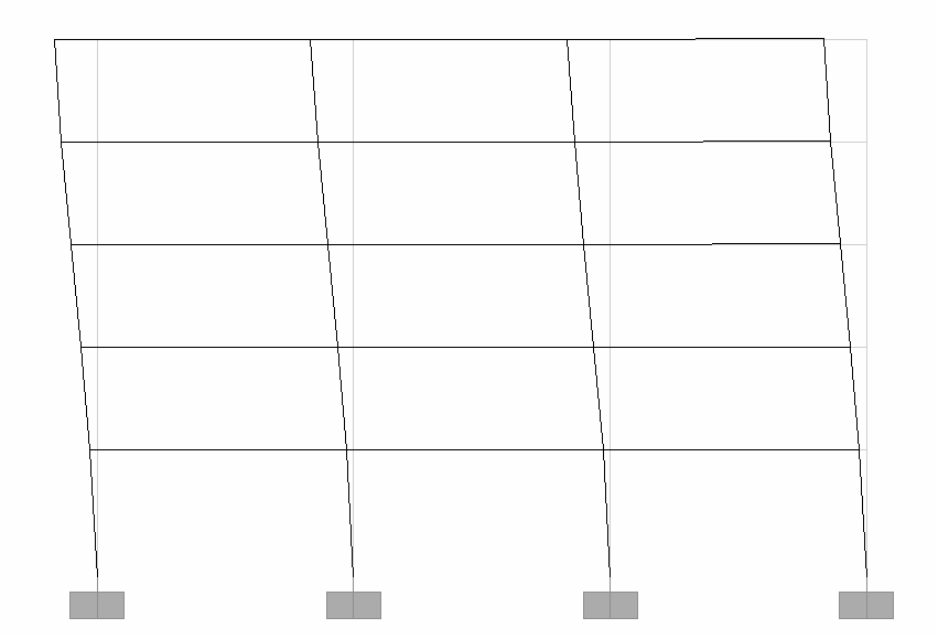

Figure 4.7 1st mode shape

Table 4.4 Response spectrum calculations of damper forces - DBE (1st mode)

Storey	ϕ_i	m_i (t)	$m_i \cdot \phi_i$	$m_i \cdot \phi_i^2$	K_i $\left(\frac{kN}{m}\right)$	C_i $\left(kN\frac{sec}{m}\right)$	δ_i (m)	Δ_{1D} (m)	∇_{1D} $\left(\frac{m}{sec}\right)$	F_D (kN)
5	1.000	222.44	222.44	222.44	32307.7	2245.4	0.149	0.025	0.105	234.8
4	0.834	224.45	187.14	156.04	42937.9	2984.2	0.124	0.034	0.143	426.0
3	0.607	224.97	136.53	82.86	57142.9	3971.4	0.090	0.034	0.143	568.1
2	0.380	225.70	85.66	32.51	70484.6	4898.7	0.057	0.032	0.135	662.2
1	0.165	226.64	37.32	6.15	98113.2	6818.9	0.025	0.025	0.104	706.4
Sum		1124.2	669.09	499.99						

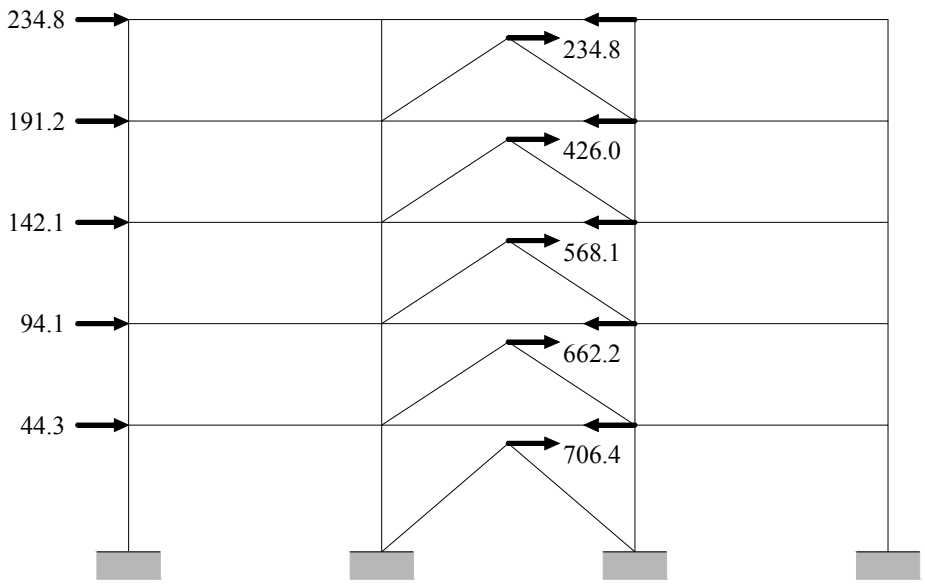

Figure 4.8 Dampers forces and horizontal restraint forces (kN) (1st mode)

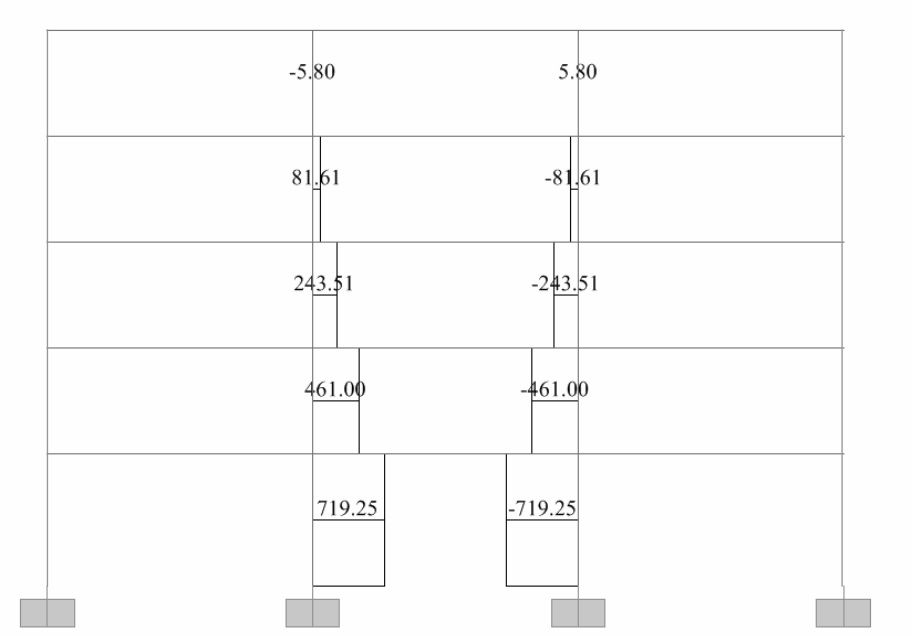

Figure 4.9 Axial forces (kN) in interior columns due to damper forces and horizontal restraint forces (1st mode)

The damping reduction factor B_{2D} is obtained from Table 3.1 for effective damping ratio equal to β_{2D}, and the roof displacement D_{2D} can be calculated from Equation (3.24):

$$D_{2D} = \frac{g}{4\pi^2} \cdot \Gamma_2 \cdot \frac{S_{D1} \cdot T_2}{B_{2D}} = \frac{g}{4\pi^2} \cdot 0.476 \cdot \frac{0.525 \cdot 0.426}{2.118} = 0.0125 \qquad \text{for } T_2 < 2\,\text{sec}$$

$$\leq \frac{g}{4\pi^2} \cdot \Gamma_2 \cdot \frac{S_{DS} \cdot T_2^2}{B_{2D}} = \frac{g}{4\pi^2} \cdot 0.476 \cdot \frac{1.05 \cdot 0.426^2}{2.118} = 0.0106$$

$$\Rightarrow D_{2D} = 0.0106\,\text{m}$$

The modal floor deflections δ_i, the storey drifts Δ_{mD}, the storey velocities ∇_{mD} and the damper forces F_D are calculated from Equations (3.20) - (3.23) and are listed in Table 4.5.

The damper forces are imposed on the braces that support the viscous dampers and horizontal restraint forces at each floor are applied such that the horizontal displacement at each level of the structure is zero (Figure 4.11). The resulting axial forces in the interior columns due to damper forces and horizontal restraint forces are shown in Figure 4.12.

Higher mode (m=3)

The damper forces of horizontal linear viscous dampers are calculated as described in Section 3.3.2. The period of the 3rd mode T_3 is equal to 0.214 sec, the masses m_i and the modal displacements ϕ_i are given in Table 4.6 and the modal participation factor Γ_3 is:

$$\Gamma_3 = \frac{\sum_{i=1}^{n} m_i \cdot \phi_{i,3}}{\sum_{i=1}^{n} m_i \cdot \phi_{i,3}^2} = \frac{261.50}{1351.96} = 0.193$$

For horizontal linear viscous dampers, the viscous damping ratio due to viscous dampers β_{Vm} is given by Equation (3.28):

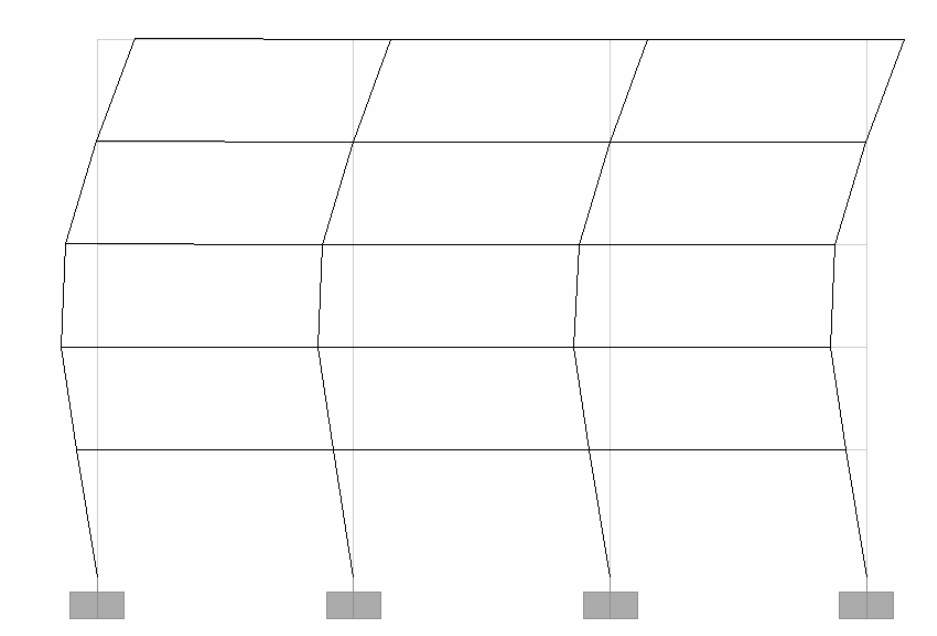

Figure 4.10 2nd mode shape

Table 4.5 Response spectrum calculations of damper forces - DBE (2nd mode)

Storey	ϕ_i	m_i (t)	$m_i \cdot \phi_i$	$m_i \cdot \phi_i^2$	δ_i (m)	Δ_{mD} (m)	∇_{mD} $\left(\frac{m}{sec}\right)$	F_D (kN)
5	1.000	222.44	222.44	222.44	0.0106	0.0108	0.159	369.9
4	-0.016	224.45	-3.48	0.05	-0.0002	0.0088	0.129	400.9
3	-0.843	224.97	-189.76	160.06	-0.0089	0.0014	0.020	84.4
2	-0.975	225.70	-219.95	214.35	-0.0103	-0.0044	-0.065	-329.0
1	-0.561	226.64	-127.05	71.22	-0.0059	-0.0059	-0.088	-620.2
Sum		1124.20	-317.80	668.12				

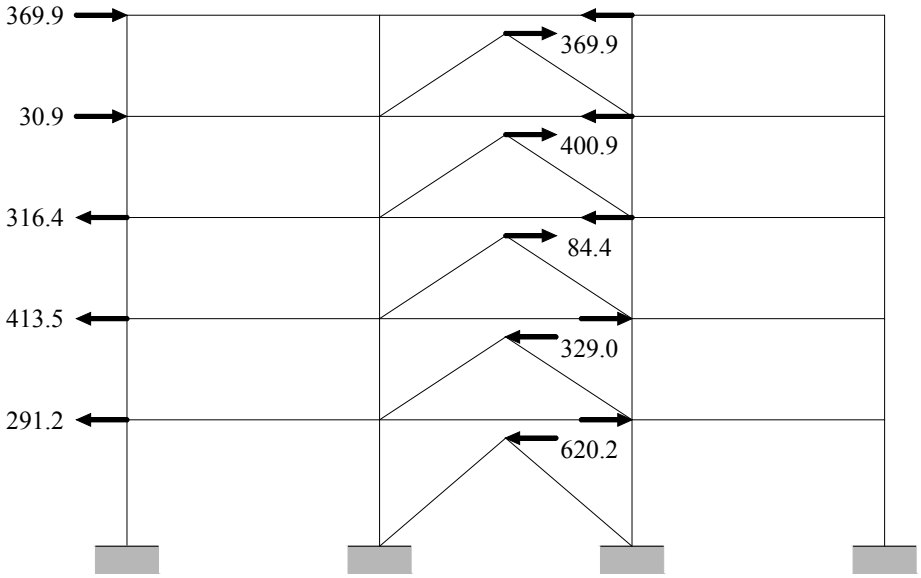

Figure 4.11 Dampers forces and horizontal restraint forces (kN) (2^{nd} mode)

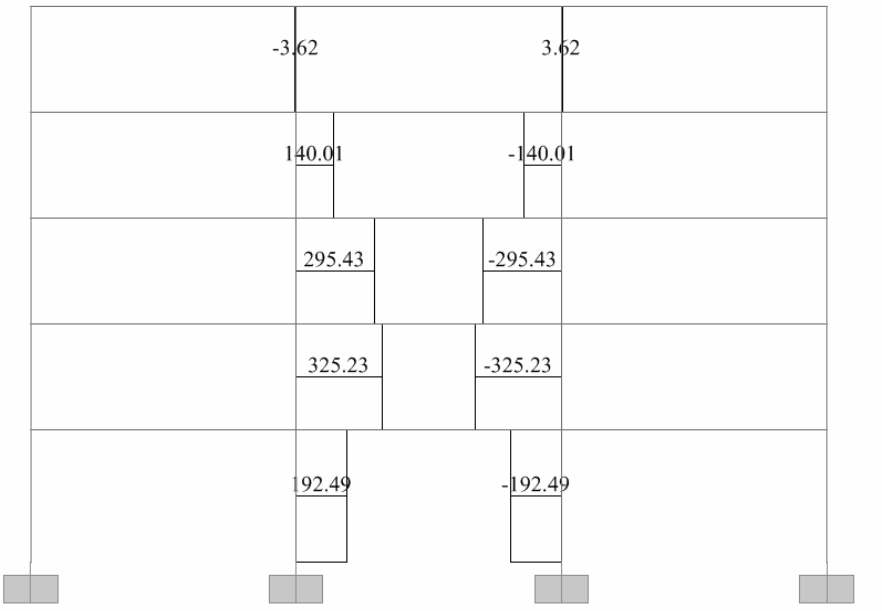

Figure 4.12 Axial forces (kN) in interior columns due to damper forces and horizontal restraint forces (2^{nd} mode)

$$\beta_{V3} = \frac{T_3}{4\pi} \frac{\sum_{i=1}^{n} C_i \cdot (\phi_{i,3} - \phi_{i-1,3})^2}{\sum_{i=1}^{n} m_i \cdot \phi_{i,3}^2} = \frac{0.214}{4\pi} \cdot \frac{37332.19}{1351.96} = 47.0\,\%$$

Then the effective damping ratios of β_{3D} is calculated:

$$\text{Eq. (3.27)} \Rightarrow \beta_{3D} = \beta_I + \beta_{V3} = 3\,\% + 47\,\% = 50\,\%$$

The damping reduction factor B_{3D} is obtained from Table 3.1 for effective damping ratio equal to β_{3D}, and the roof displacement D_{3D} can be calculated from Equation (3.24):

$$D_{3D} = \frac{g}{4\pi^2} \cdot \Gamma_3 \cdot \frac{S_{D1} \cdot T_3}{B_{3D}} = \frac{g}{4\pi^2} \cdot 0.193 \cdot \frac{0.525 \cdot 0.214}{2.40} = 0.0022 \qquad \text{for } T_3 < 2\,\text{sec}$$

$$\leq \frac{g}{4\pi^2} \cdot \Gamma_3 \cdot \frac{S_{DS} \cdot T_3^2}{B_{3D}} = \frac{g}{4\pi^2} \cdot 0.193 \cdot \frac{1.05 \cdot 0.214^2}{2.40} = 0.001$$

$$\Rightarrow D_{3D} = 0.001\,\text{m}$$

The modal floor deflections δ_i, the storey drifts Δ_{mD}, the storey velocities ∇_{mD} and the damper forces F_D are calculated from Equations (3.20) - (3.23) and are listed in Table 4.6.

The damper forces are imposed on the braces that support the viscous dampers and horizontal restraint forces at each floor are applied such that the horizontal displacement at each level of the structure is zero (Figure 4.14). The resulting axial forces in the interior columns due to damper forces and horizontal restraint forces are shown in Figure 4.15.

Higher mode (m=4)

The damper forces of horizontal linear viscous dampers are calculated as described in Section 3.3.2. The period of the 4th mode T_4 is equal to 0.135 sec, the masses m_i and the modal displacements ϕ_i are given in Table 4.7 and the modal participation factor Γ_4 is:

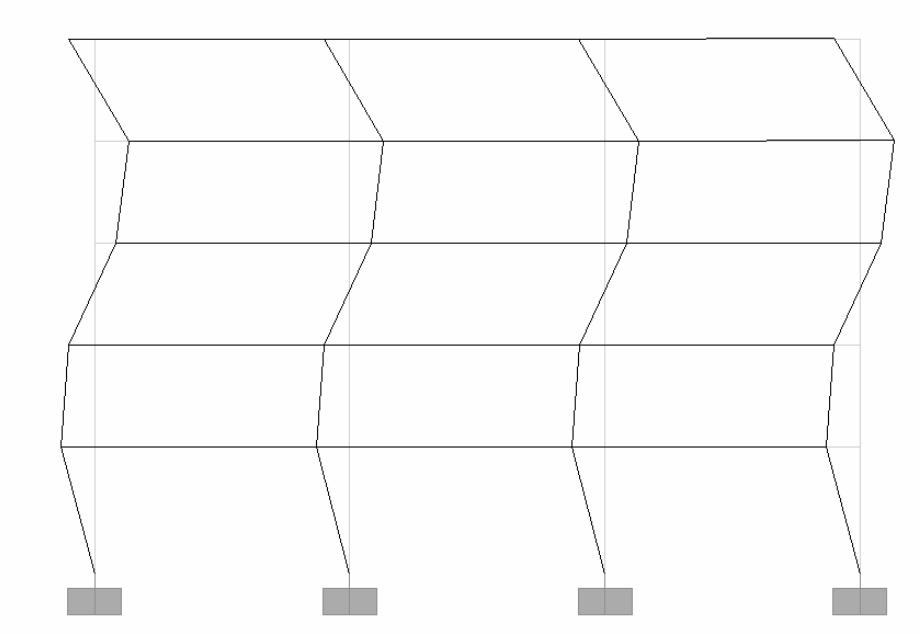

Figure 4.13 3rd mode shape

Table 4.6 Response spectrum calculations of damper forces - DBE (3rd mode)

Storey	ϕ_i	m_i (t)	$m_i \cdot \phi_i$	$m_i \cdot \phi_i^2$	δ_i (m)	Δ_{mD} (m)	∇_{mD} $\left(\frac{m}{sec}\right)$	F_D (kN)
5	1.000	222.44	222.44	222.44	0.0010	0.0023	0.068	151.9
4	-1.304	224.45	-292.64	381.56	-0.0013	-0.0005	-0.014	-42.6
3	-0.818	224.97	-184.06	150.58	-0.0008	-0.0018	-0.053	-211.6
2	0.997	225.70	224.91	224.13	0.0010	-0.0003	-0.008	-41.3
1	1.283	226.64	290.85	373.25	0.0013	0.0013	0.038	256.9
Sum		1124.2	261.50	1351.96				

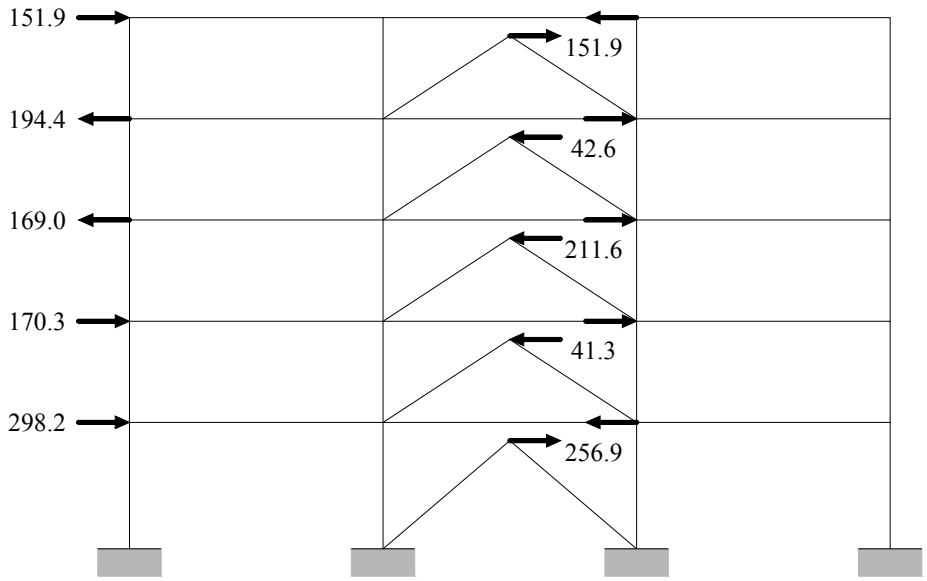

Figure 4.14 Dampers forces and horizontal restraint forces (kN) (3rd mode)

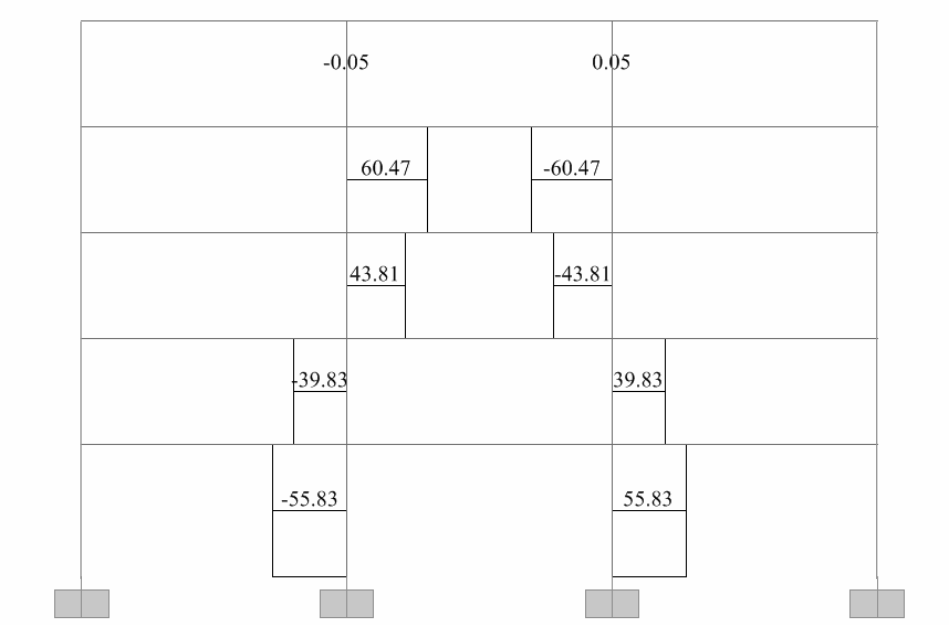

Figure 4.15 Axial forces (kN) in interior columns due to damper forces and horizontal restraint forces (3rd mode)

$$\Gamma_4 = \frac{\sum_{i=1}^{n} m_i \cdot \phi_{i,4}}{\sum_{i=1}^{n} m_i \cdot \phi_{i,4}^2} = \frac{289.22}{4219.01} = 0.069$$

For horizontal linear viscous dampers, the viscous damping ratio due to viscous dampers β_{Vm} is given by Equation (3.28):

$$\beta_{V4} = \frac{T_4}{4\pi} \frac{\sum_{i=1}^{n} C_i \cdot (\phi_{i,4} - \phi_{i-1,4})^2}{\sum_{i=1}^{n} m_i \cdot \phi_{i,4}^2} = \frac{0.135}{4\pi} \cdot \frac{194544.29}{4219.01} = 49.5\,\%$$

Then the effective damping ratios of β_{2D} is calculated:

$$\text{Eq. (3.27)} \Rightarrow \beta_{4D} = \beta_I + \beta_{V4} = 3\,\% + 49.5\,\% = 52.5\,\%$$

The damping reduction factor B_{4D} is obtained from Table 3.1 for effective damping ratio equal to β_{4D}, and the roof displacement D_{4D} can be calculated from Equation (3.24):

$$D_{4D} = \frac{g}{4\pi^2} \cdot \Gamma_4 \cdot \frac{S_{D1} \cdot T_4}{B_{4D}} = \frac{g}{4\pi^2} \cdot 0.069 \cdot \frac{0.525 \cdot 0.135}{2.476} = 0.0005 \qquad \text{for } T_4 < 2\,\text{sec}$$

$$\leq \frac{g}{4\pi^2} \cdot \Gamma_4 \cdot \frac{S_{DS} \cdot T_4^2}{B_{4D}} = \frac{g}{4\pi^2} \cdot 0.069 \cdot \frac{1.05 \cdot 0.135^2}{2.476} = 0.00013$$

$$\Rightarrow D_{4D} = 0.00013\,\text{m}$$

The modal floor deflections δ_i, the storey drifts Δ_{mD}, the storey velocities ∇_{mD} and the damper forces F_D are calculated from Equations (3.20) - (3.23) and are listed in Table 4.7.

The damper forces are imposed on the braces that support the viscous dampers and horizontal restraint forces at each floor are applied such that the horizontal displacement at each level of the structure is zero (Figure 4.17). The resulting axial forces in the interior columns due to damper forces and horizontal restraint forces are shown in Figure 4.18.

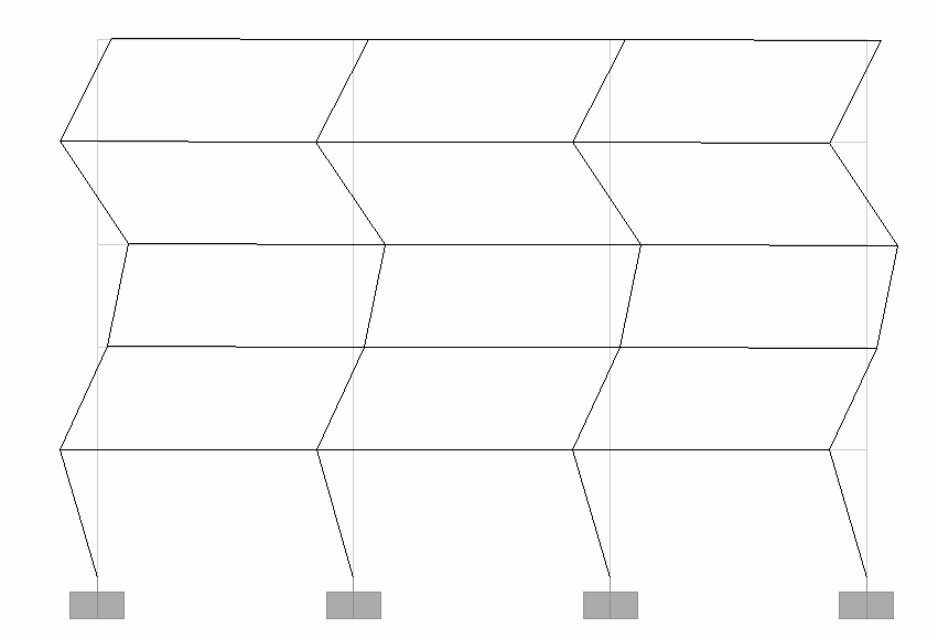

Figure 4.16 4th mode shape

Table 4.7 Response spectrum calculations of damper forces - DBE (4th mode)

Storey	ϕ_i	m_i (t)	$m_i \cdot \phi_i$	$m_i \cdot \phi_i^2$	δ_i (m)	Δ_{mD} (m)	∇_{mD} $\left(\frac{m}{sec}\right)$	F_D (kN)
5	1.000	222.44	222.44	222.44	0.00013	0.00046	0.021	48.1
4	-2.539	224.45	-569.98	1447.41	-0.00033	-0.00060	-0.028	-83.9
3	2.106	224.97	473.79	997.81	0.00027	0.00018	0.009	34.0
2	0.693	225.70	156.39	108.37	0.00009	0.00042	0.019	95.3
1	-2.523	226.64	-571.87	1442.98	-0.00033	-0.00033	-0.015	-104.1
Sum		1124.2	-289.22	4219.01				

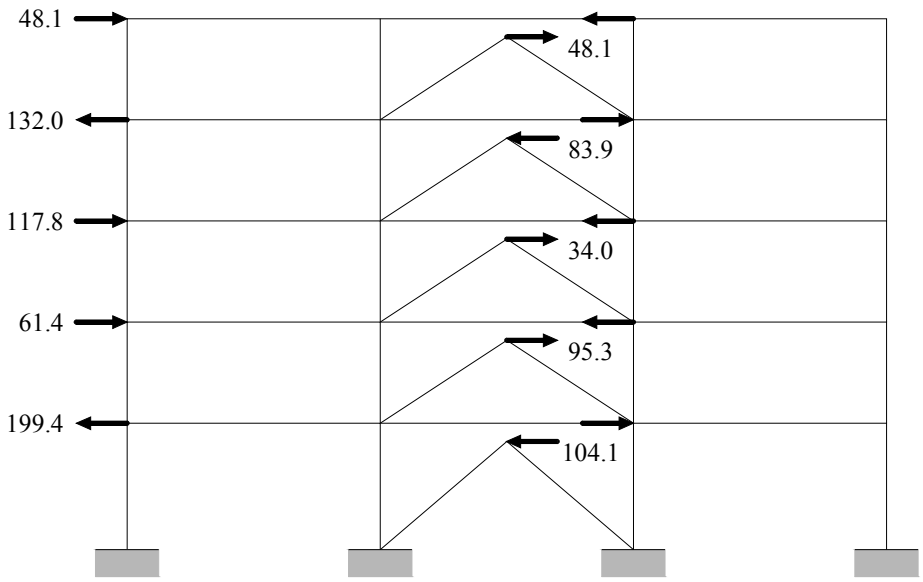

Figure 4.17 Dampers forces and horizontal restraint forces (kN) (4^{th} mode)

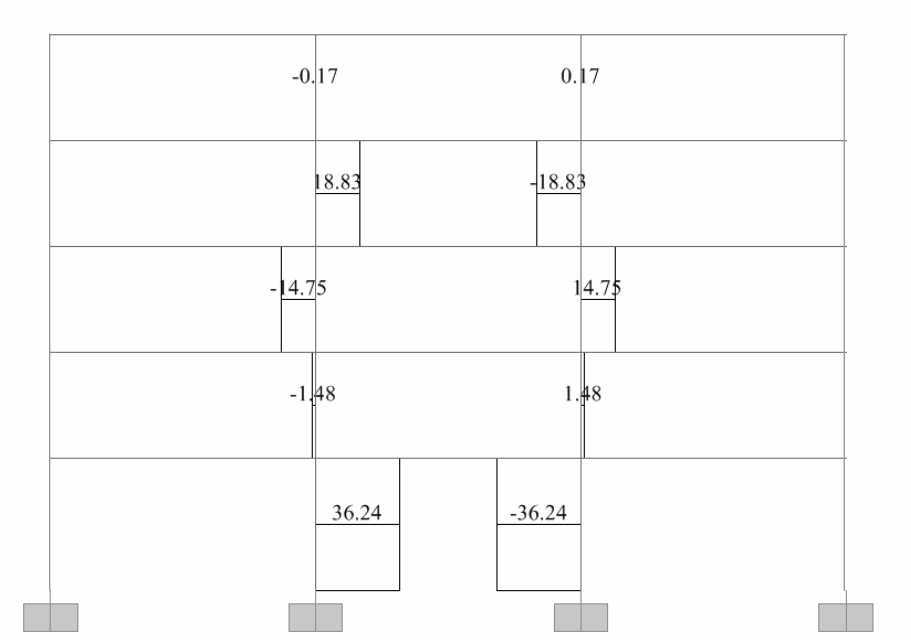

Figure 4.18 Axial forces (kN) in interior columns due to damper forces and horizontal restraint forces (4^{th} mode)

The supporting braces and the gusset plates, which are connected such as pin, are designed for the SRSS of the forces induced by each mode, combined with the gravity loads in the seismic design combination, i.e. $G + \psi_2 Q$, (peak velocity state) and such that satisfy the Equation (3.2). Given the damping coefficients, calculated in Step 7, the minimum required horizontal stiffness K_b of the bracing system for each storey can be calculated and it is shown in Figure 4.19.

The viscous dampers and their connections shall be designed to resist forces, displacements and velocities from the peak velocity state but under the MCE. This is not needed for this study, as the connections are not included in the modeling and the viscous dampers are modeled without considering limit states.

Step 9

For the columns in the force path of viscous dampers (i.e. interior columns), repeat Steps 4-6 with design axial force, as given in Step 4, modified by Equation (3.3).
The damper forces and the horizontal restraint forces of each vibration mode are combined through the SRSS rule (Figure 4.22). SF is taken equal to 1.0 and its value is re-examined in Section 4.7.

Sample calculation for the interior columns of floor 1 ($N_{Ed,G}$, $N_{Ed,E}$, $N_{Ed,E,V,SF}$ are given in Figure 4.20 - Figure 4.22):

$$N_{Ed} = N_{Ed,G} + 1.1 \cdot \gamma_{ov} \cdot \Omega \cdot \max\left(N_{Ed,E}, N_{Ed,E,V,SF=1}\right) =$$

$$= 954.60 + 1.1 \cdot 1.25 \cdot 1.019 \cdot \max\left(42.96, 747.54\right) = 2002 \text{ kN}$$

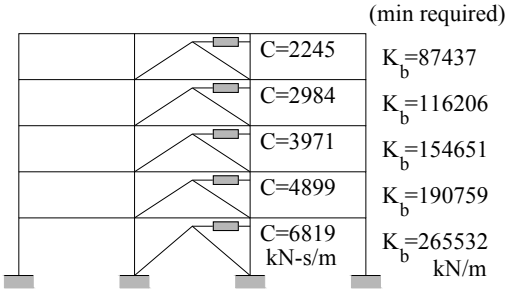

Figure 4.19 Required horizontal stiffness K_b of the bracing system

A similar expression to Equation (3.3) which will result in a slightly more conservative design, is the following:

$$N_{\mathrm{Ed}} = N_{\mathrm{Ed,G}} + 1.1 \cdot \gamma_{\mathrm{ov}} \cdot \Omega \cdot \max\left(N_{\mathrm{Ed,E}}, SF \cdot N_{\mathrm{Ed,E,V}}\right) \tag{4.2}$$

where $N_{\mathrm{Ed,E,V}}$ is the column axial force which is induced by the damper forces and the horizontal restraint forces at the peak velocity state (Step 8).

Figure 4.23 and Figure 4.24 show the elevation views along with the beam/column cross-sections and the damping coefficient of the viscous damper of the final design of the 5-storey, 10-storey and 20-storey steel MRFs with viscous dampers, while Table 4.8 lists the steel weight, the fundamental period of vibration (T_1), the IDR_{DBE} and the coefficients θ. The modified capacity design rule changed the cross-sections of the interior columns of storeys 1 to 8 of the 10-storey steel MRF and the cross-sections of the interior columns of storeys 5 to 18 of the 20-storey steel MRF as shown in Figure 4.23 and Figure 4.24, respectively. No changes were needed for the interior columns of the 5-storey steel MRF. It is also noted that the application of the modified capacity design rule increased the steel weight of the 10-storey steel MRF by 5% and the steel weight of the 20-storey steel MRF by 2%.

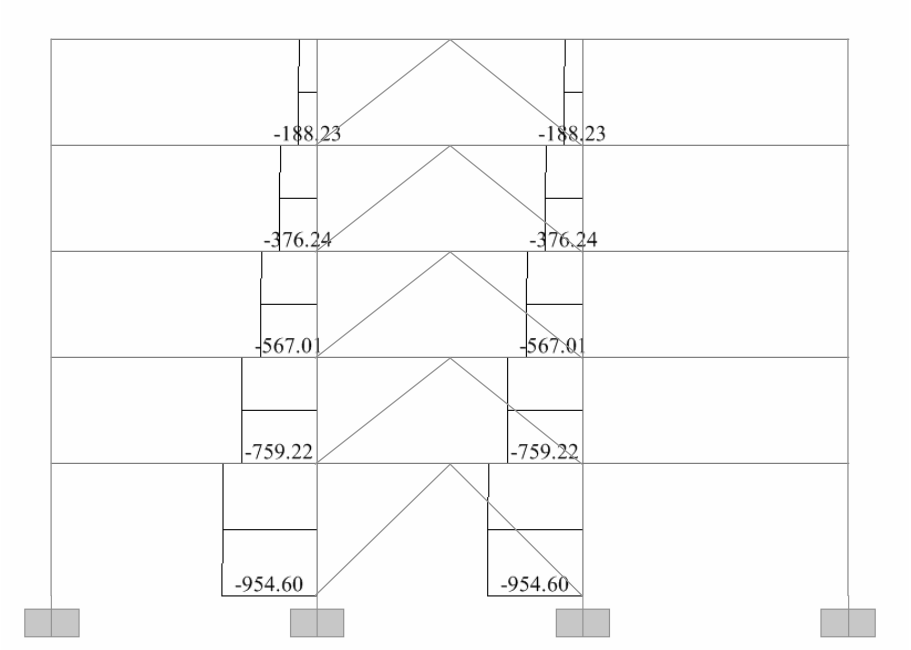

Figure 4.20 Axial forces (kN) in interior columns under the combination of $G + \psi_2 Q$

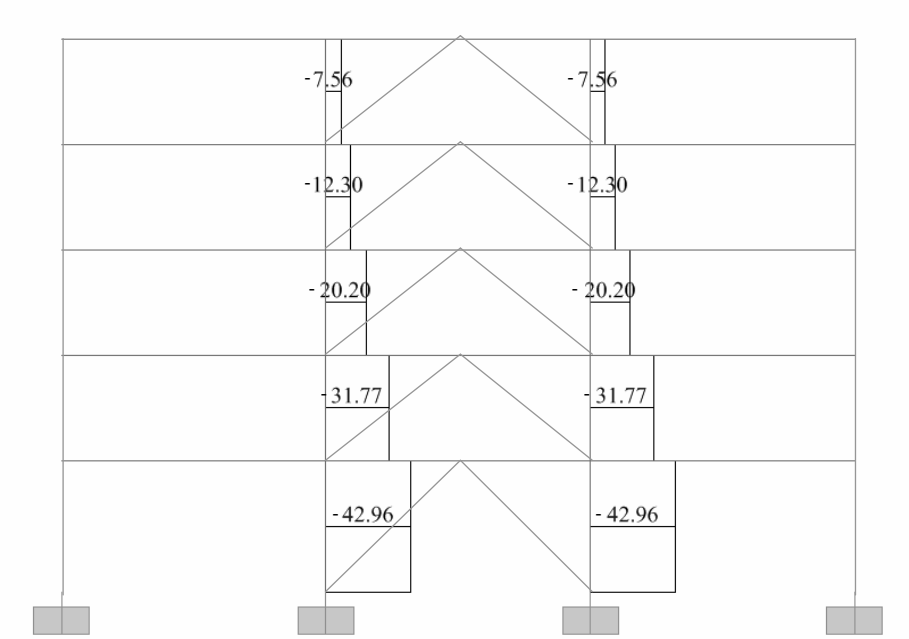

Figure 4.21 Axial forces (kN) in interior columns due to design seismic action

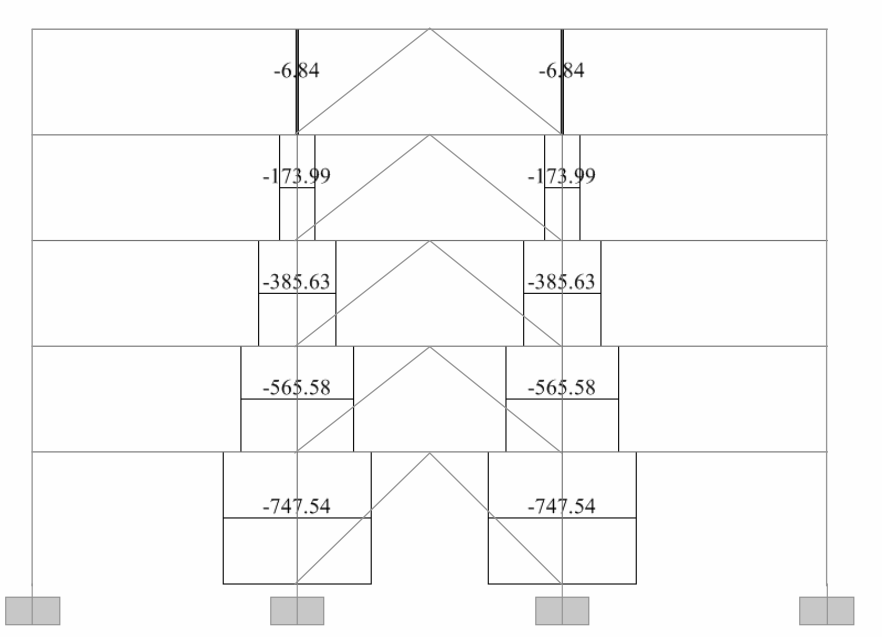

Figure 4.22 SRSS combination of axial forces (kN) in interior columns due to damper forces and horizontal restraint forces (Step 8)

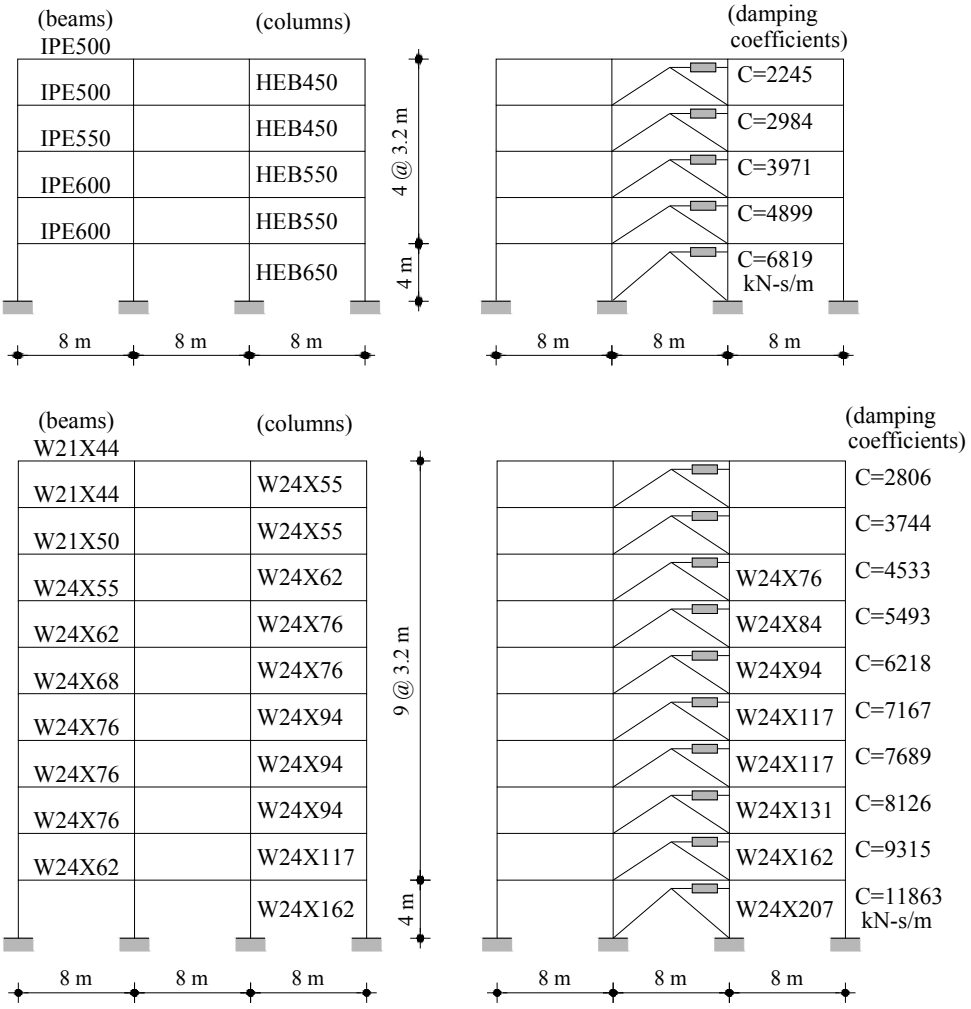

Figure 4.23 Elevation view and beam/column cross-sections of the 5-storey and the 10-storey steel MRFs with and without viscous dampers. The damping coefficients of the viscous dampers are also provided. The beam/column cross-sections of the MRFs with viscous dampers are the same with those of the corresponding MRFs without dampers apart from the indicated interior columns

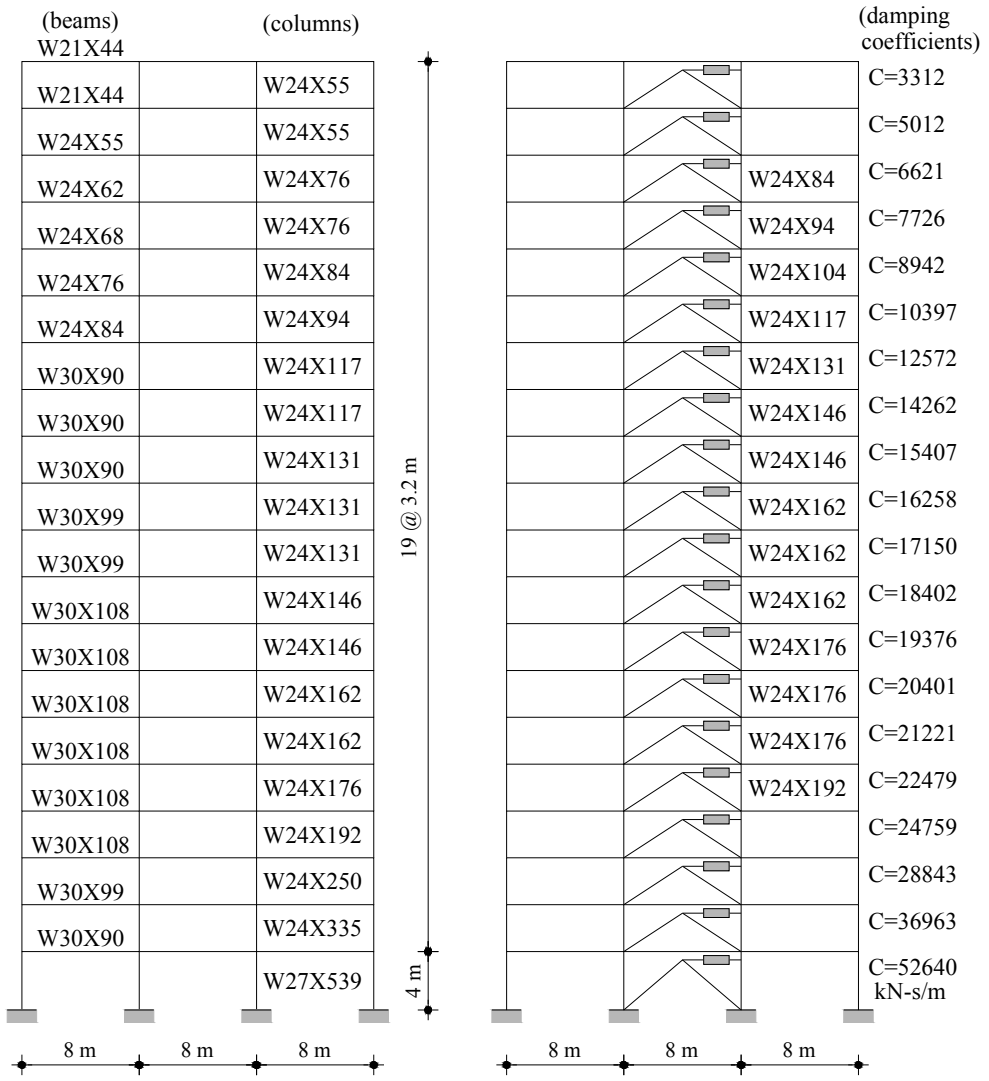

Figure 4.24 Elevation view and beam/column cross-sections of the 20-storey steel MRFs with and without viscous dampers. The damping coefficients of the viscous dampers are also provided. The beam/column cross-sections of the MRFs with viscous dampers are the same with those of the corresponding MRFs without dampers apart from the indicated interior columns

Table 4.8 Design details of the steel MRFs with viscous dampers

Frame	Steel weight (kN)	θ	T_1 (sec)	ξ_{tot} (%)	IDR_{DBE} (%)
5-storey	254	0.053	1.28		1.03
10-storey	409	0.115	2.62	20	0.89
20-storey	1254	0.080	3.83		0.52

*Braces are not included in the steel weight.

4.4 Modeling

OpenSees (2016) is employed to develop nonlinear models for the steel MRFs with and without viscous dampers as shown in Figure 4.25. Beams are modeled as elastic elements with zero length flexural plastic hinges at their ends that exhibit moment-rotation behaviour with strength and stiffness deterioration according to the rules described by Lignos and Krawinkler (2011). Panel zones are modeled using the model proposed by Krawinkler (1978). Moreover, force-based fiber elements are used to model the column to accurately capture moment-axial force interaction effects. Each fiber is assumed to exhibit uniaxial bilinear elasto-plastic stress-strain cyclic behaviour since heavy columns of low slenderness do not experience local buckling and deterioration even under large drifts (Newell and Uang 2006). Linear viscous dampers are modeled as simple dashpots without considering limit states that could occur when the piston reaches its stroke limit (Miyamoto et al. 2010). It should be noted that strokes of viscous dampers could be extensible up to ±900mm upon request (Taylor Devices Inc.), and therefore, the dampers of the steel MRFs examined in this study do not reach their limit states even under very large drifts on the basis of this assumption. The braces supporting the dampers are strong enough to resist the peak damper forces without buckling or yielding, and therefore, they are modeled as elastic truss elements. Moreover, to account for the presence of the composite slab a rigid diaphragm constraint is imposed at the nodes of each floor, while to account for the P-Δ effects of the gravity loads acting in the tributary plan area of the steel MRF a leaning column is included in the models; similarly to the models used for the design of the steel MRFs.

To integrate the equations of motion of the steel MRFs subjected to earthquake ground motion the Newmark method with constant acceleration is used. To minimise the unbalanced forces within each integration time step the Newton method with tangent stiffness is used, while an automatic technique of decreasing the time step was employed to overcome convergence issues. The inherent 3% damping ratio at the first two modes of vibration is modeled by using a Rayleigh damping matrix. A nonlinear force-controlled static analysis is first performed under the gravity loads of the seismic design combination and then nonlinear dynamic analysis is executed.

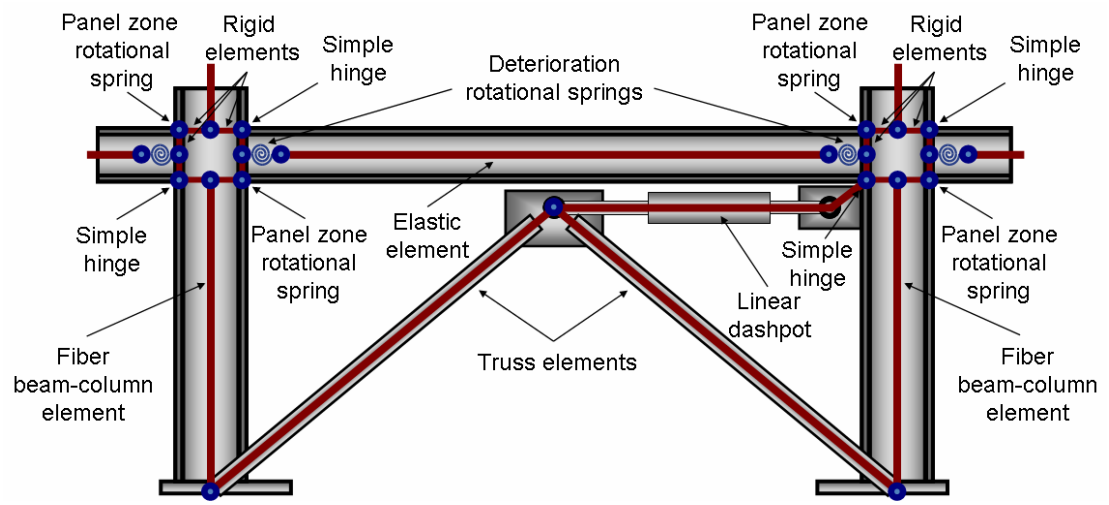

Figure 4.25 Details of the model for nonlinear static and dynamic analysis in OpenSees

4.4.1 Panel zone rotational springs

The Krawinkler model used to model the panel zone joints is shown in Figure 4.25 and it consists of 8 nodes. One of the nodes utilises a rotational spring to represent the panel zone web stiffness and strength (panel component) and another one utilises a rotational spring to represent the column flange contribution (flange component). The moment-rotation relationships of the two rotational springs are presented in Figure 4.26 and they are given by:

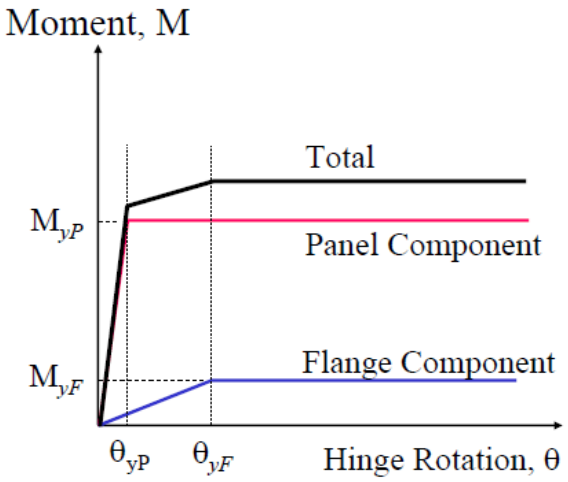

Figure 4.26 Moment-rotation relationships in Krawinkler model (FEMA 451B)

Panel component (web column and doubler plate - upper left rotational spring)

$$M_{\mathrm{yP,K}} = 0.6 \cdot F_{\mathrm{y}} \cdot a \cdot L \cdot \beta \cdot H \cdot \left(t_{\mathrm{wc}} + t_{\mathrm{d}}\right) \tag{4.3}$$

$$\theta_{\mathrm{yP,K}} = \frac{0.6 \cdot F_{\mathrm{y}}}{\mathrm{G}} \tag{4.4}$$

where $M_{\mathrm{yP,K}}$: yield moment of panel component

F_{y} : yield strength of column and doubler plate

$a \cdot L$: distance between the center of column flanges

$\beta \cdot H$: distance between the center of beam flanges

t_{wc} : thickness of column web

t_{d} : thickness of doubler plate

$\theta_{\mathrm{yP,K}}$: yield rotation of panel component

G : shear modulus of steel

Column flange component (lower right rotational spring)

$$M_{\mathrm{yF,K}} = 1.8 \cdot F_{\mathrm{y}} \cdot b_{\mathrm{cf}} \cdot t_{\mathrm{cf}}^2 \tag{4.5}$$

$$\theta_{\mathrm{yF,K}} = 4 \cdot \theta_{\mathrm{yP,K}} \tag{4.6}$$

where $M_{\mathrm{yF,K}}$: yield moment of column flange component

b_{cf} : width of column flange

t_{cf} : thickness of column flange

$\theta_{\mathrm{yF,K}}$: yield rotation of column flange component

Sample calculation for the panel zone shown in Figure 4.27:

$F_{\mathrm{y}} = 355000\,\mathrm{kPa}$

$(a \cdot L)^{\mathrm{HEB650}} = 0.65 - 0.031 = 0.619\,\mathrm{m}$

$(\beta \cdot H)^{\mathrm{IPE600}} = 0.60 - 0.019 = 0.581\,\mathrm{m}$

$t_{\mathrm{wc}}^{\mathrm{HEB650}} = 0.016\,\mathrm{m}$

$b_{\mathrm{cf}}^{\mathrm{HEB650}} = 0.30\,\mathrm{m}$

$t_{\mathrm{cf}}^{\mathrm{HEB650}} = 0.031\,\mathrm{m}$

$t_{\mathrm{d}} = 0.032\,\mathrm{m}$

$G = 80769230.8\,\mathrm{kPa}$

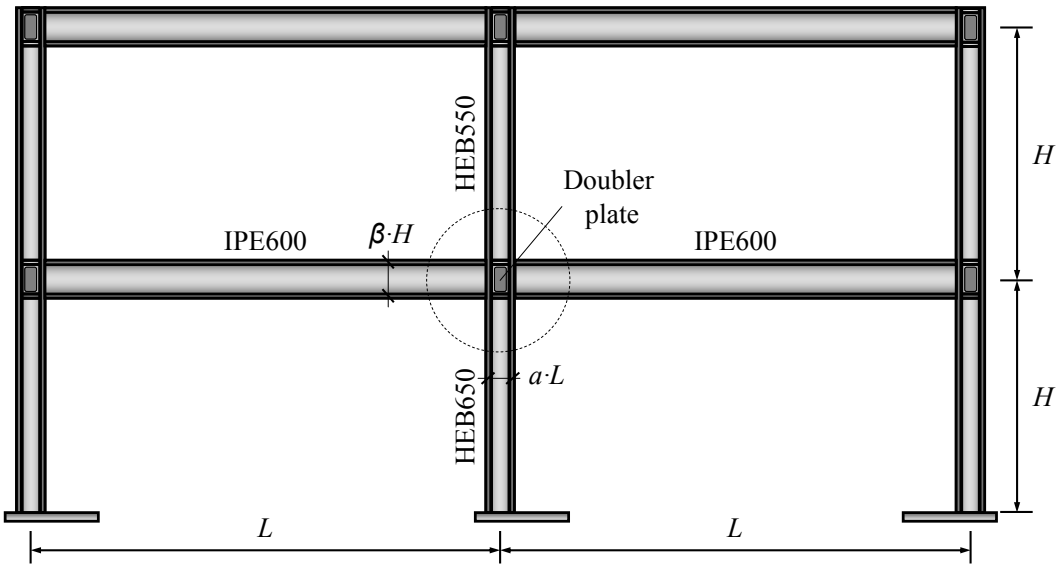

Figure 4.27 Frame with doubler plates

Panel component (web column and doubler plate - upper left rotational spring)

Eq. (4.3) $\Rightarrow M_{\mathrm{yP,K}} = 0.6 \cdot 355000 \cdot 0.619 \cdot 0.581 \cdot (0.016 + 0.032) = 3679.9\,\mathrm{kN \cdot m}$

Eq. (4.4) $\Rightarrow \theta_{\mathrm{yP,K}} = \dfrac{0.6 \cdot 355000}{80769230.8} = 0.00264\,\mathrm{rad}$

Column flange component (lower right rotational spring)

Eq. (4.5) $\Rightarrow M_{\mathrm{yF,K}} = 1.8 \cdot 355000 \cdot 0.30 \cdot 0.031^2 = 184.2\,\mathrm{kN \cdot m}$

Eq. (4.6) $\Rightarrow \theta_{\mathrm{yF,K}} = 4 \cdot 0.00264 = 0.01055\,\mathrm{rad}$

4.4.2 Beams and deterioration rotational springs

Since a beam is modeled as an elastic element connected in series with rotational springs at either end, the stiffness of these components must be modified so that the equivalent stiffness of this assembly is equivalent to the stiffness of the actual frame member. The rotational springs are made n times stiffer than the rotational stiffness of the elastic element in order to avoid numerical problems and allow all damping to be assigned to the elastic element. To ensure the equivalent stiffness of the assembly is equal to the stiffness of the actual frame member, the stiffness of the elastic element

must be $(n+1)/n$ times greater than the stiffness of the actual frame member. This is accomplished by making the elastic element's moment of inertia (I_{elastic}), $(n+1)/n$ times greater than the actual frame member's moment of inertia (I_{member}).

For a beam with actual member rotational stiffness K_{member} and with stiffness of the elastic element K_{elastic} which is modeled,

Let
$$K_{\text{spring}} = n \cdot K_{\text{elastic}} \tag{4.7}$$

The stiffnesses of the elastic element, the rotational springs, which are connected in series and the actual member, are related with the following expression:

$$K_{\text{member}} = \frac{K_{\text{spring}} \cdot K_{\text{elastic}}}{K_{\text{spring}} + K_{\text{elastic}}} \tag{4.8}$$

Substitute Eq. (4.7) into Eq. (4.8),

$$K_{\text{member}} = \frac{n \cdot K_{\text{elastic}} \cdot K_{\text{elastic}}}{n \cdot K_{\text{elastic}} + K_{\text{elastic}}} = \frac{n \cdot K_{\text{elastic}} \cdot K_{\text{elastic}}}{(n+1) \cdot K_{\text{elastic}}} = \frac{n}{(n+1)} K_{\text{elastic}} \tag{4.9}$$

$$\Rightarrow K_{\text{elastic}} = \frac{(n+1)}{n} K_{\text{member}} \tag{4.10}$$

where $K_{\text{member}} = \frac{6EI_{\text{member}}}{L}$ for beams subjected to double curvature bending, with E the modulus of elasticity. The elastic element can have the stiffness described by Equation (4.10), by using the following moment of inertia:

$$I_{\text{elastic}} = \frac{(n+1)}{n} I_{\text{member}} \tag{4.11}$$

The deterioration model by Lignos and Krawinkler (2011) that used for the rotational springs, is shown in Figure 4.28 and Figure 4.29 and is defined by the following parameters:

M_{y}: effective yield moment
M_{c}: capping moment strength
M_{r}: residual moment
θ_{y} : yield rotation
θ_{c} : capping rotation
θ_{u} : ultimate rotation capacity

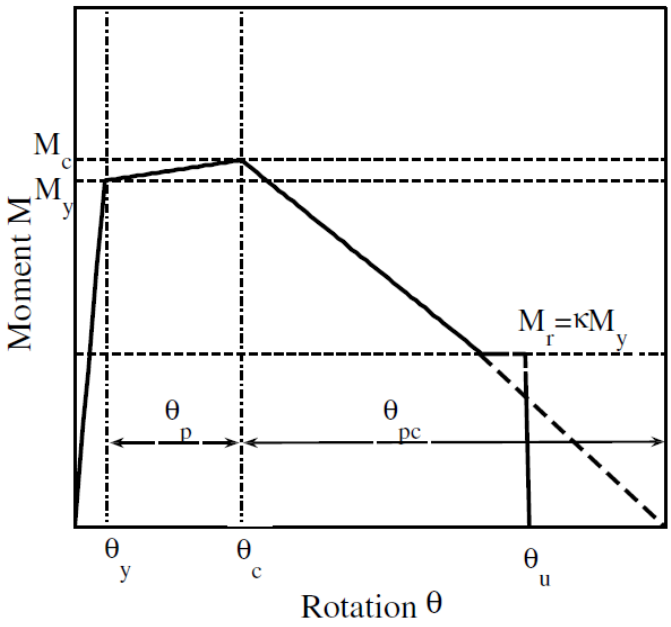

Figure 4.28 Monotonic backbone curve of the deterioration model by Lignos and Krawinkler (2011)

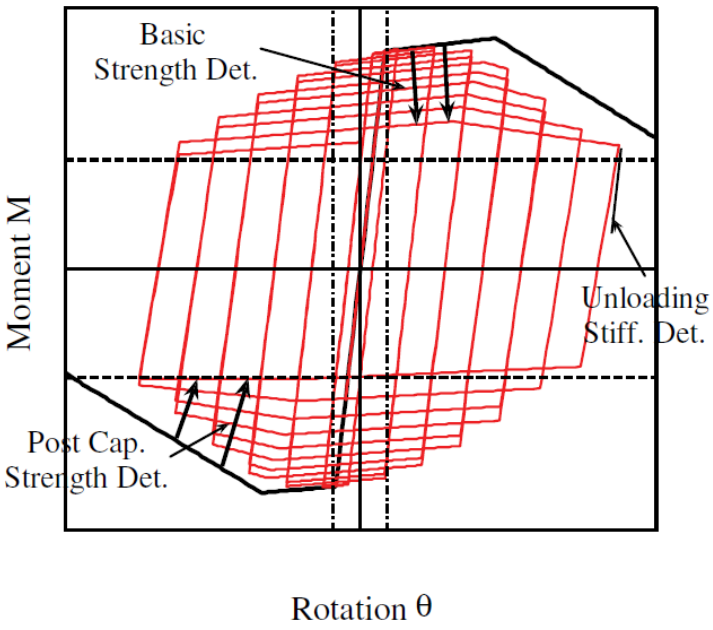

Figure 4.29 Hysteretic behaviour of the deterioration model by Lignos and Krawinkler (2011)

θ_{p} : precapping plastic rotation

θ_{pc}: postcapping plastic rotation

and

(for beams with $d < 533\,\mathrm{mm}$)

$$\theta_{\mathrm{p}} = 0.0865 \cdot \left(\frac{h}{t_{\mathrm{w}}}\right)^{-0.365} \cdot \left(\frac{b_{\mathrm{f}}}{2 \cdot t_{\mathrm{f}}}\right)^{-0.140} \cdot \left(\frac{L}{d}\right)^{0.340} \cdot \left(\frac{d}{533}\right)^{-0.721} \cdot \left(\frac{F_{\mathrm{y}}}{355}\right)^{-0.230} \tag{4.12}$$

(for beams with $d \geq 533\,\mathrm{mm}$)

$$\theta_{\mathrm{p}} = 0.318 \cdot \left(\frac{h}{t_{\mathrm{w}}}\right)^{-0.550} \cdot \left(\frac{b_{\mathrm{f}}}{2 \cdot t_{\mathrm{f}}}\right)^{-0.345} \cdot \left(\frac{L_{\mathrm{b}}}{r_{\mathrm{y}}}\right)^{-0.023} \cdot \left(\frac{L}{d}\right)^{0.090} \cdot \left(\frac{d}{533}\right)^{-0.330} \cdot \left(\frac{F_{\mathrm{y}}}{355}\right)^{-0.130} \tag{4.13}$$

(for beams with $d < 533\,\mathrm{mm}$)

$$\theta_{\mathrm{pc}} = 5.63 \cdot \left(\frac{h}{t_{\mathrm{w}}}\right)^{-0.565} \cdot \left(\frac{b_{\mathrm{f}}}{2 \cdot t_{\mathrm{f}}}\right)^{-0.800} \cdot \left(\frac{d}{533}\right)^{-0.280} \cdot \left(\frac{F_{\mathrm{y}}}{355}\right)^{-0.430} \tag{4.14}$$

(for beams with $d \geq 533\,\mathrm{mm}$)

$$\theta_{\mathrm{pc}} = 7.50 \cdot \left(\frac{h}{t_{\mathrm{w}}}\right)^{-0.610} \cdot \left(\frac{b_{\mathrm{f}}}{2 \cdot t_{\mathrm{f}}}\right)^{-0.710} \cdot \left(\frac{L_{\mathrm{b}}}{r_{\mathrm{y}}}\right)^{-0.110} \cdot \left(\frac{d}{533}\right)^{-0.161} \cdot \left(\frac{F_{\mathrm{y}}}{355}\right)^{-0.320} \tag{4.15}$$

where d : depth of section

h : depth of web

t_{w} : thickness of web

b_{f} : width of flange

t_{f} : thickness of flange

L : shear length

F_{y}: yield strength

L_{b}: lateral bracing length

r_{y} : radius of gyration about weak axis

The rate of cyclic deterioration is defined by the parameter of reference cumulative plastic rotation (Λ) and is given by:

(for beams with $d < 533\,\text{mm}$)

$$\Lambda = 495 \cdot \left(\frac{h}{t_w}\right)^{-1,340} \cdot \left(\frac{b_f}{2 \cdot t_f}\right)^{-0.595} \cdot \left(\frac{F_y}{355}\right)^{-0.360} \tag{4.16}$$

(for beams with $d \geq 533\,\text{mm}$)

$$\Lambda = 536 \cdot \left(\frac{h}{t_w}\right)^{-1,260} \cdot \left(\frac{b_f}{2 \cdot t_f}\right)^{-0.525} \cdot \left(\frac{L_b}{r_y}\right)^{-0.130} \cdot \left(\frac{F_y}{355}\right)^{-0.291} \tag{4.17}$$

In order to make the nonlinear behaviour of the assembly match that of the actual frame member, the strain hardening coefficient (the ratio of post-yield stiffness to elastic stiffness) of the plastic hinge must be modified. The strain hardening coefficient of the deterioration spring $a_{s,spring}$ is given by (OpenSees 2016):

$$a_{s,spring} = \frac{a_{s,member}}{1 + n \cdot (1 - a_{s,member})} \tag{4.18}$$

As mentioned earlier, the damping will be assigned only to the elastic element and since the stiffness of the elastic element has been modified, the stiffness proportional damping coefficient that is used with this element must also be modified (Ibarra and Krawinkler 2005, Zareian and Medina 2010). As the stiffness of the elastic element is made $(n+1)/n$ times greater than the stiffness of the actual frame member (Equation (4.10)), the stiffness proportional damping coefficient of the elastic element must also be made $(n+1)/n$ times greater than the traditional stiffness proportional damping coefficient.

Sample calculation for the beams of floor 1 shown in Figure 4.27:

Let $n = 10$

$d = 600\,\text{mm}$

$h = 562\,\text{mm}$

$t_w = 12\,\text{mm}$

$b_f = 220\,\text{mm}$

$t_f = 19\,\text{mm}$

$I = 9.208 \cdot 10^8\ \text{mm}^4$

$r_y = 46.6\,\text{mm}$

$F_y = 275\,\text{MPa}$

$E = 210000\,\text{MPa}$

The shear length L is taken equal to half of the beam length from the column faces L_{clear}:

$$L = \frac{1}{2} \cdot L_{clear} = \frac{1}{2} \cdot \left(8000 - 0.5 \cdot d^{\text{HEB650}} - 0.5 \cdot d^{\text{HEB650}}\right) =$$

$$= \frac{1}{2} \cdot \left(8000 - 0.5 \cdot 650 - 0.5 \cdot 650\right) = 3675\,\text{mm}$$

and for the calculation of the lateral bracing length L_b, the beam is assumed to be laterally supported at three points, therefore:

$$L_b = \frac{1}{4} \cdot \left(8000 - 0.5 \cdot d^{\text{HEB650}} - 0.5 \cdot d^{\text{HEB650}}\right) =$$
$$= \frac{1}{4} \cdot \left(8000 - 0.5 \cdot 650 - 0.5 \cdot 650\right) = 1837.5\,\text{mm}$$

Then,

$$\text{Eq. (4.11)} \Rightarrow I_{elastic} = \frac{(10+1)}{10} \cdot 9.208 \cdot 10^8 = 10.123 \cdot 10^8\ \text{mm}^4$$

$$\text{with } K_{member} = \frac{6EI_{member}}{L_{clear}} = \frac{6 \cdot 210000 \cdot 9.208 \cdot 10^8}{7350} = 1.58 \cdot 10^{11}\ \text{N} \cdot \text{mm}$$

$$\text{Eq.(4.10)} \Rightarrow K_{elastic} = \frac{(10+1)}{10} \cdot 1.58 \cdot 10^{11} = 1.74 \cdot 10^{11}\ \text{N} \cdot \text{mm}$$

$$\text{Eq.(4.7)} \Rightarrow K_{spring} = 10 \cdot 1.74 \cdot 10^{11} = 1.74 \cdot 10^{12}\ \text{N} \cdot \text{mm}$$

The effective yield moment M_y is taken equal to 1.1 times the plastic moment resistance $M_{pl,Rd}$ to account for the cyclic hardening (Lignos and Krawinkler 2011):

$$M_y = 1.1 \cdot M_{pl,Rd}^{\text{IPE600}} = 1.1 \cdot 965.8 \cdot 10^6 = 1062.4 \cdot 10^6\ \text{N} \cdot \text{mm}$$

The yield rotation θ_y is not needed to be calculated because the elastic branch of the curve is described by the effective yield moment M_y and the elastic stiffness of the spring K_{spring}. The capping moment strength M_c, the residual moment M_r and the ultimate rotation capacity θ_u are taken equal to the following:

$$M_c = 1.1 \cdot M_y$$

$$M_r = 0.01 \cdot M_y$$

$$\theta_u = 0.40 \text{ rad}$$

and

Eq. (4.13) $\Rightarrow$ (with $d \geq 533$ mm)

$$\theta_p = 0.318 \cdot \left(\frac{562}{12}\right)^{-0.550} \cdot \left(\frac{220}{2 \cdot 19}\right)^{-0.345} \cdot \left(\frac{1837.5}{46.6}\right)^{-0.023} \cdot \left(\frac{3675}{600}\right)^{0.090} \cdot \left(\frac{600}{533}\right)^{-0.330} \cdot \left(\frac{275}{355}\right)^{-0.130} = 0.022 \text{ rad}$$

Eq.(4.15) $\Rightarrow$ (with $d \geq 533$ mm)

$$\theta_{pc} = 7.50 \cdot \left(\frac{562}{12}\right)^{-0.610} \cdot \left(\frac{220}{2 \cdot 19}\right)^{-0.710} \cdot \left(\frac{1837.5}{46.6}\right)^{-0.110} \cdot \left(\frac{600}{533}\right)^{-0.161} \cdot \left(\frac{275}{355}\right)^{-0.320} = 0.147 \text{ rad}$$

Eq.(4.17) $\Rightarrow$ (with $d \geq 533$ mm)

$$\Lambda = 536 \cdot \left(\frac{562}{12}\right)^{-1,260} \cdot \left(\frac{220}{2 \cdot 19}\right)^{-0.525} \cdot \left(\frac{1837.5}{46.6}\right)^{-0.130} \cdot \left(\frac{275}{355}\right)^{-0.291} = 1.119 \text{ rad}$$

Assuming a 3% strain hardening coefficient of the actual beam member, the strain hardening coefficient of the deterioration spring $a_{s,spring}$ is calculated by Equation (4.18):

$$a_{s,spring} = \frac{0.03}{1 + 10 \cdot (1 - 0.03)} = 0.0028$$

4.5 Earthquake ground motions

Nonlinear dynamic analysis is performed using a set of 22 pairs of far-field ground motions (Table 4.9) developed by the FEMA P695 project (2009). The event magnitudes of the records range from 6.5 to 7.6 and are recorded on soft rock or on stiff soil. Nine of the records exhibit pulse in the velocity time history (Champion and Liel 2012). The ground motion record intensity measure is selected to be the 5% damped spectral acceleration at the fundamental period of the structure, $S_a(T_1)$.

4.6 Incremental dynamic analyses and investigation of global plastic mechanisms

Incremental dynamic analysis (IDA) (Vamvatsikos and Cornell 2002) is employed to assess and compare the plastic mechanisms of the steel MRFs with and without viscous dampers. For a pair of steel MRF and ground motion, until the drifts increase without bound given a very small increment of $S_a(T_1)$ and the MRF becomes globally unstable, the $S_a(T_1)$ is systematically scaled up in increments. The aforementioned procedure has been repeated for all steel MRFs and 44 ground motions; resulting in the IDA curves provided in Appendix C. The number of plastic hinges developed in the columns is used to assess the plastic mechanisms. For a given seismic intensity level, the steel MRFs with viscous dampers exhibit significantly lower storey drifts than those of the conventional MRFs as shown in Table 4.3 and Table 4.8 for the DBE intensity. Therefore, at specific *IDR* levels the number of column plastic hinges is recorded for fair comparisons of the effectiveness of the capacity design of columns among steel MRFs with and without viscous dampers. For this reason, the number of plastic hinges in the columns is calculated at different *IDR* levels by performing linear interpolation on the IDA results and in the comparison it is considered the number of plastic hinges, under the same ground motion, up to the minimum level of the drifts that increase without bound among the compared steel MRFs. Beyond the minimum level of drifts, which is within the range of 8% and 15%, the number of plastic hinges is assumed constant. Then, for each steel MRF from the IDA results for the 44 ground motions the median value of the number of plastic hinges in the columns is calculated

Table 4.9 Far-field ground motions

No.	Name	Year	M
1	Northridge	1994	6.7
2	Northridge	1994	6.7
3	Duzce, Turkey	1999	7.1
4	Hector Mine	1999	7.1
5	Imperial Valley	1979	6.5
6	Imperial Valley	1979	6.5
7	Kobe, Japan	1995	6.9
8	Kobe, Japan	1995	6.9
9	Kocaeli, Turkey	1999	7.5
10	Kocaeli, Turkey	1999	7.5
11	Landers	1992	7.3
12	Landers	1992	7.3
13	Loma Prieta	1989	6.9
14	Loma Prieta	1989	6.9
15	Manjil, Iran	1990	7.4
16	Superstition Hills	1987	6.5
17	Superstition Hills	1987	6.5
18	Cape Mendocino	1992	7.0
19	Chi-Chi, Taiwan	1999	7.6
20	Chi-Chi, Taiwan	1999	7.6
21	San Fernando	1971	6.6
22	Friuli, Italy	1976	6.5

at a specific *IDR* level. The total number of possible column plastic hinge locations are used to divide the aforementioned median values in order to compare the percentage of columns developing plastic hinges in steel MRFs. Without considering the bottom of the first storey columns and the top of the last storey columns, the total number of possible column plastic hinge locations is 32 for the 5-storey steel MRF, 72 for 10-storey steel MRF and 152 for the 20-storey steel MRF.

Figure 4.30 and Figure 4.31 show the median value of the percentage of column plastic hinges against *IDR* for the 5-storey, the 10-storey and the 20-storey steel MRFs with and without dampers. The 5-storey MRF with dampers has lower percentage of column plastic hinges compared to the 5-storey MRF. Plastic hinges in the 5-storey MRF with dampers develop for *IDR* larger than 7% and their median percentage value is lower than 5% for *IDR* up to 10%. The 10-storey MRF with dampers has slightly higher percentage of column plastic hinges compared to the 10-storey MRF. An appreciable difference between the plastic mechanisms of the two frames is seen for *IDR* larger than 8%. The median value of the percentage of column plastic hinges for the 10-storey steel MRF with dampers is lower than 10% for *IDR* up to 10%. The aforementioned results show that for buildings of up to 10 storeys, the proposed simple conservative capacity design rule is very effective and results in steel MRFs with viscous dampers that show plastic mechanisms similar to those of steel MRFs without dampers.

The 20-storey MRF with dampers has a significantly higher percentage of column plastic hinges compared to the 20-storey MRF. Column plastic hinges develop at *IDR* equal to 1.5% and 3% for the 20-storey MRFs with and without dampers, respectively. The percentage of the column plastic hinges at 10% *IDR* is equal to 35% and 22% for the 20-storey MRF with and without dampers, respectively. The aforementioned results show that the proposed capacity design rule needs to become stricter for highly damped steel MRFs of more than 10 storeys. Essentially this means that the SF value used in Equation (3.3) needs to become higher than 1.0 to achieve a plastic mechanism similar to that of steel MRFs without dampers. Nonlinear static analysis (pushover) is not performed to measure the influence of viscous dampers on the plastic mechanism because viscous dampers are velocity activated and pushover can not capture the effects of viscous dampers in the structure.

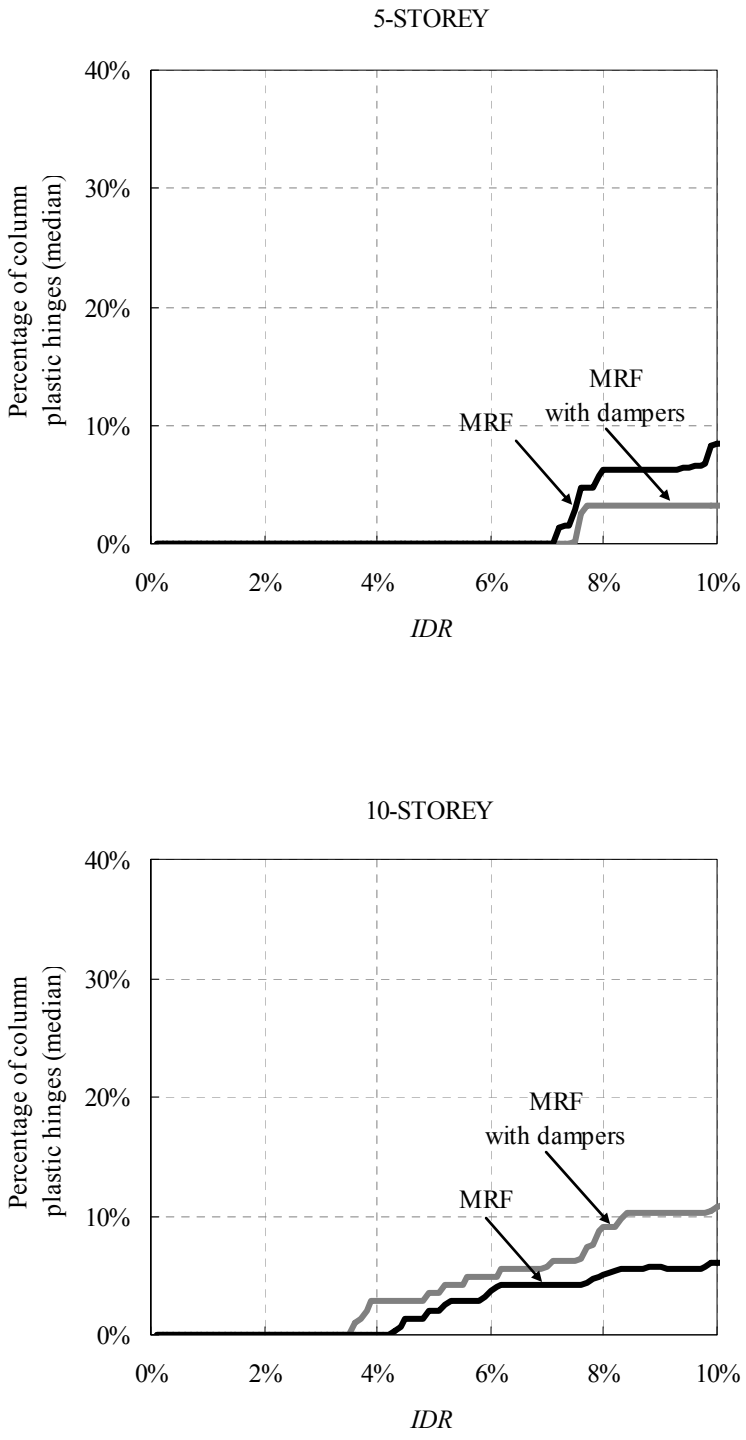

Figure 4.30 Percentage of column plastic hinges in the steel MRFs with and without dampers

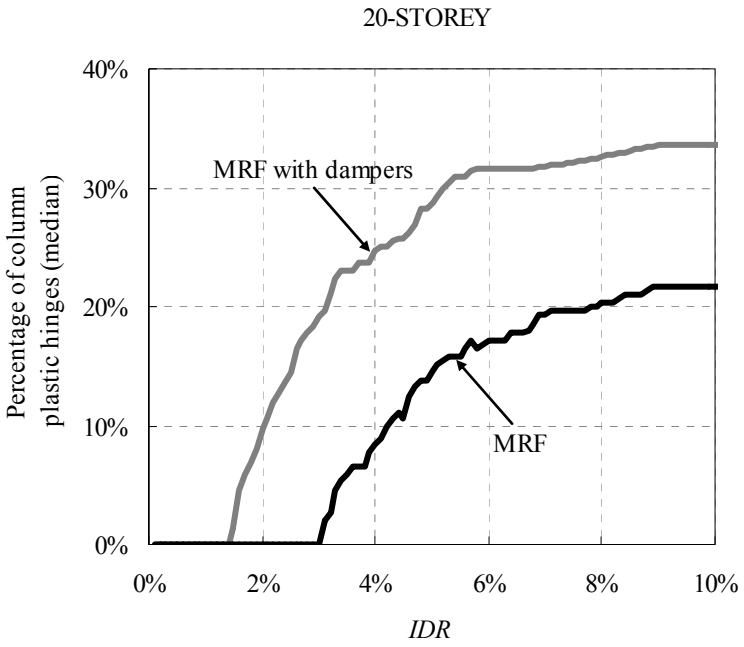

Figure 4.31 Percentage of column plastic hinges in the steel MRFs with and without dampers

Figure 4.32 and Figure 4.33 show the peak damper forces predicted by the procedure of ASCE 7-10 in comparison with the average values of the peak damper forces from nonlinear dynamic analysis of the three highly damped steel MRFs under the 44 ground motions scaled at the DBE. Figure 4.32 and Figure 4.33 also include the ratios of the average peak damper forces from analysis over the predicted ones. The values from analysis are higher than the predicted ones and their difference increases for taller steel MRFs. Moreover, their difference increases from the top to the bottom of the building. The maximum ratios are equal to 1.30, 1.95 and 2.41 for the 5-storey, 10-storey and 20-storey steel MRFs with dampers, respectively. These results indicate that the ASCE 7-10 procedure underestimates the peak damper forces in the lower storeys of tall steel MRFs and further confirm the need for a stricter capacity design rule for columns in buildings of more than 10 storeys.

Nonlinear static analysis (pushover) is not performed to measure the influence of viscous dampers on the plastic mechanism because viscous dampers are velocity activated.

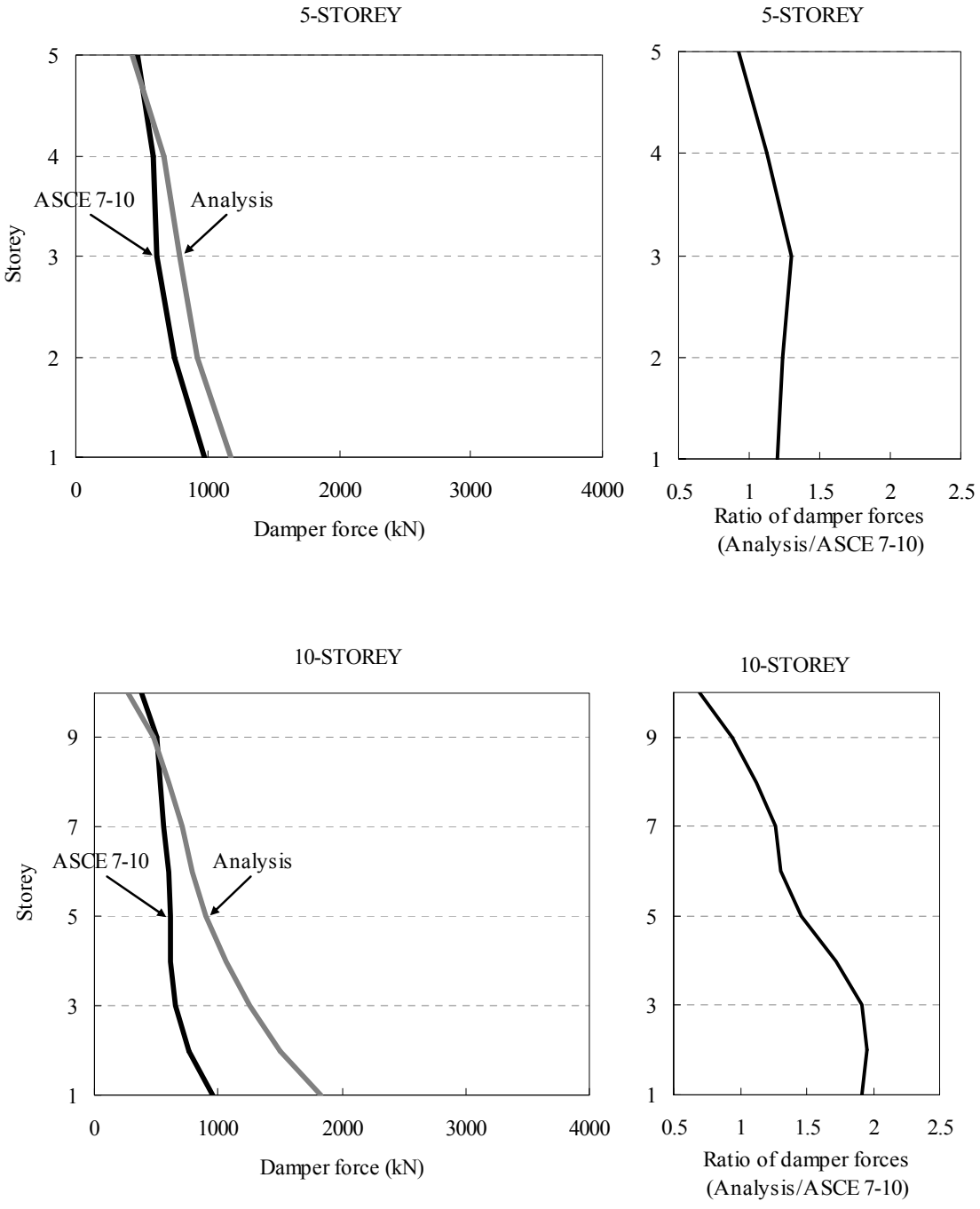

Figure 4.32 Peak damper forces predicted by ASCE 7-10 and average peak damper forces from nonlinear dynamic analysis for 44 ground motions; both calculated for the DBE seismic intensity

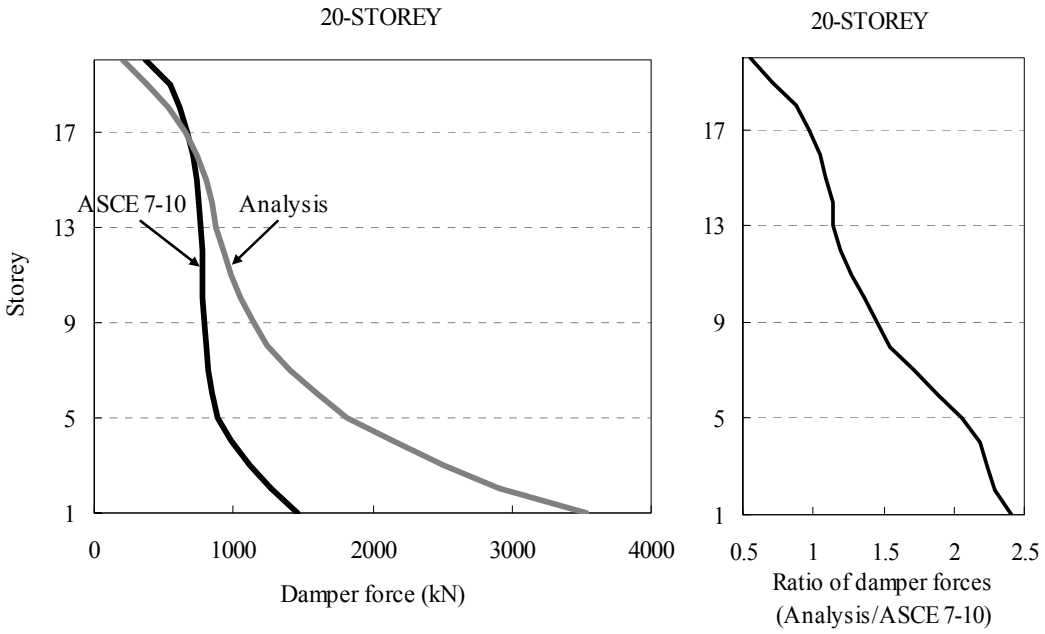

Figure 4.33 Peak damper forces predicted by ASCE 7-10 and average peak damper forces from nonlinear dynamic analysis for 44 ground motions; both calculated for the DBE seismic intensity

4.7 Re-design and assessment of the 20-storey steel MRF

The 20-storey steel MRF with viscous dampers is re-designed by using a stricter capacity design rule with the goal of achieving the desired global plastic mechanism. In particular, the design is performed on the basis of a scale factor SF (see Equation (3.3)) larger than 1.0 and then IDA is carried out to calculate the percentage of column plastic hinges at different *IDR* levels. The latter process is repeated several times until the SF factor that results in a design with plastic mechanism similar to that of the 20-steel MRF without dampers is identified.

Table 4.10 lists the steel weight, the fundamental period of vibration (T_1) and the IDR_{DBE} of the final design of the 20-storey steel MRF with viscous dampers, while Figure 4.36 shows its elevation view with the cross-sections of the beams and columns of each storey. The associated SF factor has a value equal to 3.5. The stricter capacity design rule results in changes of the interior columns in storeys 3-19 and increases the steel weight by 10% with respect to the 20-storey steel MRF with viscous dampers designed for SF equal to 1.0.

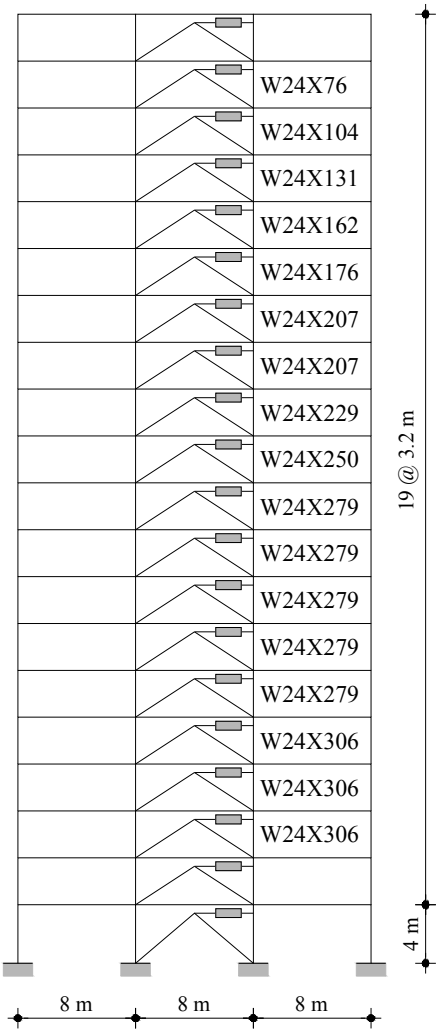

Figure 4.34 Elevation view and design details of the 20-storey steel MRF with dampers designed for SF equal to 3.5. Beams and columns are the same with those of the MRF with dampers designed for SF=1 apart from the indicated interior columns

Table 4.10 Design details of the 20-storey MRF with dampers designed with SF equal to 3.5

Frame	Steel weight (kN)	T_1 (sec)	ξ_{tot} (%)	IDR_{DBE} (%)
20-storey	1378	3.71	20	0.52

*Braces are not included in the steel weight.

Figure 4.35 shows the median value of the percentage of the column plastic hinges against *IDR* for the 20-storey MRF, the 20-storey MRF with dampers designed for SF equal to 1.0, and the 20-storey MRF with dampers designed for SF equal to 3.5. The 20-storey steel MRF with dampers designed for SF equal to 3.5 has significantly lower percentage of column plastic hinges compared to the steel MRF with dampers designed for SF equal to 1.0, and its behaviour approaches that of the steel MRF without dampers. For example, the percentage of the column plastic hinges at 10% drift is reduced from 34% for the MRF with dampers designed for SF equal to 1.0 to 25% for the MRF with dampers designed for SF equal to 3.5, while the same percentage is equal to 22% for the steel MRF without dampers.

Figure 4.36 shows the locations of the column plastic hinges for the 20-storey MRF, the 20-storey MRF with dampers designed for SF equal to 1.0, and the 20-storey MRF with dampers designed for SF equal to 3.5 from nonlinear dynamic analysis under a ground motion scaled to induce to all MRFs a *IDR* equal to 2%. The MRF does not experience column plastic hinges, the MRF with dampers and SF equal to 1.0 has 30 column plastic hinges, and the MRF with dampers and SF equal to 3.5 has 5 column plastic hinges only.

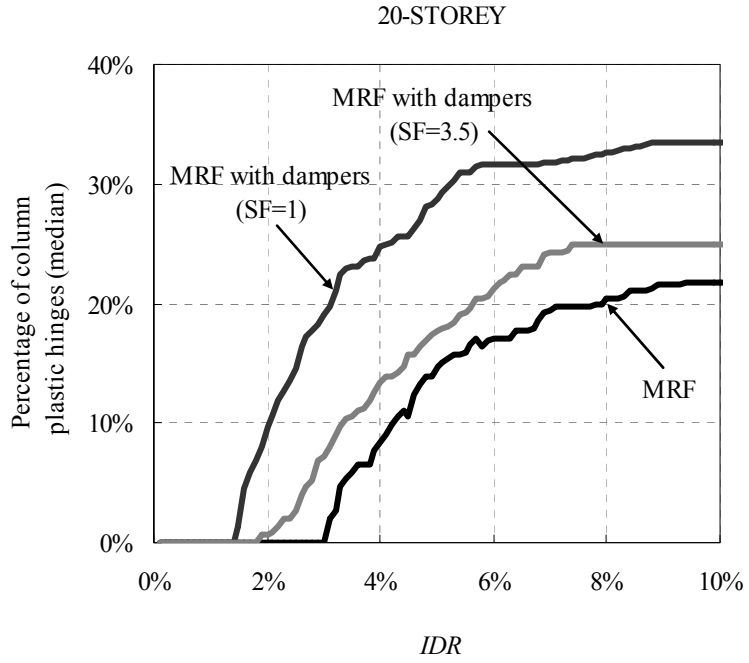

Figure 4.35 Percentage of column plastic hinges in steel MRF, MRF with dampers (SF=1) and MRF with viscous dampers (SF=3.5)

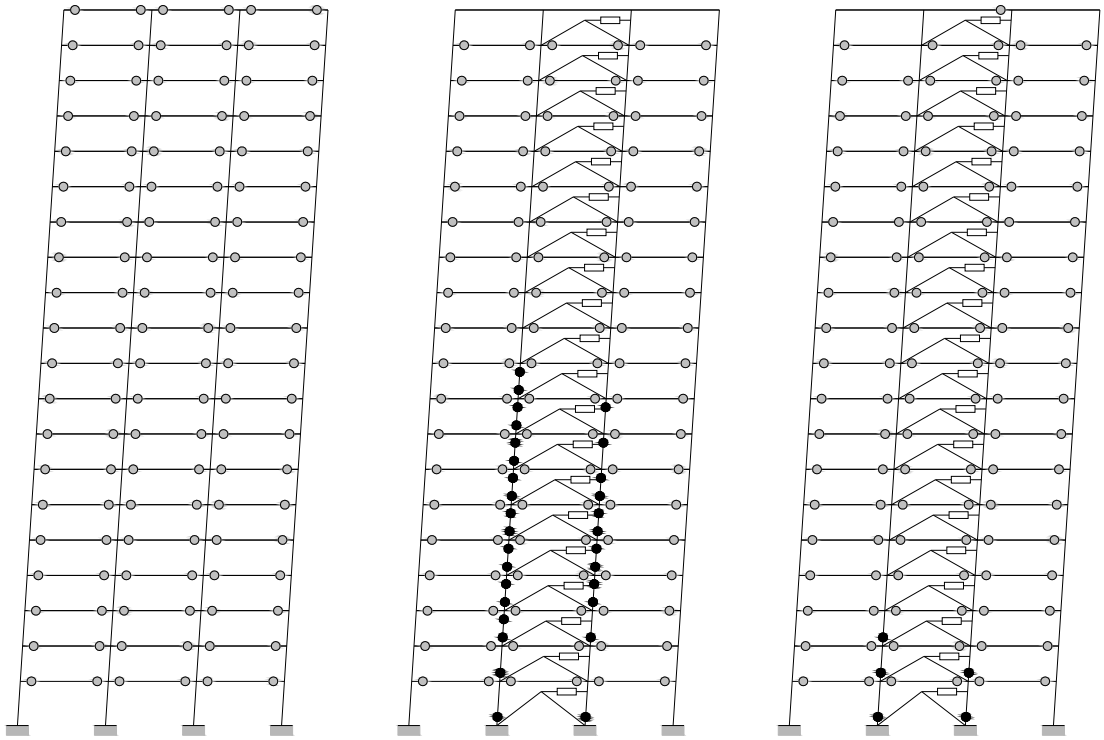

(a) (b) (c)

Figure 4.36 Locations of plastic hinges in beams and columns at *IDR* equal to 2% under ground motion No. 5 for the 20-storey a) MRF; b) MRF with dampers (SF=1); and MRF with dampers (SF=3.5)

The aforementioned results as well as those in Section 4.6 how that the proposed modified capacity design rule for columns in the force path of viscous dampers results in highly damped steel MRFs with global plastic mechanisms similar to those of conventional steel MRFs without dampers. The SF factor used in the proposed Equation (3.3) is equal to 1.0 for steel MRFs up to 10 storeys and equal to 3.5 for steel MRFs of 20 storeys. Linear interpolation can be approximately adopted to calculate the required SF value for steel MRFs with number of storeys between 10 and 20.

From each IDA curve, the $S_a(T_1)$ value leading to collapse of a steel MRF subjected to a specific ground motion can be obtained. Then the $S_a(T_1)$ values associated with collapse of the 44 ground motions are ranked in ascending order, each being treated as an equally likely outcome. A cumulative distribution function is fitted to the ranked data points assuming a lognormal distribution and the produced curve is called collapse fragility curve.

Figure 4.37 shows the collapse fragility curves of the 20-storey MRF, the 20-storey MRF with dampers and SF equal to 1.0, and the 20-storey MRF with dampers and SF

equal to 3.5, where $S_a(T_1)$ is normalised by $S_{a,MCE}(T_1)$ in order to enable the comparison of steel MRFs having different fundamental periods. The $S_a(T_1)$ at 50% probability of collapse is $6.4 \cdot S_{a,MCE}(T_1)$ for the 20-storey steel MRF with dampers and SF equal to 1.0, while the same quantity is equal to $7.3 \cdot S_{a,MCE}(T_1)$ for the 20-storey MRF with dampers and SF equal to 3.5. These values show that the application of the stricter capacity design rule for the columns of the 20-storey steel MRF with viscous dampers does not result in significant benefit in terms of the collapse resistance. However, the aforementioned 14% increase in collapse resistance could be significant in the case of lightweight steel MRFs with viscous dampers designed to have similar drift performance with that of MRFs without dampers. For such frames, achieving a global sway plastic mechanism is a fundamental requirement of seismic codes that should be satisfied before establishing other minimum requirements (e.g. allowable value of the storey drift sensitivity coefficient θ) that will allow using viscous damper to reduce steel weight without compromising the seismic performance.

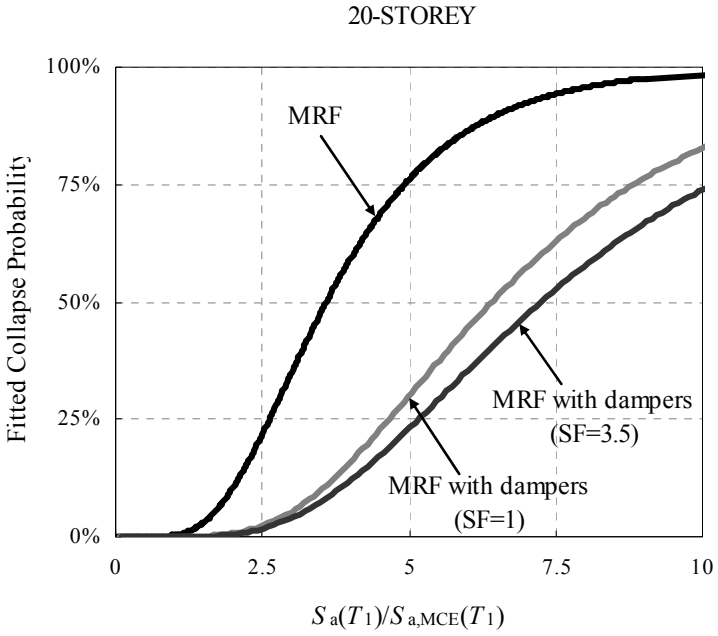

Figure 4.37 Collapse fragility curves of the 20-storey MRF, 20-storey MRF with dampers and SF equal to 1.0, and 20-storey MRF with dampers and SF equal to 3.5

4.8 Summary

In this chapter, prototype buildings of 5, 10 and 20 storeys were designed using steel MRFs with and without viscous dampers following the seismic design procedures described in the previous chapter. The MRFs with viscous dampers were designed to achieve a total viscous damping ratio, ξ_{tot}, at T_1 equal to 20%. Incremental dynamic analyses were conducted for all steel MRFs with and without viscous dampers. Their global plastic mechanisms were compared in order to explore whether more conservative capacity design rules were needed for columns in the force path of viscous dampers that will guarantee plastic mechanisms similar to those of steel MRFs without dampers. The results of analyses showed that the proposed capacity design rule resulted in highly damped steel MRFs with plastic mechanisms similar to those of steel MRFs. Such rule needs to become stricter for buildings with more than 10 storeys to address that linear elastic analysis methods for structures with dampers underestimate the peak damper forces in the lower storeys of yielding tall steel MRFs.

CHAPTER 5

PROPOSED LIMITS FOR θ

5.1 Introduction

A number of steel MRFs with viscous dampers, more flexible than the conventional steel MRFs (Section 4.2), are designed with interstorey drift equal or lower than the conventional steel MRFs. The collapse resistance of steel MRFs with viscous dampers is compared with those of steel MRFs without viscous dampers and appropriate limit values for θ are recommended for the proposed design procedure. Three cases of different damping level are investigated. The damping coefficients are selected to provide ξ_{eq} equal to 7%, 12% and 17%. The inherent damping ratio is 3%, and therefore, the MRFs with viscous dampers have total viscous damping ratio, ξ_{tot}, at T_1 equal to 10%, 15% and 20%. The upper bound of storey drift sensitivity coefficient θ, which according to EC8 is 0.30 (Step 1), is neglected. Also, their global plastic mechanisms are compared.

5.2 Design of steel MRFs with viscous dampers

The design of a more flexible steel MRF with viscous dampers than the conventional steel MRF is followed by the design of a steel MRF with viscous dampers less flexible until the collapse resistance of the steel MRF with viscous dampers becomes better than the conventional steel MRF. Elevation views along with the beam/column cross-sections and the damping coefficients of the viscous damper of the final design of the 5-storey, 10-storey and 20-storey steel MRFs with viscous dampers are provided in Appendix D. Tables with the *IDR* and the coefficients θ are included in the same Appendix.

Table 5.1 lists the steel weight, the fundamental period of vibration (T_1), the IDR_{DBE} and the coefficients θ.

Table 5.1 Design details of the steel MRFs with and without viscous dampers

Frame	ξ_{tot} (%)	Steel weight (kN)	θ	T_1 (sec)	IDR_{DBE} (%)
MRF					
5-storey	3	254	0.091	1.28	1.79
10-storey		389	0.209	2.68	1.57
20-storey		1228	0.134	3.87	0.89
MRF with dampers					
5-storey	10	203	0.154	1.69	1.79
		211	0.112	1.59	1.72
		219	0.111	1.55	1.74
	15	182	0.175	1.91	1.79
		188	0.165	1.87	1.79
		192	0.152	1.80	1.79
		199	0.144	1.73	1.68
	20	152	0.325	2.43	1.79
		176	0.188	2.00	1.74
		192	0.137	1.80	1.65
		221	0.084	1.52	1.40
10-storey	10	334	0.330	3.92	1.26
		430	0.188	3.19	1.18
	15	340	0.270	3.86	1.10
		382	0.215	3.56	1.03
		441	0.177	3.16	1.09
	20	359	0.229	3.74	1.02
		402	0.181	3.35	0.95
20-storey	10	969	0.197	5.30	0.71
		1105	0.141	4.69	0.67
		1228	0.110	4.22	0.66
	15	997	0.174	5.26	0.63
	20	1032	0.171	5.23	0.56

*Braces are not included in the steel weight of the MRFs with dampers.

5.3 Incremental dynamic analyses and establish allowable values of coefficient θ

IDA is performed to produce the collapse fragility curves of the steel MRFs and with reference the collapse resistance at the 50% probability of the steel MRFs without dampers, the allowable values of coefficient θ for the steel MRFs with dampers are established. For a pair of steel MRF and ground motion, until the drifts increase without bound given a very small increment of $S_a(T_1)$ and the MRF becomes globally unstable, the $S_a(T_1)$ is systematically scaled up in increments. The aforementioned procedure has been repeated for all steel MRFs and 44 ground motions; resulting in the IDA curves provided in Appendix E. Sources of collapse uncertainty (e.g. record-to-record, design requirement, test data and modeling) are not considered in this study.

Figure 5.1 and Figure 5.2 show the collapse fragility curves of the 5-storey steel MRFs, Figure 5.2 and Figure 5.3 show the collapse fragility curves of the 10-storey steel MRFs and Figure 5.4 and Figure 5.5 show the collapse fragility curves of the 20-storey steel MRFs. $S_a(T_1)$ is normalised by $S_{a,MCE}(T_1)$ in order to enable the comparison of steel MRFs having different fundamental periods.

The $S_a(T_1)$ at 50% probability of collapse for the 5-storey MRF is $3.74 \cdot S_{a,MCE}$, for the 10-storey MRF is $2.42 \cdot S_{a,MCE}$ and for the 20-storey MRF is $3.61 \cdot S_{a,MCE}$. The $S_a(T_1)$ at 50% probability of collapse for the 5-storey MRFs with dampers (ξ_{tot}=10%) and θ equal to 0.154, 0.112, 0.111 are $3.25 \cdot S_{a,MCE}$, $3.89 \cdot S_{a,MCE}$, $4.15 \cdot S_{a,MCE}$ respectively, for the 5-storey MRFs with dampers (ξ_{tot}=15%) and θ equal to 0.175, 0.165, 0.152, 0.144 are $3.11 \cdot S_{a,MCE}$, $3.17 \cdot S_{a,MCE}$, $3.50 \cdot S_{a,MCE}$, $3.71 \cdot S_{a,MCE}$ respectively, for the 5-storey MRFs with dampers (ξ_{tot}=20%) and θ equal to 0.325, 0.188, 0.137, 0.084 are $2.95 \cdot S_{a,MCE}$, $3.34 \cdot S_{a,MCE}$, $4.12 \cdot S_{a,MCE}$, $5.81 \cdot S_{a,MCE}$ respectively.

The $S_a(T_1)$ at 50% probability of collapse for the 10-storey MRFs with dampers (ξ_{tot}=10%) and θ equal to 0.330, 0.188 are $2.38 \cdot S_{a,MCE}$, $2.96 \cdot S_{a,MCE}$ respectively, for the 10-storey MRFs with dampers (ξ_{tot}=15%) and θ equal to 0.270, 0.215, 0.177 are $2.90 \cdot S_{a,MCE}$, $3.11 \cdot S_{a,MCE}$, $3.50 \cdot S_{a,MCE}$ respectively, for the 10-storey MRFs with dampers (ξ_{tot}=20%) and θ equal to 0.229, 0.181 are $3.49 \cdot S_{a,MCE}$, $3.69 \cdot S_{a,MCE}$ respectively. The $S_a(T_1)$ at 50% probability of collapse for the 20-storey MRFs with dampers (ξ_{tot}=10%) and θ equal to 0.197, 0.141, 0.110 are $4.17 \cdot S_{a,MCE}$, $4.36 \cdot S_{a,MCE}$,

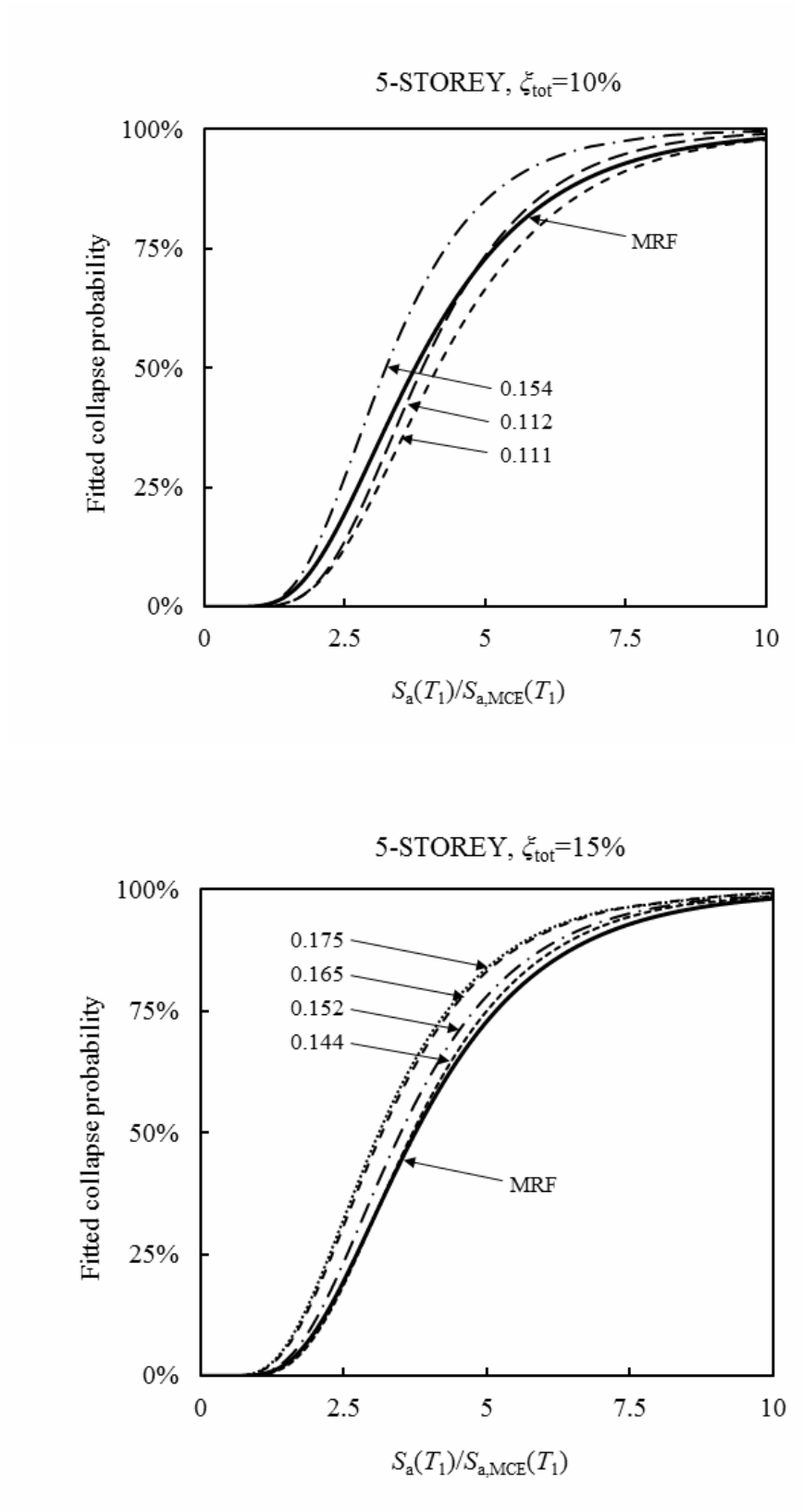

Figure 5.1 Collapse fragility curves of the steel MRF and the MRFs with viscous dampers (solid line indicates median)

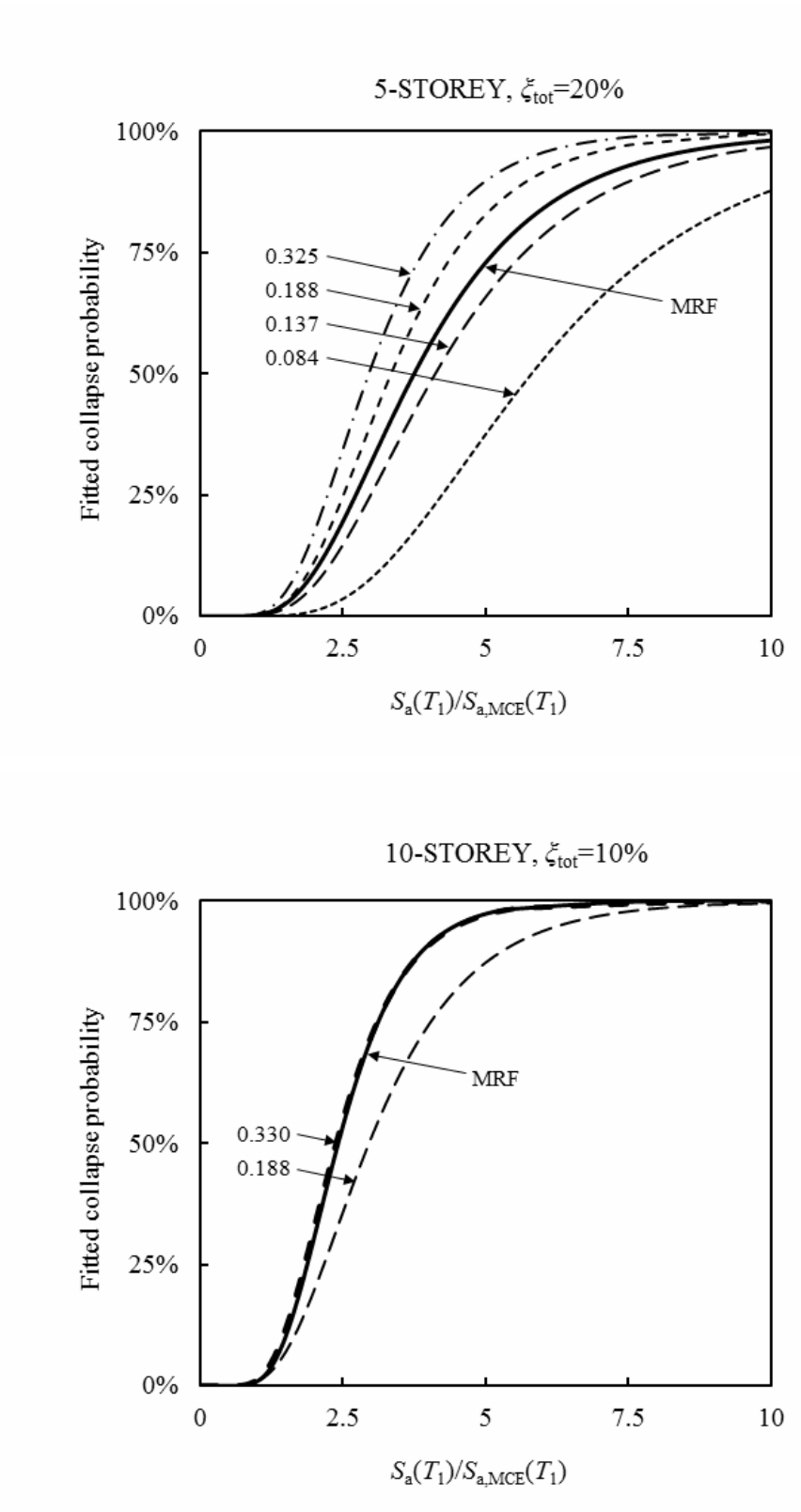

Figure 5.2 Collapse fragility curves of the steel MRFs and the MRFs with viscous dampers

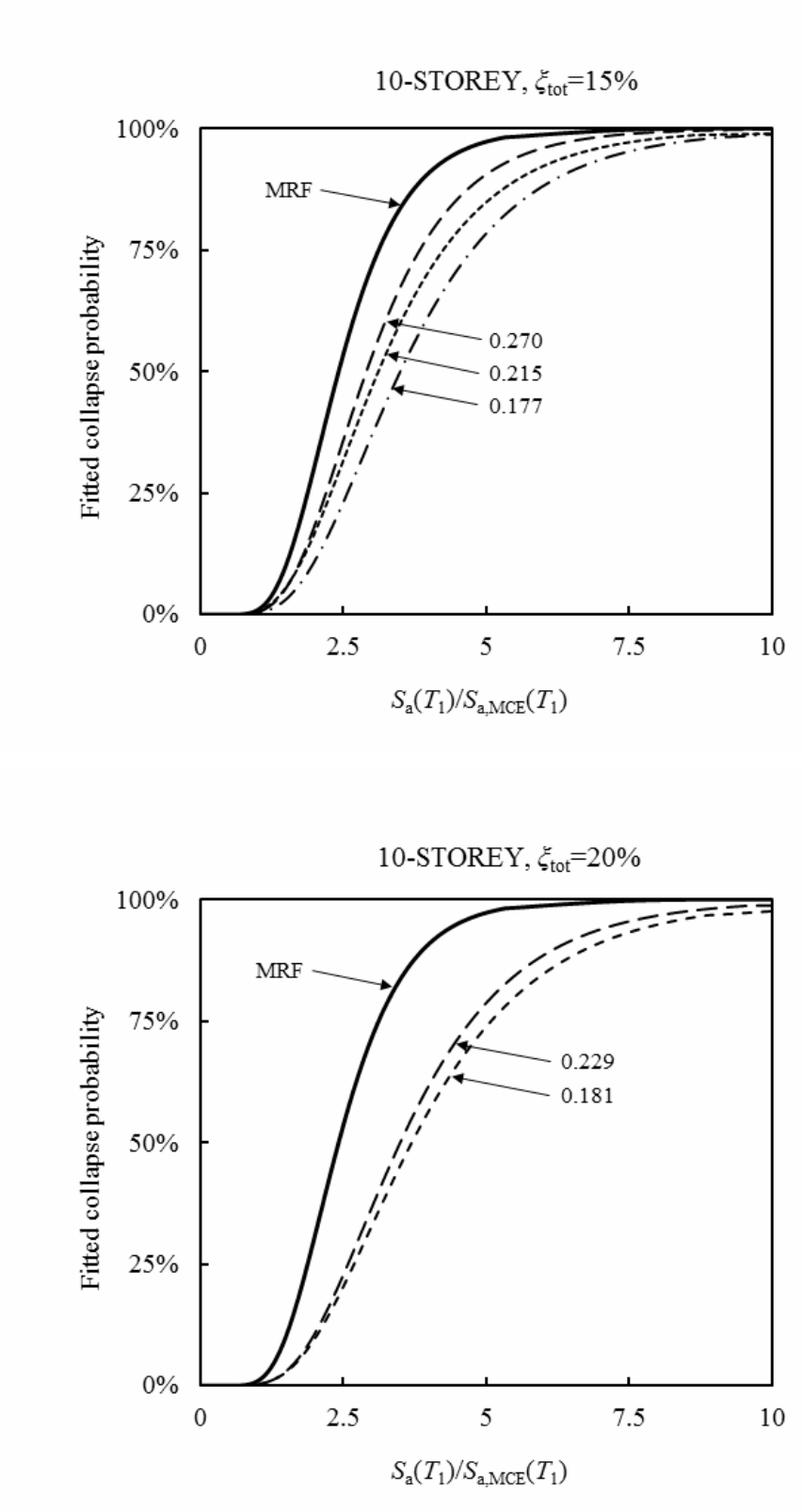

Figure 5.3 Collapse fragility curves of the steel MRF and the MRFs with viscous dampers

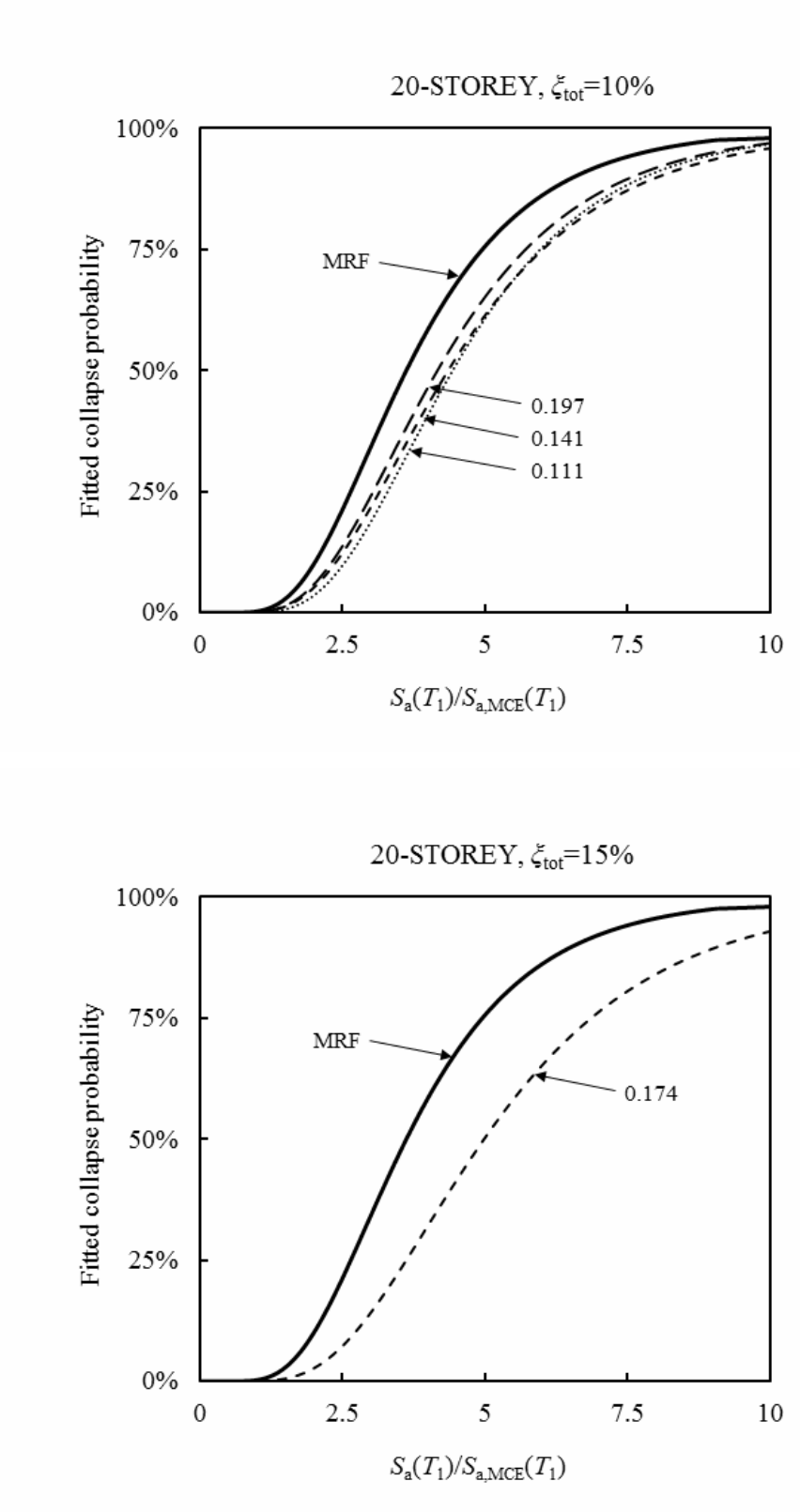

Figure 5.4 Collapse fragility curves of the steel MRF and the MRFs with viscous dampers

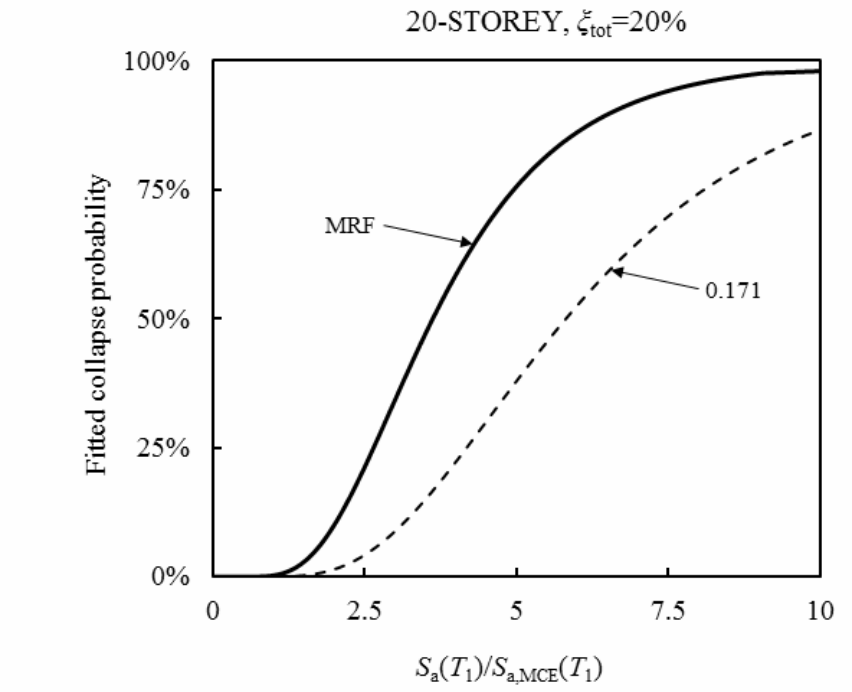

Figure 5.5 Collapse fragility curves of the steel MRF and the MRF with viscous dampers

4.43·$S_{a,MCE}$ respectively, for the 20-storey MRF with dampers (ξ_{tot}=15%) and θ equal to 0.174 is 4.98·$S_{a,MCE}$, for the 20-storey MRF with dampers (ξ_{tot}=20%) and θ equal to 0.171 is 5.81·$S_{a,MCE}$.

The 5-storey MRFs with dampers (ξ_{tot}=10%) and θ equal to 0.112, 0.111 show higher performance and with θ equal to 0.154 shows lower performance compared to the 5-storey MRF without dampers. Linear interpolation can be approximately adopted to calculate the allowable values of coefficient θ, using the $S_a(T_1)$ at 50% probability of collapse of the MRFs with θ equal to 0.154, 0.112 and the conventional MRF. The allowable value of coefficient θ for a 5-storey MRF with dampers (ξ_{tot}=10%) is equal to 0.120. The 5-storey MRFs with dampers (ξ_{tot}=15%) and θ equal to 0.175, 0.165, 0.152 show lower performance and with θ equal to 0.144 shows marginally lower performance compared to the 5-storey MRF without dampers. The allowable value of coefficient θ for a 5-storey MRF with dampers (ξ_{tot}=15%) is equal to 0.142 after performing linear interpolation on the $S_a(T_1)$ at 50% probability of collapse of the MRFs with θ equal to 0.152 and 0.144 and the conventional MRF. The

5-storey MRFs with dampers (ξ_{tot}=20%) and θ equal to 0.137, 0.084 show higher performance and with θ equal to 0.325, 0.188 show lower performance compared to the 5-storey MRF without dampers. The allowable value of coefficient θ for a 5-storey MRF with dampers (ξ_{tot}=20%) is equal to 0.158 after performing linear interpolation on the $S_a(T_1)$ at 50% probability of collapse of the MRFs with θ equal to 0.188 and 0.137 and the conventional MRF.

The 10-storey MRF with dampers (ξ_{tot}=10%) and θ equal to 0.188 shows higher performance and with θ equal to 0.330 shows lower performance compared to the 5-storey MRF without dampers. The allowable value of coefficient θ for a 10-storey MRF with dampers (ξ_{tot}=10%) is equal to 0.317 after performing linear interpolation on the $S_a(T_1)$ at 50% probability of collapse of the MRFs. The 10-storey MRFs with dampers (ξ_{tot}=15%, 20%) and the 20-storey MRFs with dampers (ξ_{tot}=10%, 15%, 20%) show higher performance compared to the corresponding MRFs without dampers. In particular, the more flexible MRFs with dampers show lower performance compared to stiffer MRFs with dampers but still higher performance than the conventional MRFs. In these cases of MRFs with dampers, limit of coefficient θ can be neglected in the design procedure and other loading conditions, such as wind, is expected to result in designs of similar or less flexible MRFs that are considered in this study.

The allowable values of coefficient θ for the 5-storey and the 10-storey MRFs with dampers are shown in Figure 5.6. Linear interpolation is suggested to approximately calculate the allowable values of coefficient θ for total viscous damping ratio between 3-10%, 10-15% and 15-20% for 5-storey MRFs with dampers and between 3-10% for 10-storey MRFs with dampers.

5.4 Assessment of global plastic mechanisms

The number of plastic hinges developed in the columns is used to assess the plastic mechanisms. The number of plastic hinges in the columns is calculated at different *IDR* levels by performing linear interpolation on the IDA results. Then, for each steel MRF from the IDA results for the 44 ground motions the median value of the number of plastic hinges in the columns is calculated at a specific *IDR* level. The total number

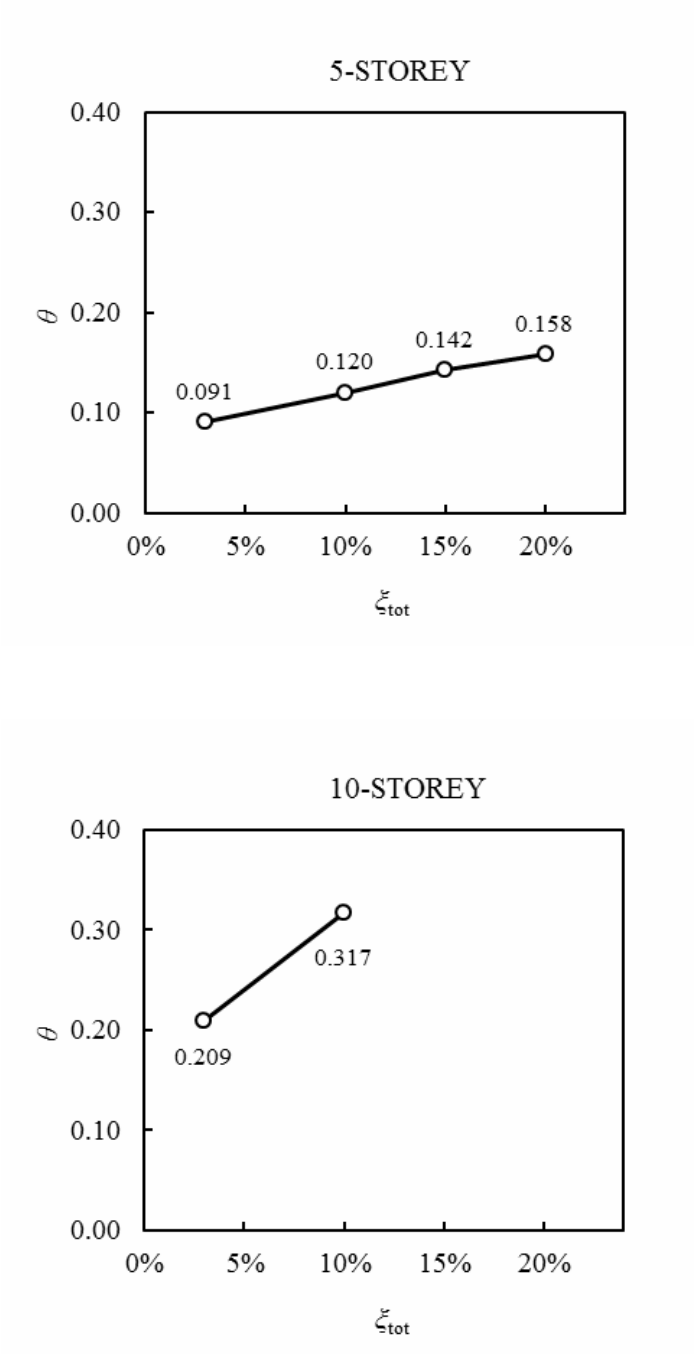

Figure 5.6 Allowable values of coefficient θ for the steel MRFs with viscous dampers

of possible column plastic hinge locations are used to divide the aforementioned median values in order to compare the percentage of columns developing plastic hinges in steel MRFs. Without considering the bottom of the first storey columns and the top of the last storey columns, the total number of possible column plastic hinge locations is 32 for the 5-storey steel MRF, 72 for 10-storey steel MRF and 152 for the 20-storey steel MRF. Figure 5.7 and Figure 5.8 show the median value of the percentage of column plastic hinges against *IDR* for the 5-storey steel MRFs, Figure 5.8 and Figure 5.9 show the median value of the percentage of column plastic hinges against *IDR* for the 10-storey steel MRFs and Figure 5.10 and Figure 5.11 show the median value of the percentage of column plastic hinges against *IDR* for the 20-storey steel MRFs.

In the 5-storey MRFs with dampers (ξ_{tot}=10%) as θ decreases the percentage of column plastic hinges increases. The MRF with dampers (ξ_{tot}=10%) and θ equal to 0.154 does not develop plastic hinges in columns for *IDR* up to 10%. The percentage of column plastic hinges for the 5-storey MRF is lower than 9% for *IDR* up to 10% and for the MRF with dampers (ξ_{tot}=10%) that has the highest percentage is lower than 16%. In the 5-storey MRFs with dampers (ξ_{tot}=15%) as θ decreases the percentage of column plastic hinges decreases. The percentage of column plastic hinges for the 5-storey MRF with dampers (ξ_{tot}=15%) that has the highest percentage is lower than 6% for *IDR* up to 10% and develop for *IDR* larger than the MRF. In the 5-storey MRFs with dampers (ξ_{tot}=20%) as θ decreases the percentage of column plastic hinges increases. The percentage of column plastic hinges for the 5-storey MRF with dampers (ξ_{tot}=20%) that has the highest percentage is lower than 16% for *IDR* up to 10%. For the proposed allowable values of coefficient θ for the three damping levels, the results indicate that the 5-storey MRFs with dampers will develop similar or lower percentage of column plastic hinges than the MRF.

In the 10-storey MRFs with dampers (ξ_{tot}=10%) as θ decreases the percentage of column plastic hinges decreases. The percentage of column plastic hinges for the 10-storey MRF is lower than 6% for *IDR* up to 10% and for the 10-storey MRF with dampers (ξ_{tot}=10%) that has the highest percentage is lower than 8% and develop for *IDR* larger than the MRF. The percentage of column plastic hinges for the 10-storey MRF with dampers (ξ_{tot}=15%) that has the highest percentage is lower than 13% for *IDR* up to 10%. In the 10-storey MRFs with dampers (ξ_{tot}=20%) as θ decreases the percentage of column plastic hinges decreases. The percentage of column plastic

hinges for the 10-storey MRF with dampers (ξ_{tot}=20%) that has the highest percentage is lower than 16% for *IDR* up to 10%. For the proposed allowable value of coefficient θ for ξ_{tot}=10%, the results indicate that the 10-storey MRF with dampers will develop similar or lower percentage of column plastic hinges than the MRF, while for the 10-storey MRFs with dampers (ξ_{tot}=15%, 20%) a stricter capacity design rule could be proposed.

The 20-storey MRFs with dampers (ξ_{tot}=10%, 15%, 20%) have significantly lower percentage of column plastic hinges compared to the 20-storey MRF due to the stricter capacity design of columns in the force path of viscous dampers. Plastic hinges in the 20-storey MRFs with and without dampers develop for *IDR* larger than 3% and their median percentage value for the MRF with dampers that has the highest percentage is lower than 7% and for the MRF without dampers is lower than 22% for *IDR* up to 10%. These results indicate that a SF less than 3.5 could be used in the modified capacity design rule for the interior columns in the force path of viscous dampers.

It can also be noted that the 5-storey and the 10-storey MRFs with dampers with lower performance compared to the MRFs have lower percentage of column plastic hinges compared to the MRFs and with higher performance have higher percentage of column plastic hinges. This observation does not apply to the 20-storey MRFs due to the stricter capacity design rule.

Moreover, it is important to note that none of the 5-storey and the 20-storey MRFs with dampers experience column plastic hinges under the MCE seismic intensities while few plastic hinges were observed for some ground motions in the 10-storey MRFs with dampers.

The benefits of using viscous dampers in steel reduction, shall not be extracted from this study, as the section group that is assigned to columns (i.e. HEB, W12, W24) might not be the optimum.

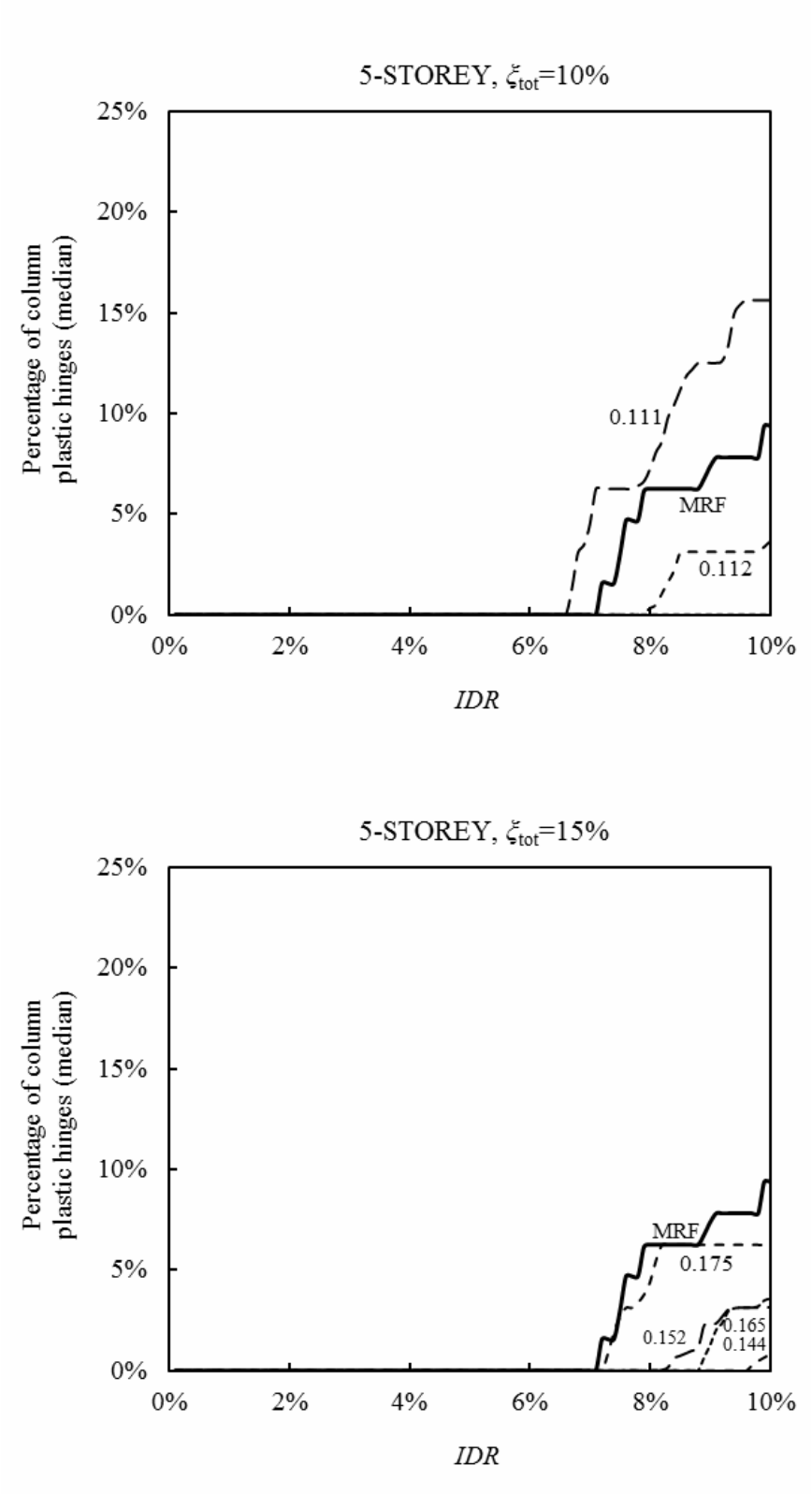

Figure 5.7 Percentage of column plastic hinges in the steel MRF and the MRFs with dampers

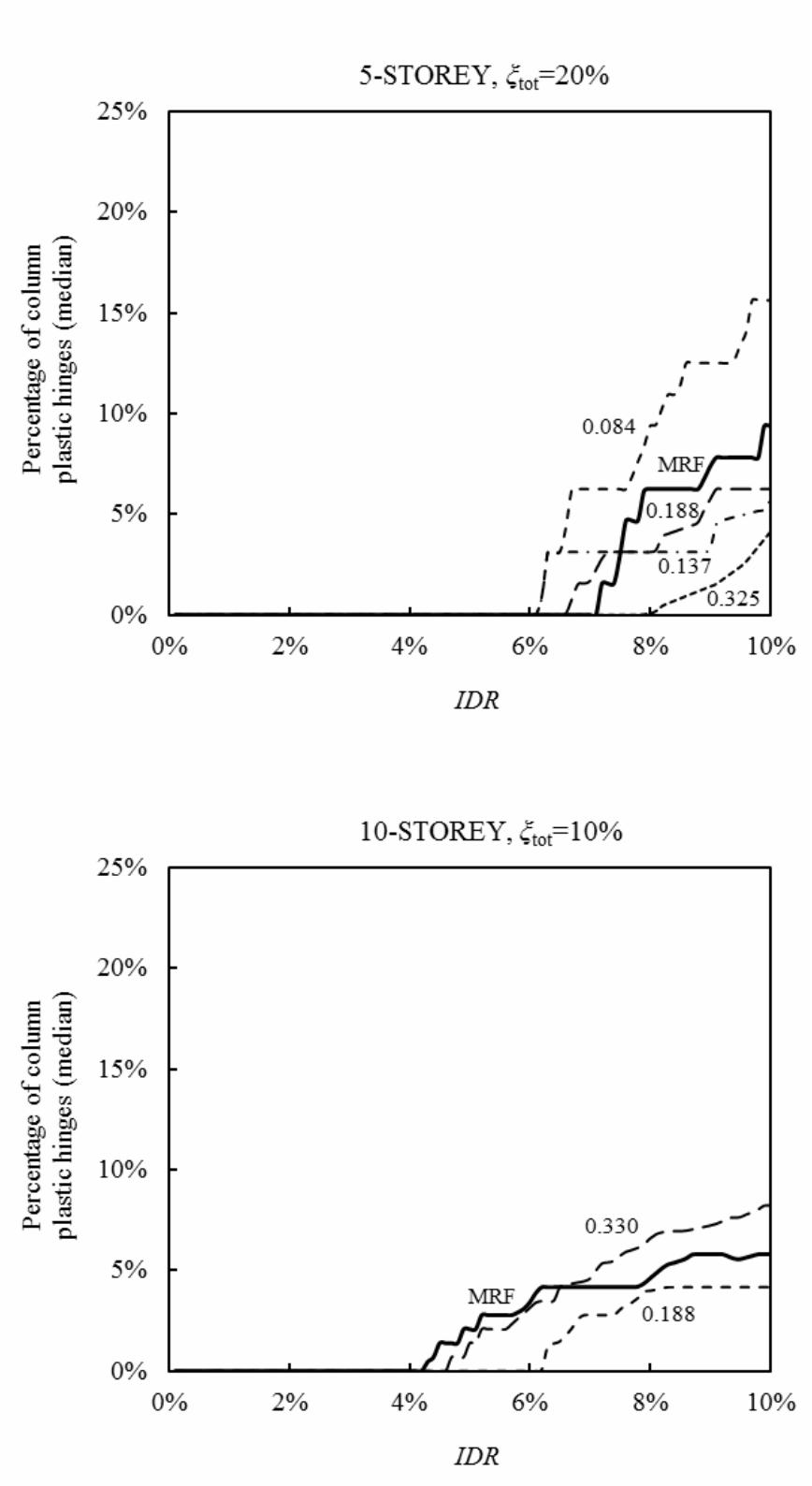

Figure 5.8 Percentage of column plastic hinges in the steel MRFs and the MRFs with dampers

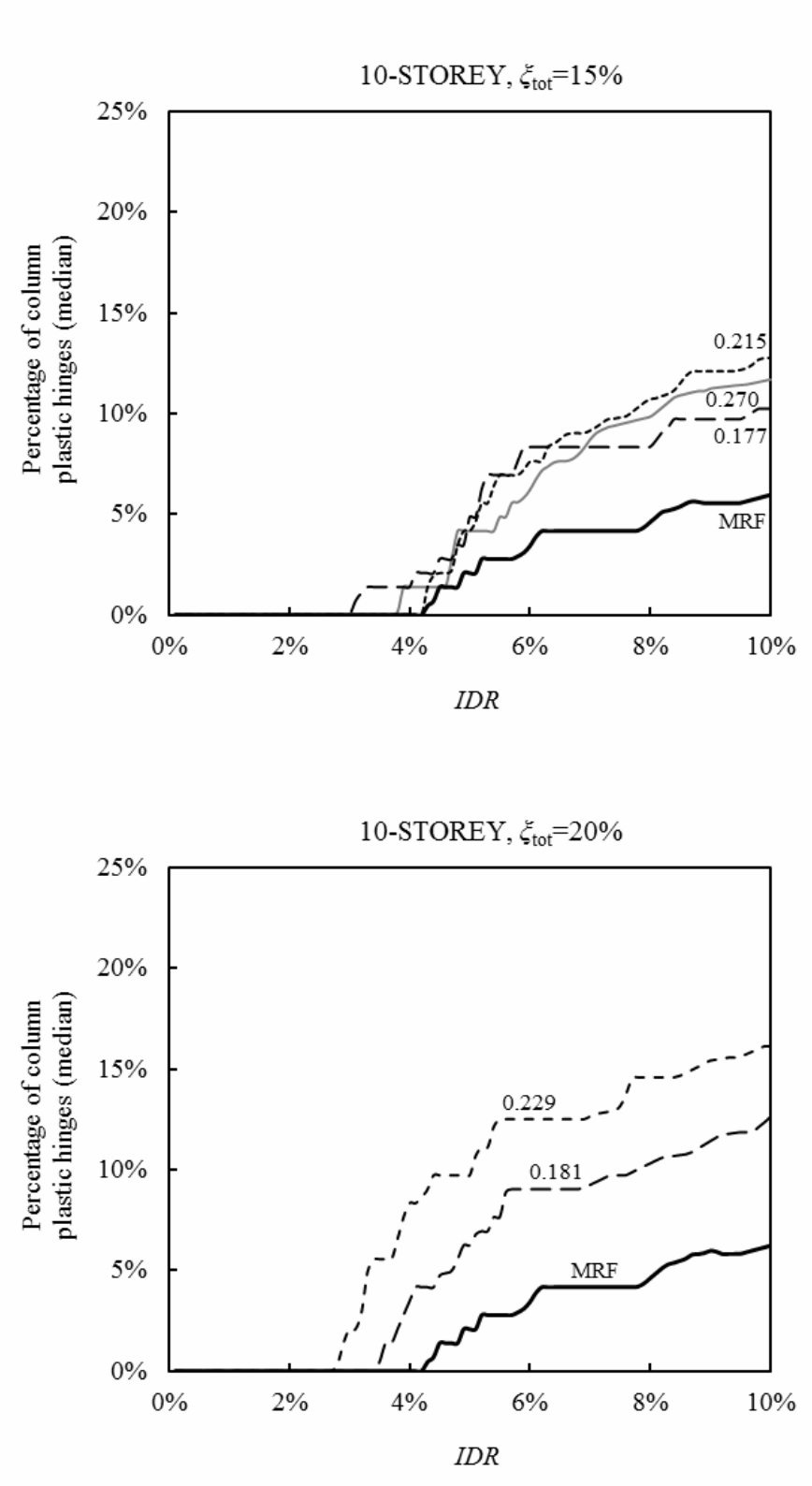

Figure 5.9 Percentage of column plastic hinges in the steel MRF and the MRFs with dampers

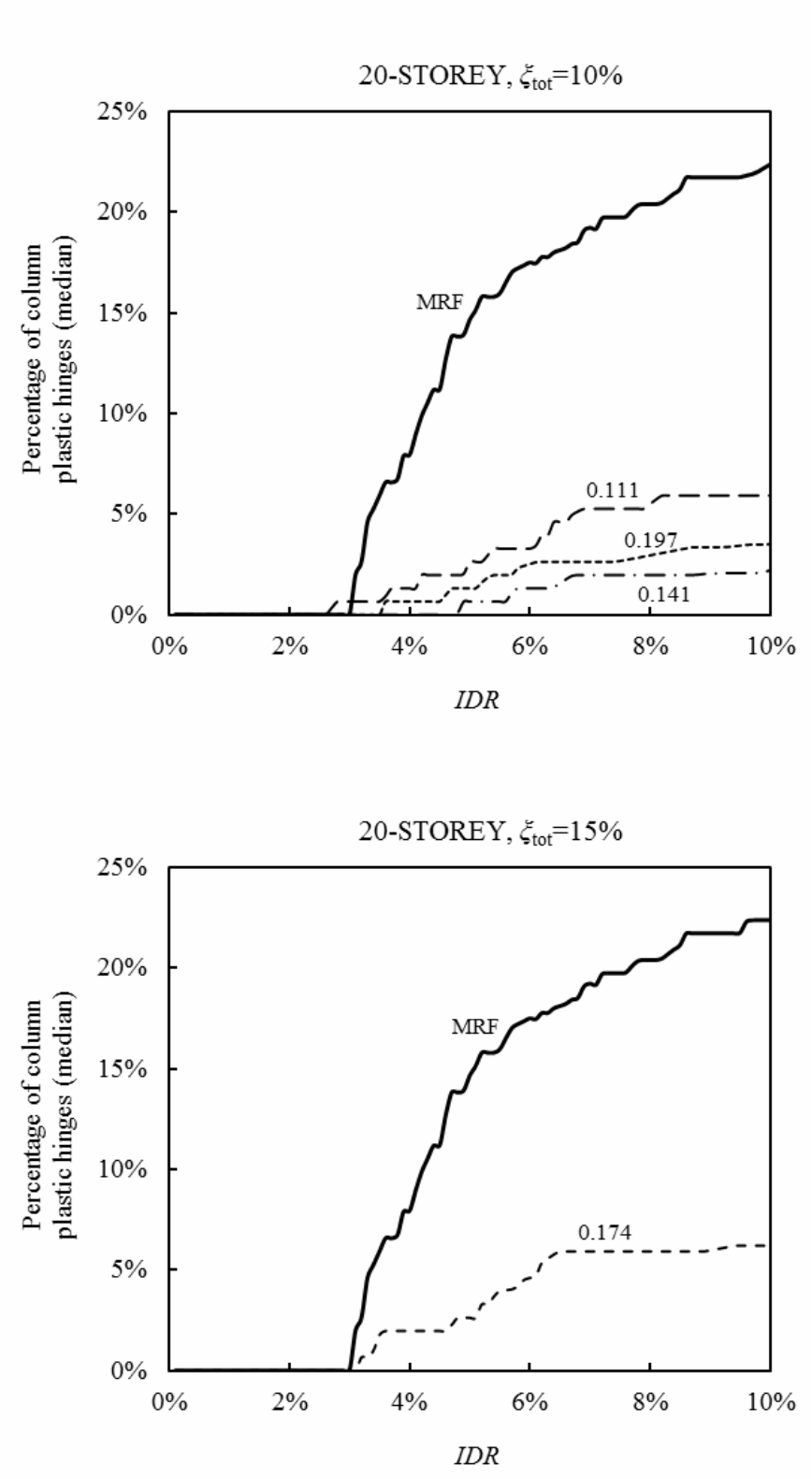

Figure 5.10 Percentage of column plastic hinges in the steel MRF and the MRFs with dampers

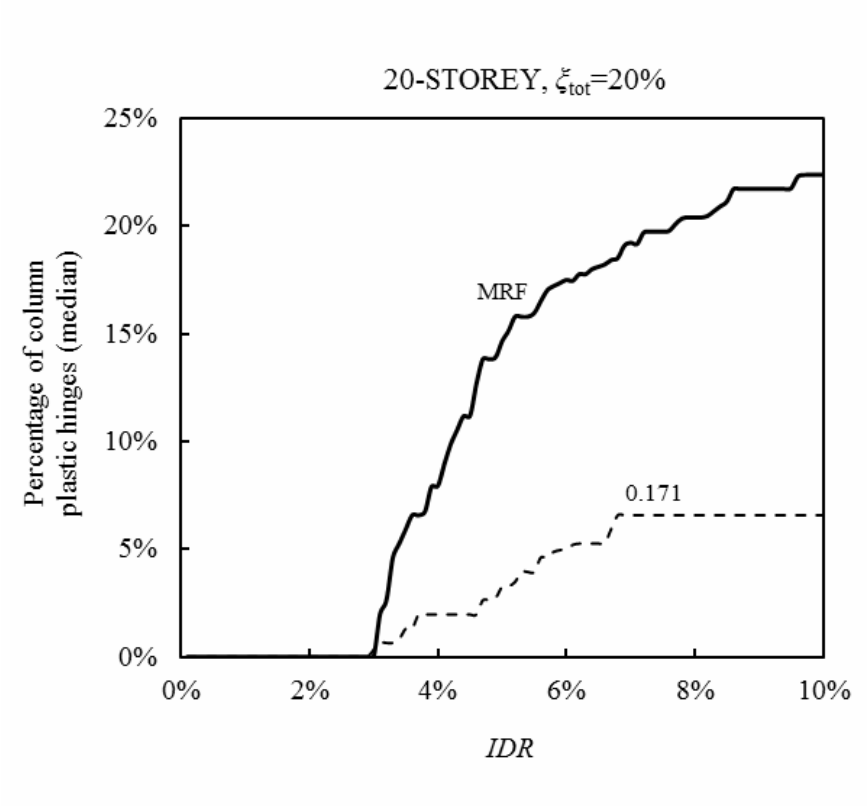

Figure 5.11 Percentage of column plastic hinges in the steel MRF and the MRF with dampers

5.5 Summary

In this chapter, a number of steel MRFs with viscous dampers, more flexible than the conventional steel MRFs, following the proposed seismic design procedure were designed with interstorey drift equal or lower than the conventional steel MRFs. The upper bound of storey drift sensitivity coefficient θ of the proposed design procedure was neglected. Three groups of MRFs with viscous dampers were designed to achieve a total viscous damping ratio, ξ_{tot}, at T_1 equal to 10%, 15% and 20%, respectively. Incremental dynamic analyses were conducted for steel MRFs with viscous dampers and their collapse resistance was compared with those of steel MRFs without viscous dampers. Appropriate limit values for the storey drift sensitivity coefficient θ were recommended to guarantee for steel MRFs with viscous dampers collapse resistance similar to those of steel MRFs without dampers. For buildings with more than 10 storeys and total viscous damping ratio more than 15%, limit values for the storey

drift sensitivity coefficient θ were not recommended as other loading conditions, such as wind, are expected to result in MRFs with collapse resistance similar or better than that of steel MRFs without dampers. Also, a comparison of their global plastic mechanisms was provided.

CHAPTER 6

CONCLUSIONS AND RECOMMENDATIONS FOR FUTURE RESEARCH

6.1 Conclusions

In this PhD thesis, the benefits of passive dampers were first outlined and a brief description of viscous dampers was presented. Then, a literature review of research on structures equipped with viscous dampers was provided. The existing studies highlight the benefits of the incorporation of viscous dampers in structures and they explore the influence of different parameters on the response. Structures with viscous dampers are prone to plastic mechanisms that involve hinges in columns because of the large column axial forces due to the large damper forces. Eurocode 8 does not provide design procedures for steel buildings with viscous dampers and the development of design procedures is needed with emphasis on design criteria related to sway plastic mechanism and collapse resistance.

The seismic design procedure for steel MRFs was provided, which satisfies the requirements of Eurocode 8. Then, a seismic design procedure for steel MRFs with viscous dampers was developed within the framework of Eurocode 8. A conservative design rule was proposed for the capacity design of the columns in the force path of viscous dampers. More specifically, the column axial force used to perform the capacity design is the envelope of the axial force from the peak drift state and the axial force from the peak velocity state. For the calculation of the damper forces which are needed for the proposed procedure, the response spectrum procedure of ASCE 7-10 was adopted and appropriate relations were derived to correlate the response spectrums of ASCE 7-10 and EC8.

Prototype buildings of 5, 10 and 20 storeys were designed using steel MRFs with and without viscous dampers. The MRFs with viscous dampers were designed to achieve a total viscous damping ratio, ξ_{tot}, at T_1 equal to 20%. Incremental dynamic analyses were conducted for all steel MRFs with and without viscous dampers. Their global plastic mechanisms were compared in order to explore whether more

conservative capacity design rules were needed for columns in the force path of viscous dampers that will guarantee plastic mechanisms similar to those of steel MRFs without dampers. The results of analyses showed that the proposed capacity design rule resulted in highly damped steel MRFs with plastic mechanisms similar to those of steel MRFs without dampers and needed to become stricter for buildings with more than 10 storeys to address that linear elastic analysis methods for structures with dampers underestimate the peak damper forces in the lower storeys of yielding tall steel MRFs.

A number of steel MRFs with viscous dampers, more flexible than the conventional steel MRFs, following the proposed seismic design procedure were designed with interstorey drift equal or lower than the conventional steel MRFs. The upper bound of storey drift sensitivity coefficient θ of the proposed design procedure was neglected. Three groups of MRFs with viscous dampers were designed to achieve a total viscous damping ratio, ξ_{tot}, at T_1 equal to 10%, 15% and 20%, respectively. Incremental dynamic analyses were conducted for steel MRFs with viscous dampers and their collapse resistance was compared with that of steel MRF without viscous dampers. Appropriate limit values for the storey drift sensitivity coefficient θ were recommended to guarantee for steel MRFs with viscous dampers collapse resistance similar to those of steel MRFs without dampers. For buildings with more than 10 storeys and total viscous damping ratio more than 15%, limit values for the storey drift sensitivity coefficient θ were not recommended as other loading conditions, such as wind, are expected to result in MRFs with collapse resistance similar or better than that of steel MRFs without dampers. Also, a comparison of their global plastic mechanisms was provided.

The conclusions drawn from this research are the following:

- Linear elastic analysis methods for structures with dampers underestimate the peak damper forces in the lower storeys of yielding tall steel MRFs and the capacity design rule of the proposed design procedure addresses this issue by becoming stricter for buildings with more than 10 storeys. The scale factor used in the capacity design rule of the proposed design procedure is equal to 1.0 for buildings with up to 10 storeys and equal to 3.5 for buildings of 20 storeys. Linear interpolation is suggested to approximately calculate the

appropriate scale factor value for buildings with number of storeys between 10 and 20.

- The proposed design procedure for steel MRFs with viscous dampers, for the case of incorporation of viscous dampers in an existing 5-storey steel MRF to provide total viscous damping ratio equal to 20%, results in a steel MRF with lower percentage of column plastic hinges compared to the steel MRF without dampers. Plastic hinges in the steel MRF with dampers develop for *IDR* larger than 7% and their median percentage value is lower than 5% for *IDR* up to 10%.

- The proposed design procedure for steel MRFs with viscous dampers, for the case of incorporation of viscous dampers in an existing 10-storey steel MRF to provide total viscous damping ratio equal to 20%, results in a steel MRF with slightly higher percentage of column plastic hinges compared to steel MRF without dampers. An appreciable difference between the plastic mechanisms of the two frames is seen for *IDR* larger than 8%. The median value of the percentage of column plastic hinges for the steel MRF with dampers is lower than 10% for *IDR* up to 10%.

- The proposed design procedure for steel MRFs with viscous dampers, for the case of incorporation of viscous dampers in an existing 20-storey steel MRF to provide total viscous damping ratio equal to 20%, results in a steel MRF with slightly higher percentage of column plastic hinges compared to steel MRF without dampers. The median value of the percentage of column plastic hinges for the steel MRF with dampers is equal to 25% for *IDR* equal to 10%, while the same percentage for the steel MRF without dampers is equal to 22%.

- The proposed design procedure for steel MRFs with viscous dampers, for the case of incorporation of viscous dampers in an existing steel MRF to provide total viscous damping ratio equal to 20%, results in no increase of steel weight for the case of a 5-storey steel MRF, in 5% increase for a 10-storey steel MRF and in 10% increase for a 20-storey steel MRF.

- The average values of the peak damper forces from nonlinear dynamic analysis of highly damped steel MRFs are higher than the peak damper forces predicted by the procedure of ASCE 7-10 and their difference increases for taller steel MRFs. Moreover, their difference increases from the top to the bottom of the building. The maximum ratios are equal to 1.30, 1.95 and 2.41 for a 5-storey, 10-storey and 20-storey steel MRF with dampers, respectively.

- Reduction in the steel weight of the steel MRFs with viscous dampers can be achieved without compromising the seismic performance.

- For a 5-storey steel MRF with viscous dampers, the limit values for the storey drift sensitivity coefficient θ which are recommended to guarantee collapse resistance similar to that of a steel MRF without dampers, are equal to 0.120, 0.142 and 0.158 for total viscous damping ratio of 10%, 15% and 20%, respectively.

- For a 10-storey steel MRF with viscous dampers, the limit value for the storey drift sensitivity coefficient θ which is recommended to guarantee collapse resistance similar to that of a steel MRF without dampers, is equal to 0.317 for total viscous damping ratio of 10%. Limit values for total viscous damping ratio more than 15% are not recommended as other loading conditions, such as wind, will result in an MRF with collapse resistance similar or better than that of a steel MRF without dampers.

- For a 20-storey steel MRF with viscous dampers, limit values are not recommended as other loading conditions, such as wind, will result in an MRF with collapse resistance similar or better than that of a steel MRF without dampers.

6.2 Recommendations for future research

- Evaluation of the proposed design procedure employing nonlinear models that account for the moment-axial force interaction effects, the strength and the stiffness deterioration effects in the columns.

- Evaluation of the proposed design procedure employing nonlinear models that consider the limit states of viscous dampers that could occur when the piston reaches its stroke limit.

- Evaluation of the proposed design procedure accounting for the sources of collapse uncertainty (e.g. record-to-record, design requirement, test data and modeling).

- Evaluation of the proposed design procedure using ground motions that exhibit near-fault pulse characteristics.

- Establishment of the allowable values of the storey drift sensitivity coefficient θ for the proposed design procedure within the framework of EC8 for other seimic zones than the selected in this study and for buildings with other limitations of interstorey drift as described in EC8.

- Evaluation of the proposed design procedure for buildings with nonlinear viscous dampers and development of similar design procedures for buildings with other passive supplemental devices such as viscoelastic dampers, friction dampers and metallic dampers.

- Evaluation of the economic seismic losses in buildings with viscous dampers designed with the proposed procedure.

REFERENCES

Aiken I, Kelly J (1990) Earthquake simulator testing and analytical studies of two energy absorbing systems for multistory structures. Report No. UCB/EERC 90/03, University of California, Berkeley, CA

ASCE 7-10 (2010) Minimum Design Loads for Buildings and Other Structures. American Society of Civil Engineers, Reston, Virginia

Bergman D, Hanson R (1993) Viscoelastic mechanical damping devices tested at real earthquake displacements. Earthq Spectra 9(3):389–418

Bisch P, Carvalho E, Degee H, Fajfar P, Fardis M, Franchin P, Kreslin M, Pecker A, Pinto P, Plumier A, Somja H, Tsionis G (2012) Eurocode 8: Seismic design of buildings worked examples. JRC, European Commission

Black C, Makris N, Aiken I (2004) Component testing, seismic evaluation and characterization of buckling-restrained braces. J Struct Eng 130(6):880–894

Chang K, Soong T, Lai M, Nielsen E (1993) Development of a design procedure for structures with added viscoelastic dampers. ATC-17–1 Seminar on Seismic Isolation, Passive Energy Dissipation and Active Control, Vol. 2, ATC 473–484

Champion C, Liel A (2012) The effect of near-fault directivity on building seismic collapse risk. Earthq Eng Struct Dynam 41:1391-1409

Christopoulos C, Filiatrault A (2006) Principles of passive supplemental damping and isolation. IUSS press

Constantinou M, Symans M (1992) Experimental and analytical investigation of seismic response of structures with supplemental fluid viscous dampers. NCEER-92-0032. National Center for Earthquake Engineering Research, Technical report, Buffalo, New York

Dong B, Sause R, Ricles JM (2016) Seismic response and performance of a steel MRF building with nonlinear viscous dampers under DBE and MCE. J Struct Eng 142(6)

Eurocode 3 (2009) Design of Steel Structures. European Committee for Standardization (CEN), Brussels

Eurocode 8 (2013) Design of Structures for Earthquake Resistance. European Committee for Standardization (CEN), Brussels

FEMA 273 (1997) NEHRP Guidelines for the seismic rehabilitation of buildings. Building Seismic Safety Council National Institute of Building Sciences, Washington D.C.

FEMA 274 (1997) NEHRP Guidelines for the seismic rehabilitation of buildings (Commentary). Building Seismic Safety Council National Institute of Building Sciences, Washington D.C.

FEMA 356 (2000) Prestandard and Commentary for the seismic rehabilitation of buildings. Federal Emergency Management Agency, Washington D.C.

FEMA 368 (2000) NEHRP Recommended provisions for seismic regulations for new buildings and other structures. Building Seismic Safety Council National Institute of Building Sciences, Washington D.C.

FEMA 369 (2000) NEHRP Recommended provisions for seismic regulations for new buildings and other structures (Commentary). Building Seismic Safety Council National Institute of Building Sciences, Washington D.C.

FEMA 450 (2003) NEHRP Recommended provisions for seismic regulations for new buildings and other structures. Building Seismic Safety Council National Institute of Building Sciences, Washington D.C.

FEMA 451B (2007) NEHRP Recommended provisions for new buildings and other structures: Training and instructional materials. Building Seismic Safety Council National Institute of Building Sciences, Washington D.C.

FEMA P695 (2009) Quantification of building seismic performance factors. Report. Federal Emergency Management Agency, Washington D.C.

Goel R (2002) Influence of inclined viscous damper on column axial force. Report no. CP/SEAM-2002/03, California Polytechnic State University, San Luis Obispo, CA

Grigorian C, Yang T, Popov E (1993) Slotted bolted connection energy dissipators. Earthq Spectra 9(3):491–504

Guo JWW, Christopoulos C (2013a) Performance spectra-based design method for the seismic design of structures equipped with passive supplemental damping systems. Earthq Eng Struct Dynam 42(6):935-952

Guo JWW, Christopoulos C (2013b) A procedure for generating performance spectra for structures equipped with passive supplemental dampers. Earthq Eng Struct Dynam 42(9):1321-1338

Ibarra L, Krawinkler H (2005) Global collapse of frame structures under seismic excitations. Report no 152. The John A. Blume Earthquake Engineering Center, Stanford, California

Karavasilis TL, Seo C-Y (2011) Seismic structural and non-structural performance evaluation of highly damped self-centering and conventional systems. Eng Struct 33:2248-2258

Karavasilis TL (2016) Assessment of capacity design of columns in steel moment resisting frames with viscous dampers. Soil Dynam Earthq Eng 88:215-222

Kasai K, Fu Y (1998) Comparative study of frames using viscoelastic and viscous dampers. J Struct Eng 124(5):513-522

Kasai K, Motoyui S, Ozaki H, Ishii M, Ito H, Kajiwara K, Hikino T (2009) Full-scale tests of passively-controlled 5-story steel building using E-Defense shake table. Part 1: Test concept, method, and building specimen. Proceedings of the sixth international conference on behaviour of steel structures in seismic areas. Philadelphia

Krawinkler H (1978) Shear design of steel frame joints. Eng J AISC 15(2):82-91

Landolfo R (2013) Assessment of EC8 provisions for seismic design of steel structures. European Convention for Constructional Steelwork (ECCS), Technical Committee 13 Seismic Design

Lignos DG, Krawinkler H (2011) Deterioration modeling of steel components in support of collapse prediction of steel moment frames under earthquake loading. J Struct Eng 137(11):1291–1302

Lin R, Liang Z, Soong T, Zhang R (1988) An experimental study of seismic structural response with added viscoelastic dampers. NCEER-88-0018. National Center for Earthquake Engineering Research, Technical report, Buffalo, New York

Lin W, Chopra A (2002) Earthquake response of elastic SDF Systems with non-linear fluid viscous dampers. Earthq Eng Struct Dynam 31:1623-1642

Lin W, Chopra A (2003) Earthquake response of elastic single-degree-of-freedom systems with nonlinear viscoelastic dampers. J Eng Mech 129(6):597-606

Miyamoto HK, Gilani AS, Wada A, Ariyaratana C (2010) Limit states and failure mechanisms of viscous dampers and the implications for large earthquakes. Earthq Eng Struct Dynam 39(11):1279-1297

New Zealand (2013) Treasury Budget Speech. Available online: http://www.treasury.govt.nz/ budget/2013/speech/06.htm (accessed on 14 May 2014)

Newell J, Uang CM (2006) Cyclic behaviour of steel columns with combined high axial load and drift demand. Report No. SSRP-06/22. Department of Structural Engineering, University of California, San Diego, La Jolla

OpenSees (2016) Open system for earthquake engineering simulation. Pacific Earthquake Engineering Research Center, University of California at Berkeley, Berkeley, CA

Pall A, Marsh C (1982) Seismic response of friction damped braced frames. J Struct Div 108(6):1313–1323

Pavlou E, Constantinou MC (2006) Response of nonstructural components in structures with damping systems. J Struct Eng 132(7):1108-1117

Polat E, Constantinou M (2017) Open-space damping system description, theory and verification. J Struct Eng 143(4)

Ramirez OM, Constantinou MC, Kircher CA, Whittaker AS, Johnson MW, Gomez JD, Chrysostomou CZ (2000) Development and evaluation of simplified procedures for analysis and design of buildings with passive energy dissipation systems. MCEER-00-0010. Multidisciplinary Center for Earthquake Engineering Research, Technical report, Buffalo, New York

Ramirez OM, Constantinou MC, Gomez JD, Whittaker AS, Chrysostomou CZ (2002a) Evaluation of simplified methods of analysis of yielding structures with damping systems. Earthq Spectra 18(3):501-530

Ramirez OM, Constantinou MC, Whittaker AS, Kircher CA, Chrysostomou CZ (2002b) Elastic and inelastic seismic response of buildings with damping systems. Earthq Spectra 18(3):531-547

Ramirez O, Constantinou M, Whittaker A, Kircher C, Johnson M, Chrysostomou C (2003) Validation of 2000 NEHRP provisions' equivalent lateral force and modal

analysis procedures for buildings with damping systems. Earthq Spectra 19(4):981-999

Robinson W, Greenbank L (1976) An extrusion absorber suitable for the protection of structures during an earthquake. Earthq Eng Struct Dynam 4:251-259

Seleemah A, Constantinou MC (1997) Investigation of seismic response of buildings with linear and nonlinear fluid viscous dampers. NCEER-97–0004. National Center for Earthquake Engineering Research, Technical report, Buffalo, New York

Seo C-Y, Karavasilis TL, Ricles JM, Sause R (2014) Seismic performance and probabilistic collapse resistance of steel moment resisting frames with fluid viscous dampers. Earthq Eng Struct Dynam 43(14):2135-2154

Symans M, Charney F, Whittaker A, Constantinou M, Kircher C, Johnson M, McNamara R (2008) Energy dissipation systems for seismic applications: current practice and recent developments. J Struct Eng 134(1):3-21

Taylor Devices Inc. Accessible to http://www.taylordevices.com

Tsai K, Chen H, Hong C, Su Y (1993) Design of steel triangular plate energy absorbers for seismic-resistant construction. Earthq Spectra 9(3):505-528

Vamvatsikos D, Cornell CA (2002) Incremental dynamic analysis. Earthq Eng Struct Dynam 31(3):491-514

Wanitkorkul A, Filiatrault A (2008) Influence of passive supplemental damping systems on structural and nonstructural seismic fragilities of a steel building. Eng Struct 30(3):675-682

Whittaker A, Bertero V, Thompson C, Alonso L (1991) Seismic testing of steel-plate energy dissipating devices. Earthq Spectra 7(4):563–604

Whittaker A, Constantinou M, Ramirez O, Johnson M, Chrysostomou C (2003) Equivalent lateral force and modal analysis procedures of the 2000 NEHRP provisions for buildings with damping systems. Earthq Spectra 19(4):959-980

Whittle J, Williams MS, Karavasilis TL, Blakeborough A (2012) A comparison of viscous damper placement methods for improving seismic building design. J Earthq Eng 16:540-560

Zareian F, Medina R (2010) A practical method for proper modeling of structural damping in inelastic plane structural systems. Comp and Struct 88:45-53

APPENDIX A

DESIGN OF STEEL MRFS WITHOUT DAMPERS

The seismic design procedure for steel MRFs without dampers which satisfies the requirements of Eurocode 8 is the following:

Step 1

Design the structural elements of the structure, using the design spectrum, to satisfy the limitation of interstorey drift ratio (*IDR*) given in Section 4.4.3.2 of Eurocode 8 (EC8) and the limitation of storey drift sensitivity coefficient θ given in Section 4.4.2.2(2) of EC8:

$$\theta = \frac{P_{\text{tot}} \cdot d_r}{V_{\text{tot}} \cdot h} \tag{A.1}$$

where P_{tot} : total axial forces at the bottom of the columns of the storey due to gravity loads in the seismic design combination (i.e. $G + \psi_2 Q$)

d_{r} : design interstorey drift

V_{tot} : total seismic shear at the bottom of the storey

h : storey height

If the coefficient θ is less than 0.10, P-Δ effects need not to be accounted. It shall not exceed the value of 0.30 and for values between 0.10-0.20, the P-Δ effects need to be accounted as described in Section 4.4.2.2(2) of EC8.

Step 2

Check the dissipative elements of MRF (i.e. beams, bottom of base columns, top of columns in the upper storey (Figure A.1)) that comply with the required cross-sectional class given in Section 6.5.3 of EC8 depending on the ductility class and the behaviour factor q used in the design.

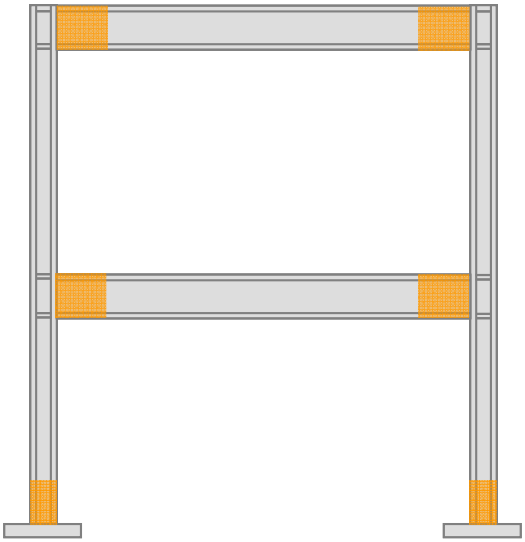

Figure A.1 Dissipative zones in MRFs

Step 3

The beams should verify the following expressions to ensure that their full plastic moment of resistance and rotation capacity are not decreased by compression and shear forces, for cross-sectional class 1,2 (Section 6.6.2(2) of EC8):

$$\frac{N_{Ed}}{N_{pl,Rd}} \leq 0.15 \tag{A.2}$$

$$\frac{V_{Ed}}{V_{pl,Rd}} \leq 0.50 \tag{A.3}$$

where N_{Ed} : design axial force

V_{Ed} : design shear force (Figure A.2)

$N_{pl,Rd}$: plastic axial resistance

$V_{pl,Rd}$: plastic shear resistance

and

$$V_{Ed} = V_{Ed,G} + \frac{M_{pl,Rd}^{\text{one end}} + M_{pl,Rd}^{\text{other end}}}{L} \tag{A.4}$$

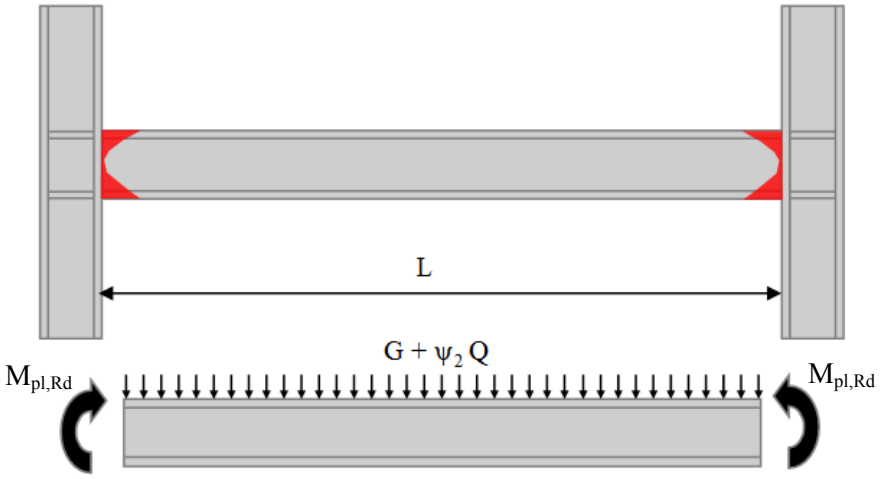

Figure A.2 Loading condition to consider in the calculation of V_{Ed}

where $V_{Ed,G}$: shear force due to non seismic actions

$M_{pl,Rd}$: plastic moment resistance

L : beam length

Step 4

The columns should satisfy the following expression (Section 6.6.3(4) of EC8):

$$\frac{V_{Ed}}{V_{pl,Rd}} \leq 0.50 \tag{A.5}$$

where V_{Ed} : design shear force

$V_{pl,Rd}$: plastic shear resistance

Also, the columns should be checked against axial forces, bending moments and shear forces (and their combinations) calculated from (Section 6.6.3(1) of EC8):

$$N_{Ed} = N_{Ed,G} + 1.1 \cdot \gamma_{ov} \cdot \Omega \cdot N_{Ed,E} \tag{A.6}$$

$$M_{Ed} = M_{Ed,G} + 1.1 \cdot \gamma_{ov} \cdot \Omega \cdot M_{Ed,E} \tag{A.7}$$

$$V_{Ed} = V_{Ed,G} + 1.1 \cdot \gamma_{ov} \cdot \Omega \cdot V_{Ed,E} \tag{A.8}$$

where N_{Ed} : design axial force

M_{Ed} : design bending moment

V_{Ed} : design shear force

$N_{Ed,G}$, $M_{Ed,G}$, $V_{Ed,G}$: axial force, bending moment, shear force due to non-seismic actions in the seismic design combination

$N_{Ed,E}$, $M_{Ed,E}$, $V_{Ed,E}$: axial force, bending moment, shear force due to the design seismic action

γ_{ov} : material overstrength factor (Section 6.2 of EC8)

Ω : overstrength factor (minimum $\frac{M_{pl,Rd}}{M_{Ed}}$ of all beams in the seismic design situation)

Step 5

All joints must satisfy the weak beam-strong column capacity design rule given in Section 4.4.2.3(4) of EC8:

$$\sum M_{Rc} \geq 1.3 \sum M_{Rb} \tag{A.9}$$

where ΣM_{Rc} : sum of the plastic moments of resistance of the columns framing the joint

ΣM_{Rb} : sum of the plastic moments of resistance of the beams framing the Joint

Note that in the calculation of ΣM_{Rc}, the column axial forces in the columns due to the amplified combination of actions in the seismic design situation as described in step 4, shall be used. This capacity design rule is waived at the beam-column joints in the upper storey.

Step 6

For acting moment equal to $M_{Pl,Rd}$ at the bottom of the base columns and the top of the columns in the upper storey, these columns shall satisfy all the member verifications.

Steps 1-6 need to be repeated until there is no change in the sections of the structural members.

APPENDIX B

DESIGN OF 5-STOREY STEEL MRF WITHOUT DAMPERS

The design steps of the 5-storey steel MRF without dampers in Chapter 4, as described in APPENDIX A with sample calculations, follow:

Step 1

Design the structural elements of the frame under the design load combinations of $1.35G + 1.5Q$ and $G + \psi_2 Q + E$ to satisfy the limitation of interstorey drift ratio under the DBE (IDR_{DBE}) for buildings having ductile non-structural elements:

$$IDR_{\mathrm{DBE}} = \frac{d_{\mathrm{r}}}{h} \le \frac{0.0075}{\nu} = 1.875\% \tag{B.1}$$

where $d_{\mathrm{r}} = q \cdot \left(d_{\mathrm{e}}^{\text{story top}} - d_{\mathrm{e}}^{\text{story bottom}} \right)$: design interstorey drift

q : behaviour factor

d_{e} : displacement based on the design spectrum

h : storey height

ν : reduction factor (= 0.4 for importance class II)

In the calculation of the displacement $q \cdot d_{\mathrm{e}}$ of a joint, does not need to be larger than the displacement calculated using the elastic spectrum. Also, the limitation of storey drift sensitivity coefficient θ shall be satisfied:

$$\theta = \frac{P_{\mathrm{tot}} \cdot d_r}{V_{\mathrm{tot}} \cdot h} \le 0.30 \tag{B.2}$$

where P_{tot} : total axial forces at the bottom of the columns of the storey due to gravity loads in the seismic design combination (i.e. $G + \psi_2 Q$)

V_{tot} : total seismic shear at the bottom of the storey

In this study, for coefficients θ within the range of 0.10-0.30, P-Δ effects are accounted through a second-order analysis. To satisfy the conditions of Equations (B.1) and (B.2), lower value of behaviour factor is used in the design (i.e. q = 2.3). Figure B.1 shows the cross-sections of the beams and columns. Figure B.2 shows the axial forces in columns due to gravity loads in the seismic design combination (i.e. $G + \psi_2 Q$) and Figure B.3 shows the shear forces in columns in the seismic design combination (i.e. $G + \psi_2 Q + E$). The calculations of the interstorey drift ratio under the DBE and the storey drift sensitivity coefficient θ are listed in Table B.1 for behaviour factor equal to 2.3. For the first time of the Step 1, the maximum *IDR* (i.e. 2.32%) is selected to exceed the limit such as after the completion of the other steps, the maximum *IDR* to meet the limit (i.e. 1.875%).

Step 2

The beams, the bottom of base columns and the top of columns in the upper storey are checked to comply with the required cross-sectional class of EC8 for the behaviour factor q used in the design. The behaviour factor used in the design is equal to 2.3 and the required cross-sectional class is 1 or 2. The class of all members of this frame is 1.

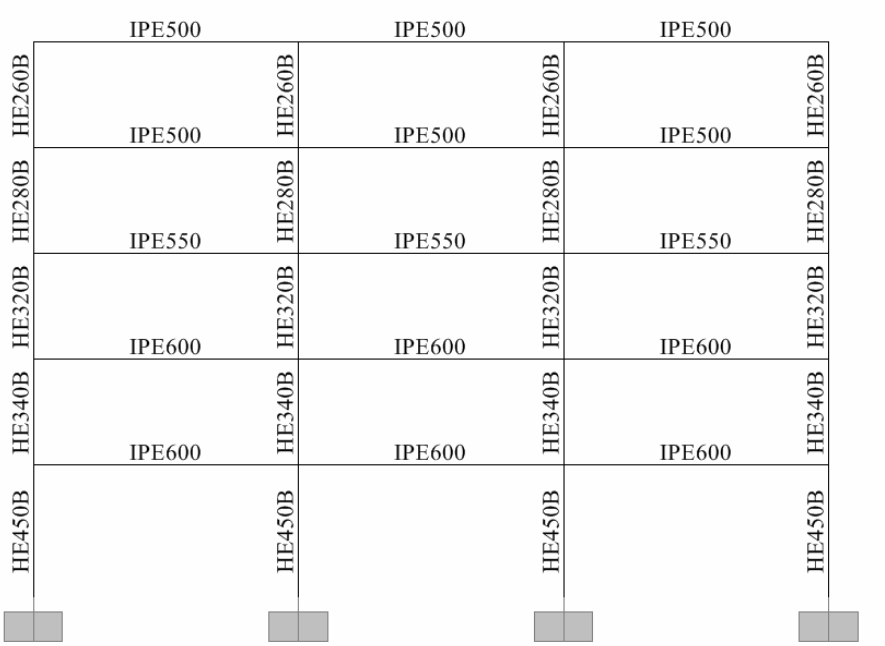

Figure B.1 Beam/column cross-sections

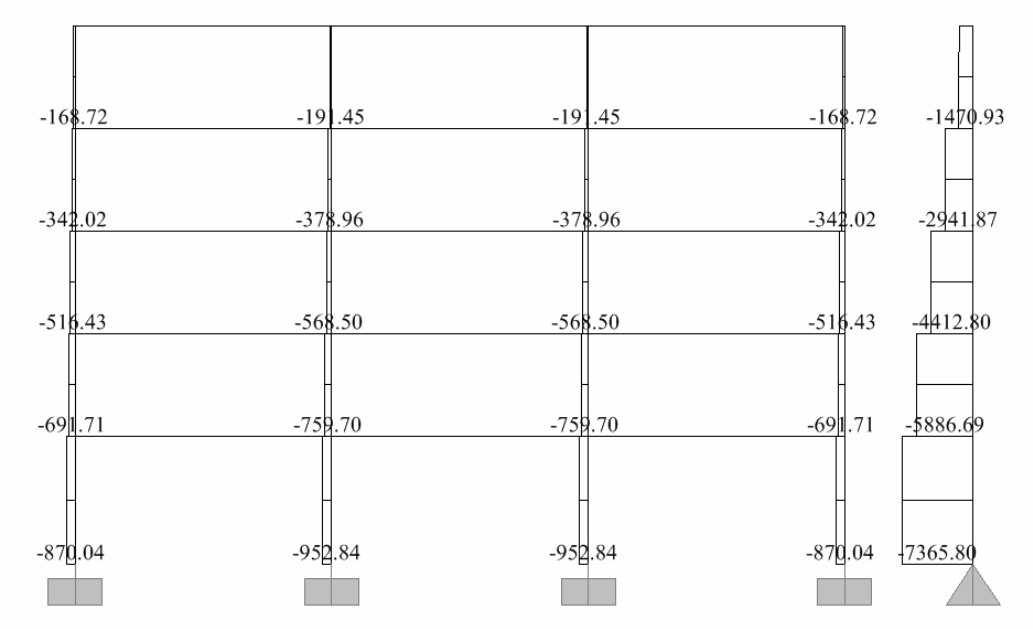

Figure B.2 Column axial forces (kN) under the combination of $G + \psi_2 Q$

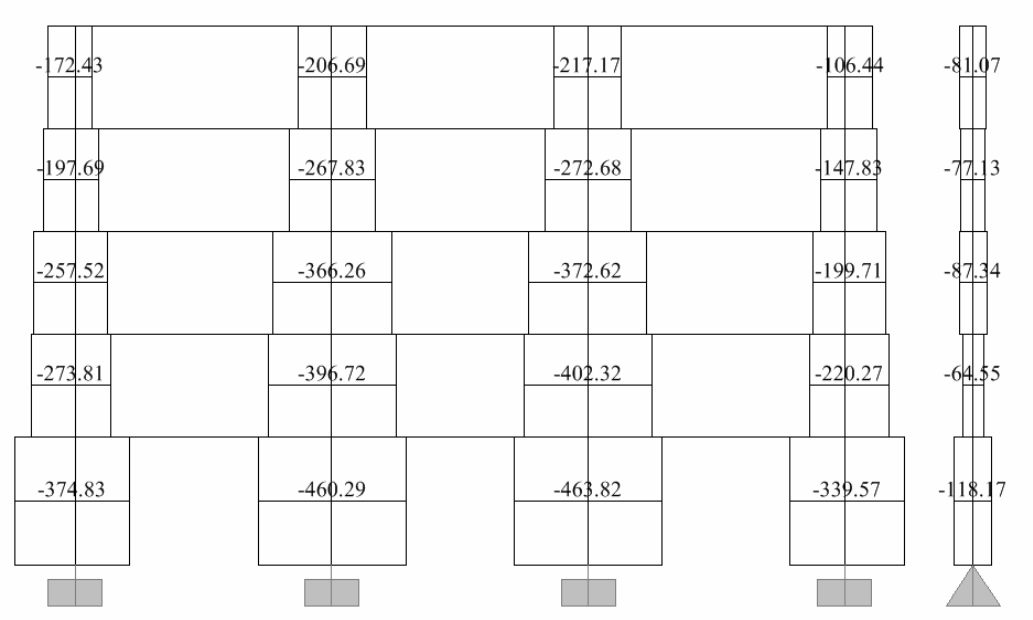

Figure B.3 Column shear forces (kN) under the combination of $G + \psi_2 Q + E$

Table B.1 *IDR* and θ

Storey	d_e (m)	d_r (m)	*IDR*	P_{tot} (kN)	V_{tot} (kN)	θ
1	0.028	0.064	1.61%	11011.57	1756.67	0.101
2	0.060	0.074	2.31%	8789.51	1357.67	0.150
3	0.092	0.074	2.31%	6582.66	1283.46	0.118
4	0.124	0.074	2.32%	4383.83	963.16	0.106
5	0.151	0.062	1.92%	2191.27	783.80	0.054

Step 3

The axial forces developed in beams under the design seismic combination are very small, therefore the condition that the axial forces shall be under 15% of their plastic axial resistance is satisfied (Equation (A.2)).

Also the following expression needs to be satisfied:

$$\frac{V_{Ed}}{V_{pl,Rd}} \leq 0.50 \tag{B.3}$$

Sample calculation for the beam of floor 3 shown in Figure B.4:

$$\text{Eq. (A.4)} \Rightarrow V_{Ed} = V_{Ed,G} + \frac{M_{pl,Rd}^{IPE550} + M_{pl,Rd}^{IPE550}}{L} = 90 + \frac{766.43 + 766.43}{8 - 2 \cdot \frac{0.32}{2}} = 289.59 \text{ kN}$$

$$\text{Eq. (B.3)} \Rightarrow V_{Ed} = 289.59 \text{ kN} < 0.50 V_{pl,Rd} = 0.50 \cdot 969.30 = 484.65 \text{ kN}$$

Step 4

The columns should satisfy the following expression:

$$\frac{V_{Ed}}{V_{pl,Rd}} \leq 0.50 \tag{B.4}$$

where V_{Ed} : design shear force

$V_{pl,Rd}$: plastic shear resistance

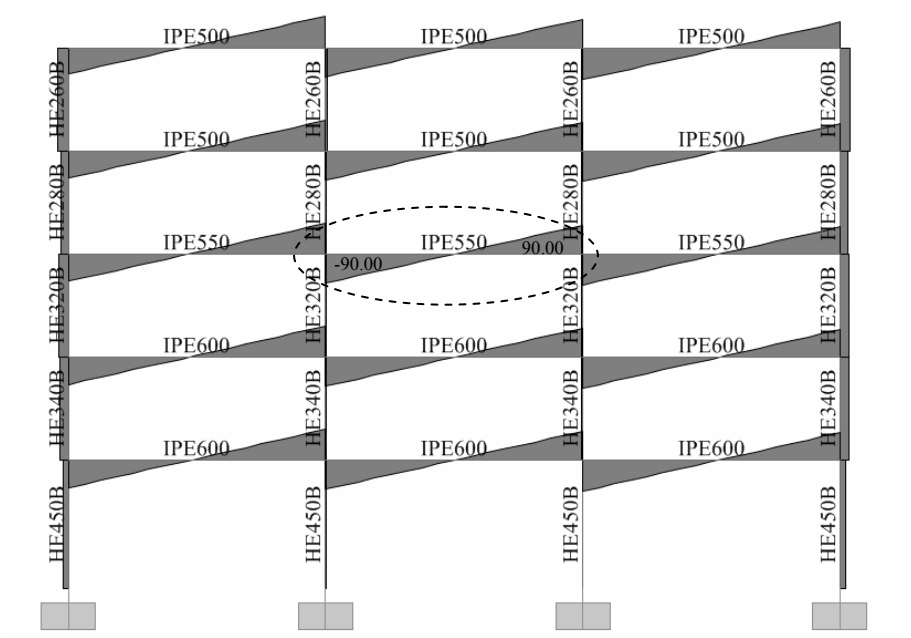

Figure B.4 Beam shear forces (kN) under the combination of $G + \psi_2 Q + E$

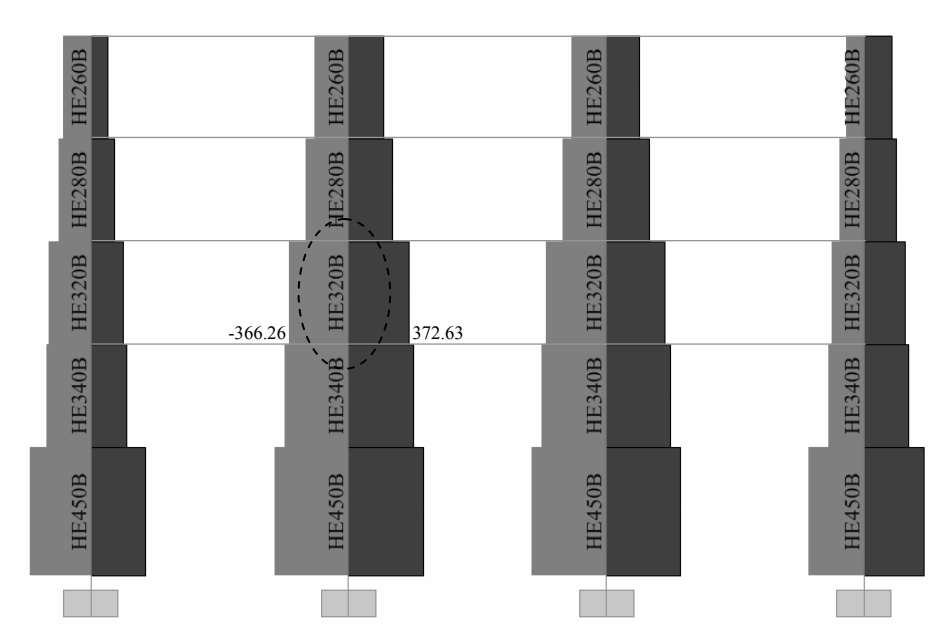

Figure B.5 Column shear forces (kN) under the combination of $G + \psi_2 Q + E$

Sample calculation for the interior column of floor 3 shown in Figure B.5:

$$\frac{V_{\text{Ed}}}{V_{\text{pl,Rd}}^{\text{HEB320}}} = \frac{372.63}{754.25} = 0.49 < 0.50$$

Also, the columns should be checked against axial forces, bending moments and shear forces (and their combinations) calculated from:

$$N_{\text{Ed}} = N_{\text{Ed,G}} + 1.1 \cdot \gamma_{\text{ov}} \cdot \Omega \cdot N_{\text{Ed,E}} \quad \text{(B.5)}$$

$$M_{\text{Ed}} = M_{\text{Ed,G}} + 1.1 \cdot \gamma_{\text{ov}} \cdot \Omega \cdot M_{\text{Ed,E}} \quad \text{(B.6)}$$

$$V_{\text{Ed}} = V_{\text{Ed,G}} + 1.1 \cdot \gamma_{\text{ov}} \cdot \Omega \cdot V_{\text{Ed,E}} \quad \text{(B.7)}$$

where

N_{Ed} : design axial force

M_{Ed} : design bending moment

V_{Ed} : design shear force

$N_{\text{Ed,G}}$, $M_{\text{Ed,G}}$, $V_{\text{Ed,G}}$: axial force, bending moment, shear force due to non-seismic actions in the seismic design combination

$N_{\text{Ed,E}}$, $M_{\text{Ed,E}}$, $V_{\text{Ed,E}}$: axial force, bending moment, shear force due to the design seismic action

γ_{ov} : material overstrength factor = 1.25 (section 6.2 of EC8)

Ω : overstrength factor (minimum $\frac{M_{\text{pl,Rd}}}{M_{\text{Ed}}}$ of all beams in the seismic design situation)

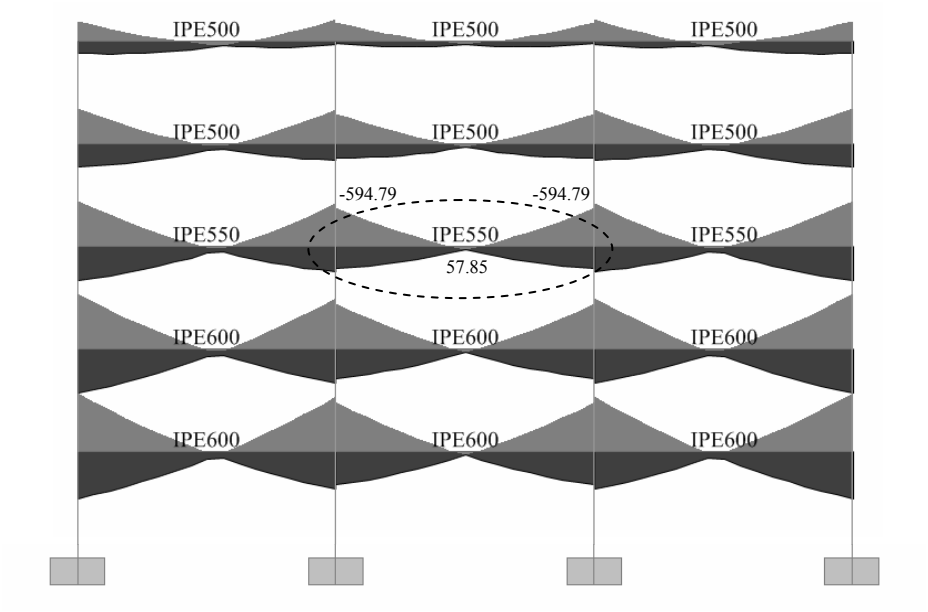

Figure B.6 Beam bending moments (kN·m) under the combination of $G + \psi_2 Q + E$

Sample calculation of the overstrength factor Ω for the beam of floor 3 shown in Figure B.6:

Middle of beam

$$\Omega = \frac{M_{\text{pl,Rd}}^{\text{IPE550}}}{M_{\text{Ed}}} = \frac{766.43}{57.85} = 13.249$$

End of beam

$$\Omega = \frac{M_{\text{pl,Rd}}^{\text{IPE550}}}{M_{\text{Ed}}} = \frac{766.43}{|-594.79|} = 1.289$$

Minimum Ω of all beams

$$\Omega = \text{minimum } \frac{M_{\text{pl,Rd}}}{M_{\text{Ed}}} = 1.055$$

The resulting cross-sections from this step are show in Figure B.7.

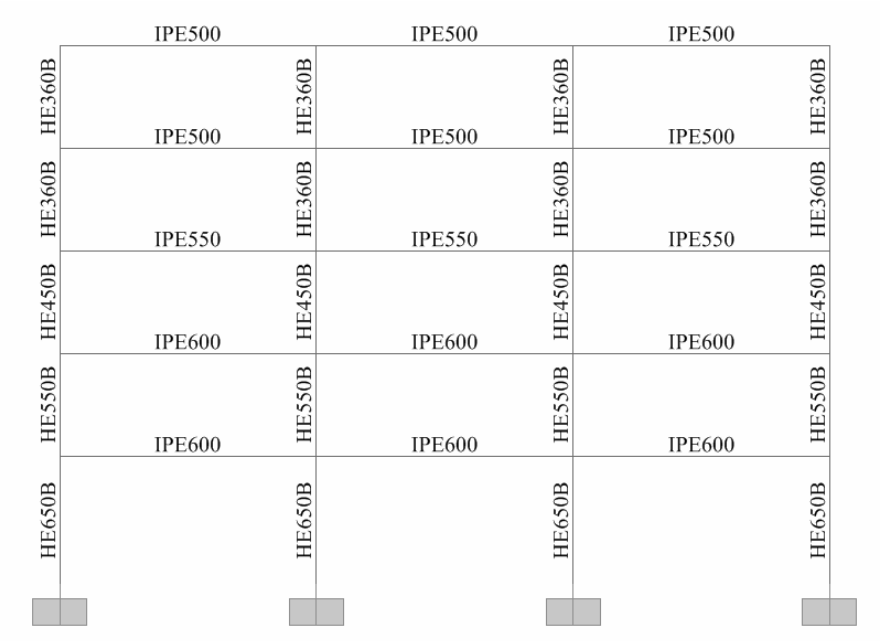

Figure B.7 Beam/column cross-sections

Step 5

All joints must satisfy the weak beam-strong column capacity design rule given in Section 4.4.2.3(4) of EC8:

$$\sum M_{\mathrm{Rc}} \geq 1.3 \sum M_{\mathrm{Rb}} \tag{B.8}$$

where ΣM_{Rc} : sum of the plastic moments of resistance of the columns framing the joint

ΣM_{Rb} : sum of the plastic moments of resistance of the beams framing the joint

Note that in the calculation of ΣM_{Rc}, the column axial forces in the columns due to the amplified combination of actions in the seismic design situation as described in step 4, shall be used (Bisch et al. 2012). This capacity design rule is waived at the beam-column joints in the upper storey.

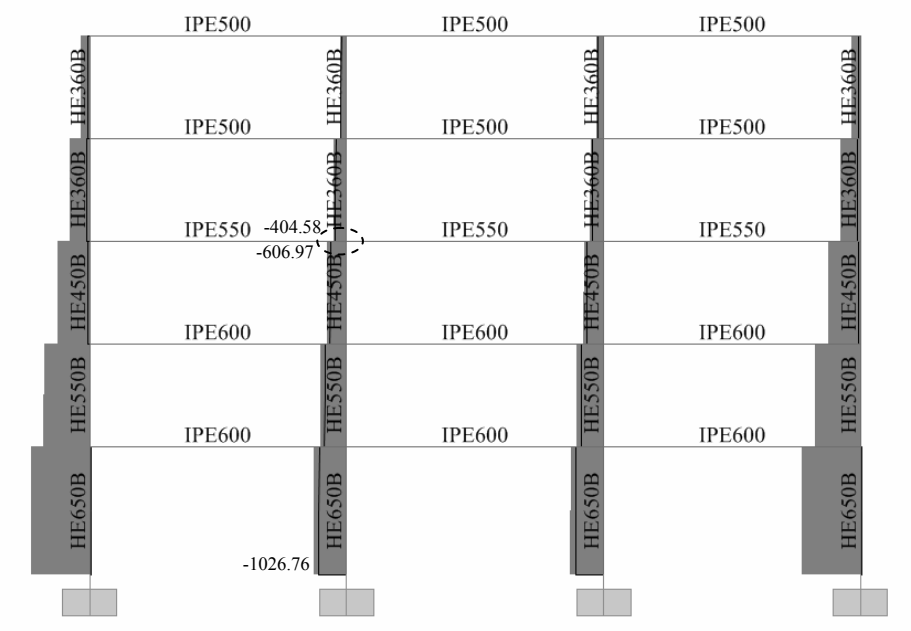

Figure B.8 Column axial forces (kN) under the combination of $G+\psi_2 Q+1.1\gamma_{ov}\Omega E$

Sample calculation for the interior joint of floor 3 shown in Figure B.8:

$$\sum M_{\mathrm{Rc}} \geq 1.3\sum M_{\mathrm{Rb}}$$

$$\Rightarrow M_{\mathrm{N,Rd}}^{\mathrm{HEB360}} + M_{\mathrm{N,Rd}}^{\mathrm{HEB450}} \geq 1.3\left(M_{\mathrm{pl,Rd}}^{\mathrm{IPE550}} + M_{\mathrm{pl,Rd}}^{\mathrm{IPE550}}\right)$$

$$\Rightarrow 952.47 + 1413.61 \geq 1.3\left(766.43 + 766.43\right)$$

$$\Rightarrow 2366.08\ \mathrm{kN \cdot m} \geq 1992.72\ \mathrm{kN \cdot m}$$

As pointed by Landolfo (2013), it is unclear why this double capacity design (i.e. use of Equations (B.5)-(B.7) and Equation (B.8)) is necessary, or which method should be given preference in terms of simplicity and efficiency in promoting a global sway plastic mechanism.

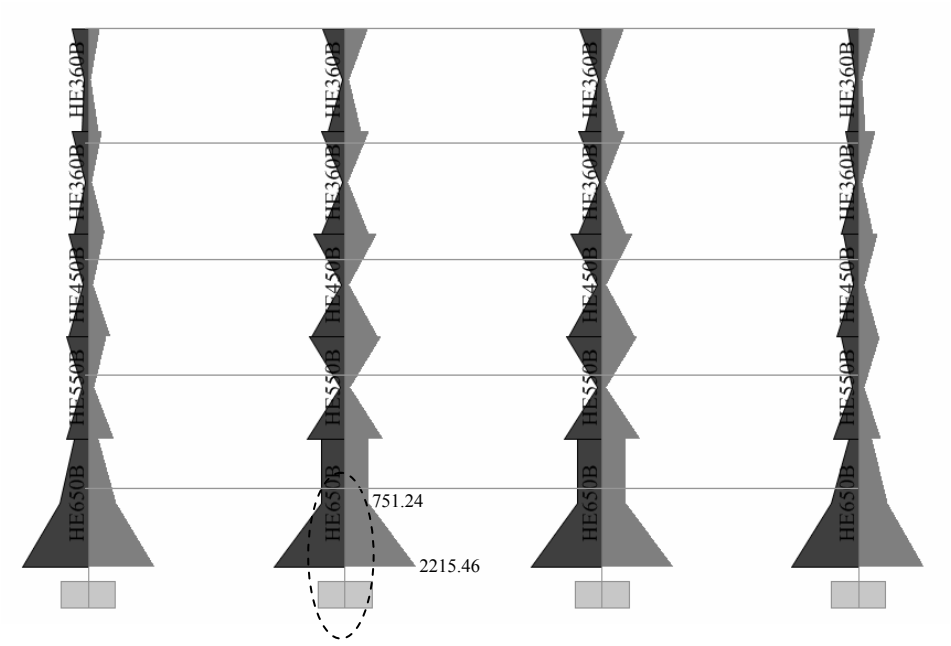

Figure B.9 Column bending moments (kN·m) under the combination of

$$G+\psi_2 Q+1.1\gamma_{ov}\Omega E$$

Step 6

The base columns are checked for the amplified axial forces, bending moments and shear forces but for acting moment at the bottom equal to $M_{pl,Rd}$.

Sample calculation for the interior base column shown in Figure B.9:

$M_{Ed}^{top} = 751.24\,\text{kN}\cdot\text{m}$

$M_{Ed}^{bottom} = 2215.46\,\text{kN}\cdot\text{m}$

$N_{Ed} = -1026.76\,\text{kN}$ (Figure B.8)

$V_{Ed} = 732.70\,\text{kN}$

$M_{pl,Rd}^{HEB650} = 2598.60\,\text{kN}\cdot\text{m}$

Bending and shear force (§6.2.8 of EC3):

For $V_{Ed} = 732.70 < 0.50\cdot V_{pl,Rd} = 0.50\cdot 2185.56 = 1092.78$,

$$M_{V,Rd} = 2598.60\,\text{kN}\cdot\text{m} > M_{Ed}^{top} = 751.24\,\text{kN}\cdot\text{m}$$

and

$$M_{\mathrm{V,Rd}} = 2598.60\,\mathrm{kN\cdot m} \geq M_{\mathrm{Ed}}^{\mathrm{bottom,acting}} = M_{\mathrm{pl,Rd}}^{\mathrm{HEB650}} = 2598.60\,\mathrm{kN\cdot m}$$

where $M_{\mathrm{V,Rd}}$: plastic moment resistance reduced due to shear force

Bending and axial force (§6.2.9 of EC3):

$$M_{\mathrm{N,Rd}} = 2598.60\,\mathrm{kN\cdot m} > M_{\mathrm{Ed}}^{\mathrm{top}} = 751.24\,\mathrm{kN\cdot m}$$

and

$$M_{\mathrm{N,Rd}} = 2598.60\,\mathrm{kN\cdot m} \geq M_{\mathrm{Ed}}^{\mathrm{bottom,acting}} = M_{\mathrm{pl,Rd}}^{\mathrm{HEB650}} = 2598.60\,\mathrm{kN\cdot m}$$

where $M_{\mathrm{N,Rd}}$: plastic moment resistance reduced due to axial force

Bending, shear and axial force (§6.2.10 of EC3):

For $V_{\mathrm{Ed}} = 732.70 < 0.50 \cdot V_{\mathrm{pl,Rd}} = 0.50 \cdot 2185.56 = 1092.78$,

$$M_{\mathrm{N,V,Rd}} = M_{\mathrm{N,Rd}} = 2598.60\,\mathrm{kN\cdot m} > M_{\mathrm{Ed}}^{\mathrm{top}} = 751.24\,\mathrm{kN\cdot m}$$

and

$$M_{\mathrm{N,V,Rd}} = M_{\mathrm{V,Rd}} = 2598.60\,\mathrm{kN\cdot m} \geq M_{\mathrm{Ed}}^{\mathrm{bottom,acting}} = M_{\mathrm{pl,Rd}}^{\mathrm{HEB650}} = 2598.60\,\mathrm{kN\cdot m}$$

where $M_{\mathrm{N,V,Rd}}$: plastic moment resistance reduced due to axial and shear force

Buckling resistance under bending and axial compression (§6.3.3 of EC3):

Unfavourable case:

For $M_{\mathrm{Ed}}^{\mathrm{top}} = 751.24\,\mathrm{kN\cdot m}$, $M_{\mathrm{Ed}}^{\mathrm{bottom,acting}} = 2598.60\,\mathrm{kN\cdot m}$ and $N_{\mathrm{Ed}} = 1026.76\,\mathrm{kN}$,

$$\frac{N_{\mathrm{Ed}}}{\chi_{\mathrm{y}} \cdot A \cdot f_{\mathrm{y}} / \gamma_{\mathrm{M1}}} + \frac{k_{\mathrm{yy}} \cdot M_{\mathrm{Ed}}^{\mathrm{bottom,acting}}}{\chi_{\mathrm{LT}} \cdot w_{\mathrm{pl,y}} \cdot f_{\mathrm{y}} / \gamma_{\mathrm{M1}}} \leq 1$$

$$\Rightarrow \frac{1026.76}{1.0 \cdot 0.0286 \cdot 355000/1.0} + \frac{0.715 \cdot 2598.60}{0.937 \cdot 0.00732 \cdot 355000/1.0} = 0.865 < 1$$

and

$$\frac{N_{\mathrm{Ed}}}{\chi_{\mathrm{z}} \cdot A \cdot f_{\mathrm{y}} / \gamma_{\mathrm{M1}}} + \frac{k_{\mathrm{zy}} \cdot M_{\mathrm{Ed}}^{\mathrm{bottom,acting}}}{\chi_{\mathrm{LT}} \cdot w_{\mathrm{pl,y}} \cdot f_{\mathrm{y}} / \gamma_{\mathrm{M1}}} \leq 1$$

$$\Rightarrow \frac{1026.76}{0.755 \cdot 0.0286 \cdot 355000/1.0} + \frac{0.429 \cdot 2598.60}{0.937 \cdot 0.00732 \cdot 355000/1.0} = 0.593 \leq 1$$

where k_{yy} : interaction factor (member not sucsceptible to torsional deformations and with non-sway buckling mode)

χ_y, χ_z : reduction factors due to flexural buckling

χ_{LT} : reduction factor due to lateral torsional buckling

A : cross-sectional area

f_{y} : yield strength

γ_{M1} : partial factor

$w_{\mathrm{pl,y}}$: plastic section modulus

Step 1 is repeated. *IDR* and coefficients θ are calculated and are listed in Table B.2. IDR exceeds the allowable *IDR* of 1.875%, therefore the Steps need to be repeated for a lower value of q until the allowable value to be met. Table B.3 - Table B.5 list the *IDR* and the coefficients θ of the final design of the 5-storey, 10-storey and 20-storey steel MRFs.

Table B.2 *IDR* and θ

Storey	d_{e} (m)	d_{r} (m)	*IDR*	P_{tot} (kN)	V_{tot} (kN)	θ
1	0.018	0.044	1.11%	11044.88	1980.03	0.062
2	0.042	0.055	1.73%	8814.43	1618.75	0.094
3	0.068	0.062	1.95%	6599.42	1442.21	0.089
4	0.095	0.065	2.04%	4394.96	1132.85	0.079
5	0.116	0.050	1.56%	2197.48	907.00	0.038

Table B.3 *IDR* and θ (5-storey, MRF, q = 2.4)

Storey	d_e (m)	d_r (m)	*IDR*	P_{tot} (kN)	V_{tot} (kN)	θ
1	0.019	0.045	1.13%	11055.71	2024.90	0.062
2	0.042	0.056	1.76%	8825.27	1705.94	0.091
3	0.066	0.057	1.79%	6610.25	1489.36	0.079
4	0.090	0.057	1.78%	4402.25	1186.69	0.066
5	0.108	0.044	1.38%	2201.13	881.21	0.034

Table B.4 *IDR* and θ (10-storey, MRF, q = 3.3)

Storey	d_e (m)	d_r (m)	*IDR*	P_{tot} (kN)	V_{tot} (kN)	θ
1	0.012	0.041	1.02%	22056.44	2012.64	0.112
2	0.027	0.049	1.52%	19811.97	1442.27	0.209
3	0.042	0.050	1.57%	17587.45	1483.15	0.186
4	0.056	0.046	1.44%	15367.19	1398.16	0.158
5	0.069	0.043	1.33%	13156.78	1328.53	0.132
6	0.082	0.043	1.33%	10949.12	1117.98	0.131
7	0.094	0.041	1.28%	8747.09	1026.63	0.109
8	0.107	0.041	1.28%	6555.32	824.05	0.102
9	0.118	0.038	1.19%	4368.02	640.88	0.081
10	0.127	0.030	0.93%	2184.01	500.81	0.040

Table B.5 *IDR* and θ (20-storey, MRF, q = 2.8)

Storey	d_e (m)	d_r (m)	*IDR*	P_{tot} (kN)	V_{tot} (kN)	θ
1	0.006	0.016	0.39%	44810.08	4991.78	0.035
2	0.013	0.022	0.67%	42429.70	2561.50	0.111
3	0.023	0.026	0.81%	40126.36	2481.64	0.131
4	0.032	0.028	0.86%	37835.74	2428.80	0.134
5	0.042	0.027	0.85%	35568.68	2547.56	0.119
6	0.051	0.026	0.81%	33304.53	2454.14	0.110
7	0.060	0.024	0.75%	31042.93	2518.83	0.093
8	0.068	0.022	0.70%	28791.58	2331.74	0.086
9	0.076	0.021	0.66%	26543.22	2313.34	0.076
10	0.083	0.021	0.64%	24297.95	2098.98	0.074
11	0.090	0.019	0.61%	22062.84	2032.57	0.066
12	0.097	0.019	0.59%	19830.95	1925.59	0.061
13	0.103	0.019	0.58%	17599.05	1786.49	0.057
14	0.110	0.019	0.61%	15379.62	1684.10	0.056
15	0.118	0.022	0.70%	13162.21	1443.66	0.064
16	0.127	0.025	0.77%	10951.80	1339.27	0.063
17	0.136	0.026	0.82%	8753.93	1144.03	0.063
18	0.146	0.027	0.84%	6559.78	1001.01	0.055
19	0.156	0.028	0.89%	4368.02	738.80	0.052
20	0.165	0.025	0.79%	2184.01	566.06	0.030

APPENDIX C

IDA CURVES FOR STEEL MRFS IN CHAPTER 4

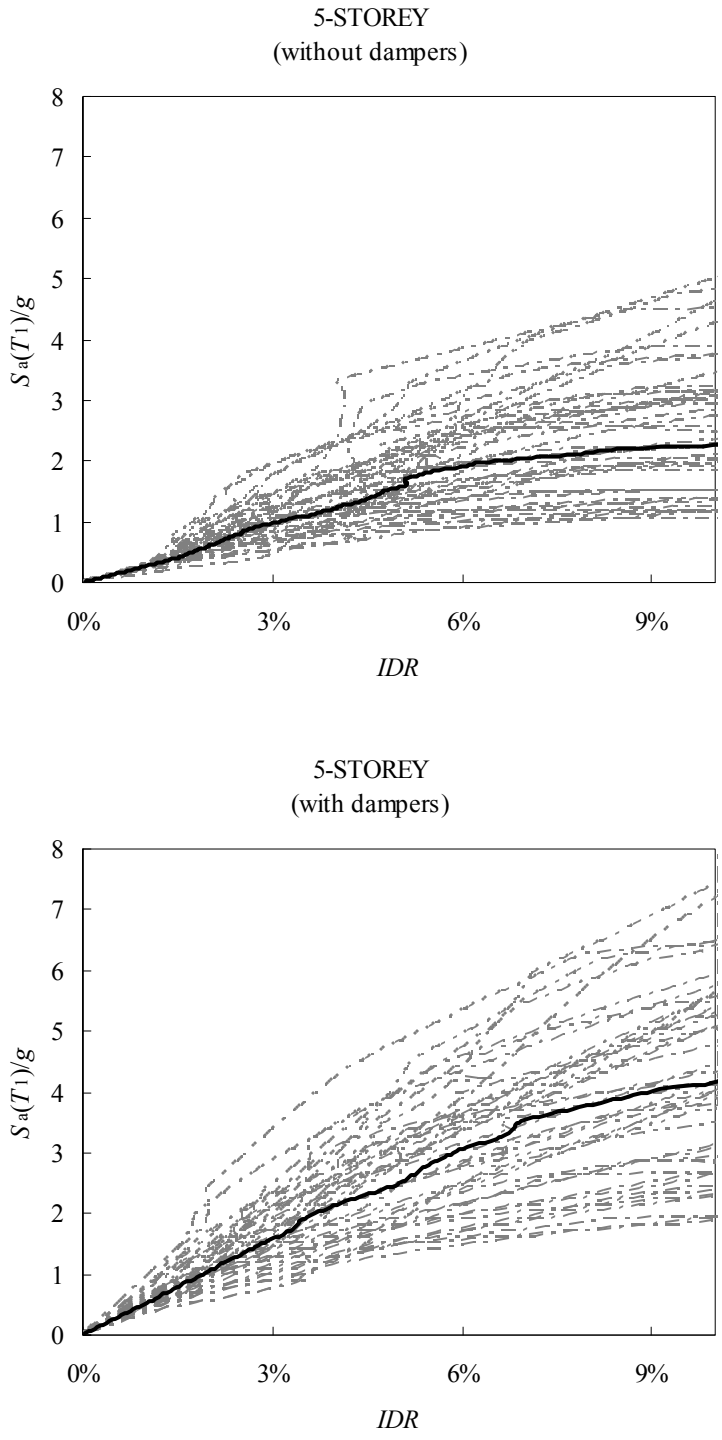

Figure C.1 IDA curves for the steel MRFs with and without viscous dampers (solid line indicates median)

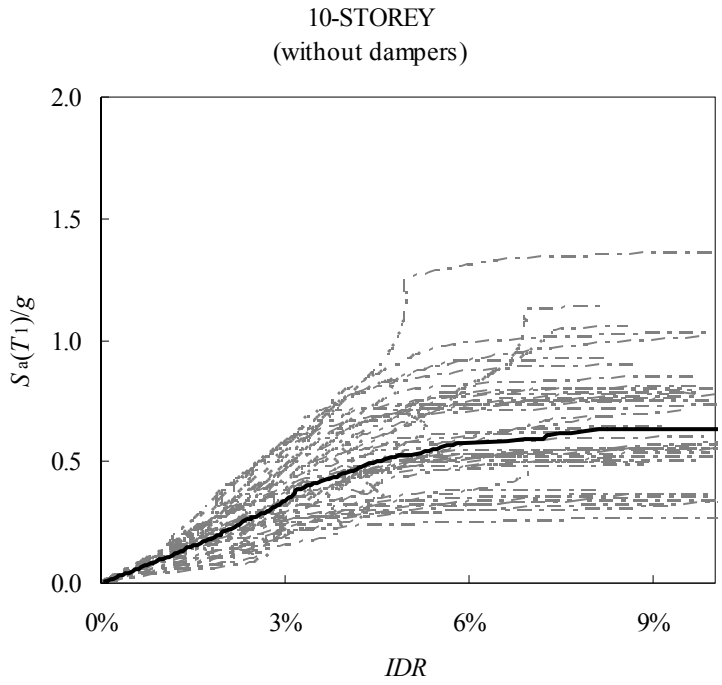

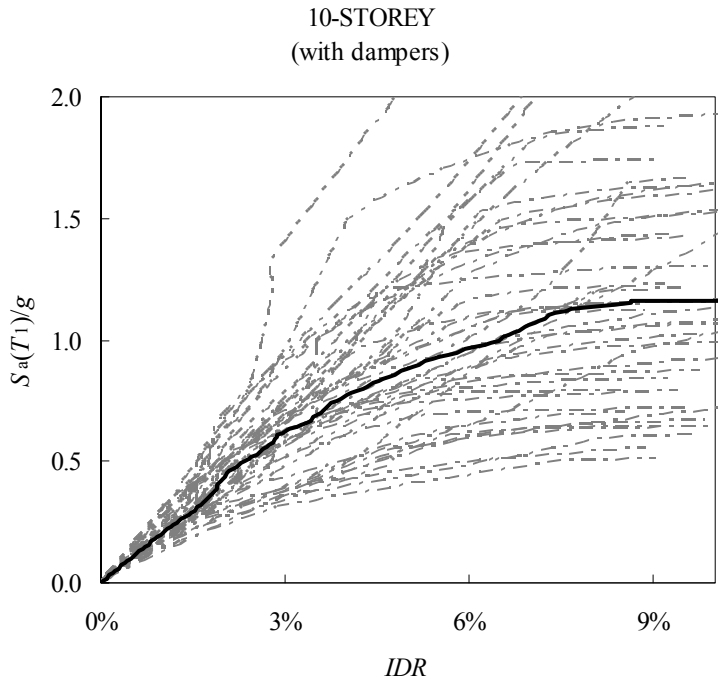

Figure C.2 IDA curves for the steel MRFs with and without viscous dampers (solid line indicates median)

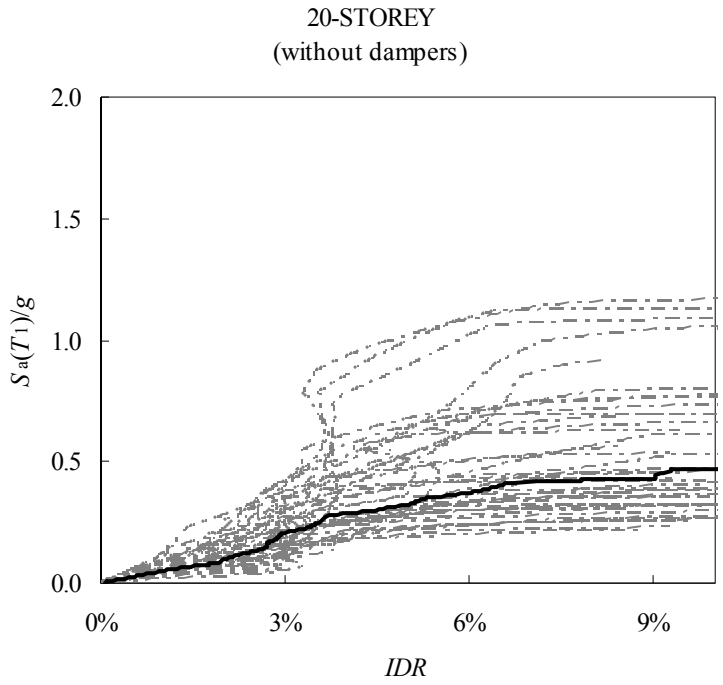

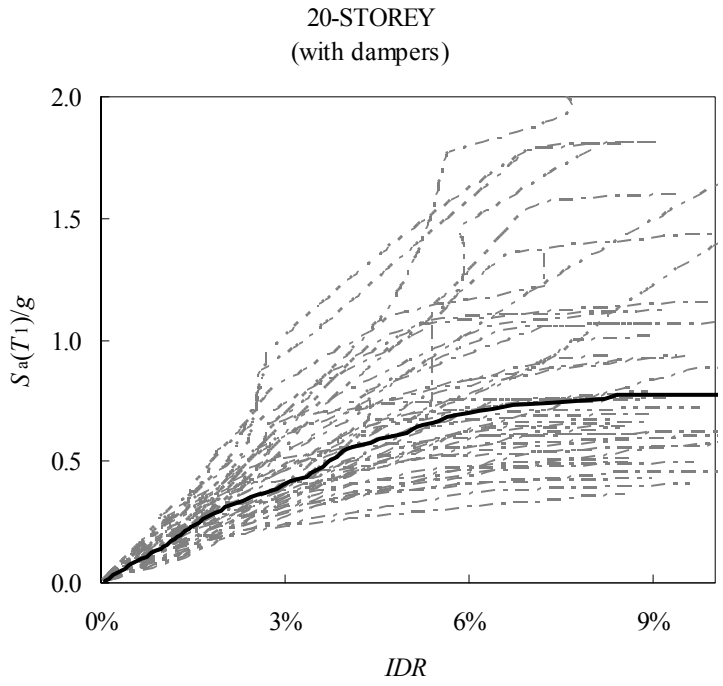

Figure C.3 IDA curves for the steel MRFs with and without viscous dampers (solid line indicates median)

APPENDIX D

DESIGN DETAILS OF STEEL MRFS WITH AND WITHOUT VISCOUS DAMPERS IN CHAPTER 5

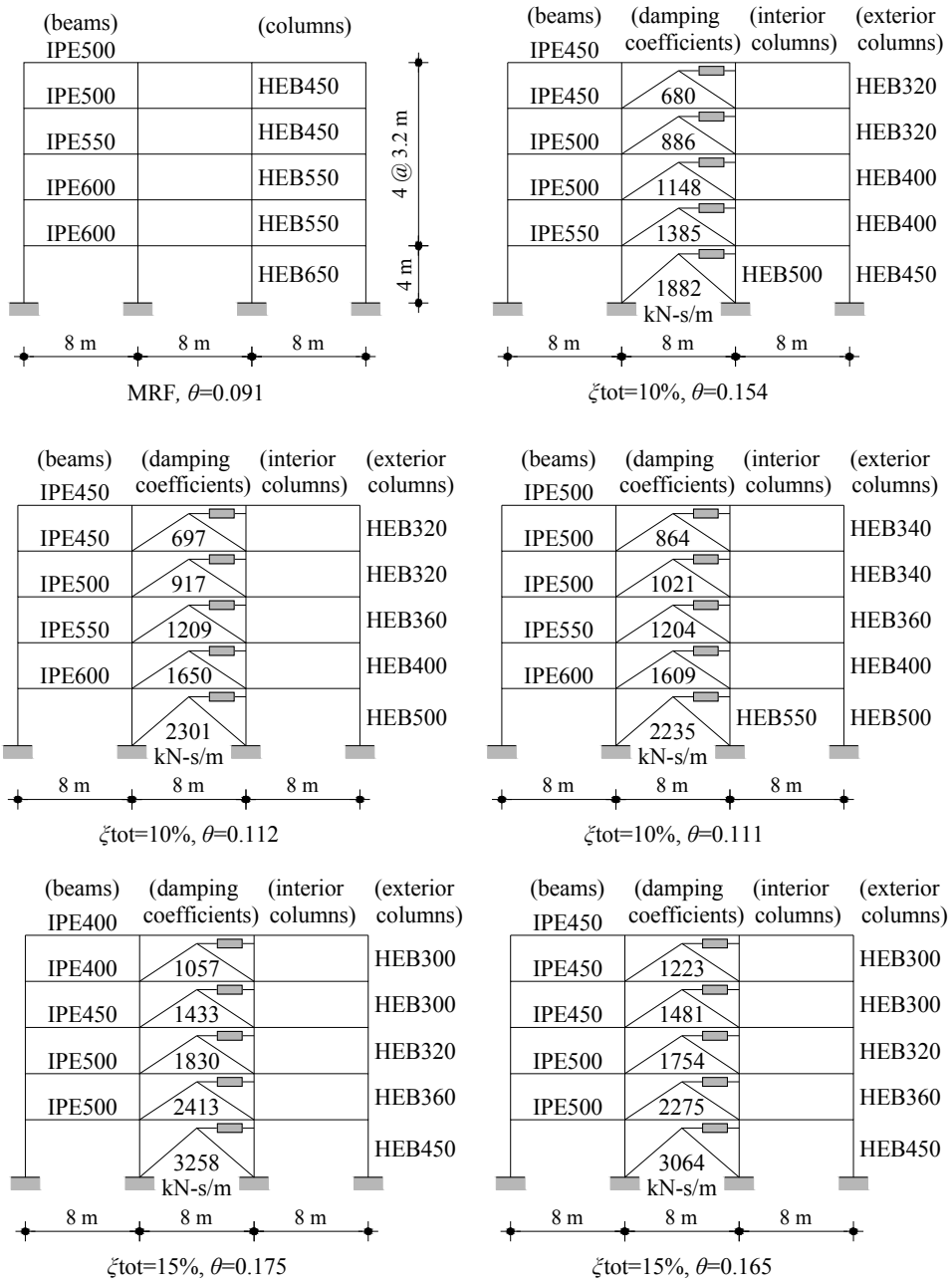

Figure D.1 Elevation view and beam/column cross-sections of the 5-storey steel MRF and the MRFs with viscous dampers. The damping coefficients of the viscous dampers are also provided. The interior column cross-sections of the MRFs with viscous dampers are the same with the exterior apart from the indicated

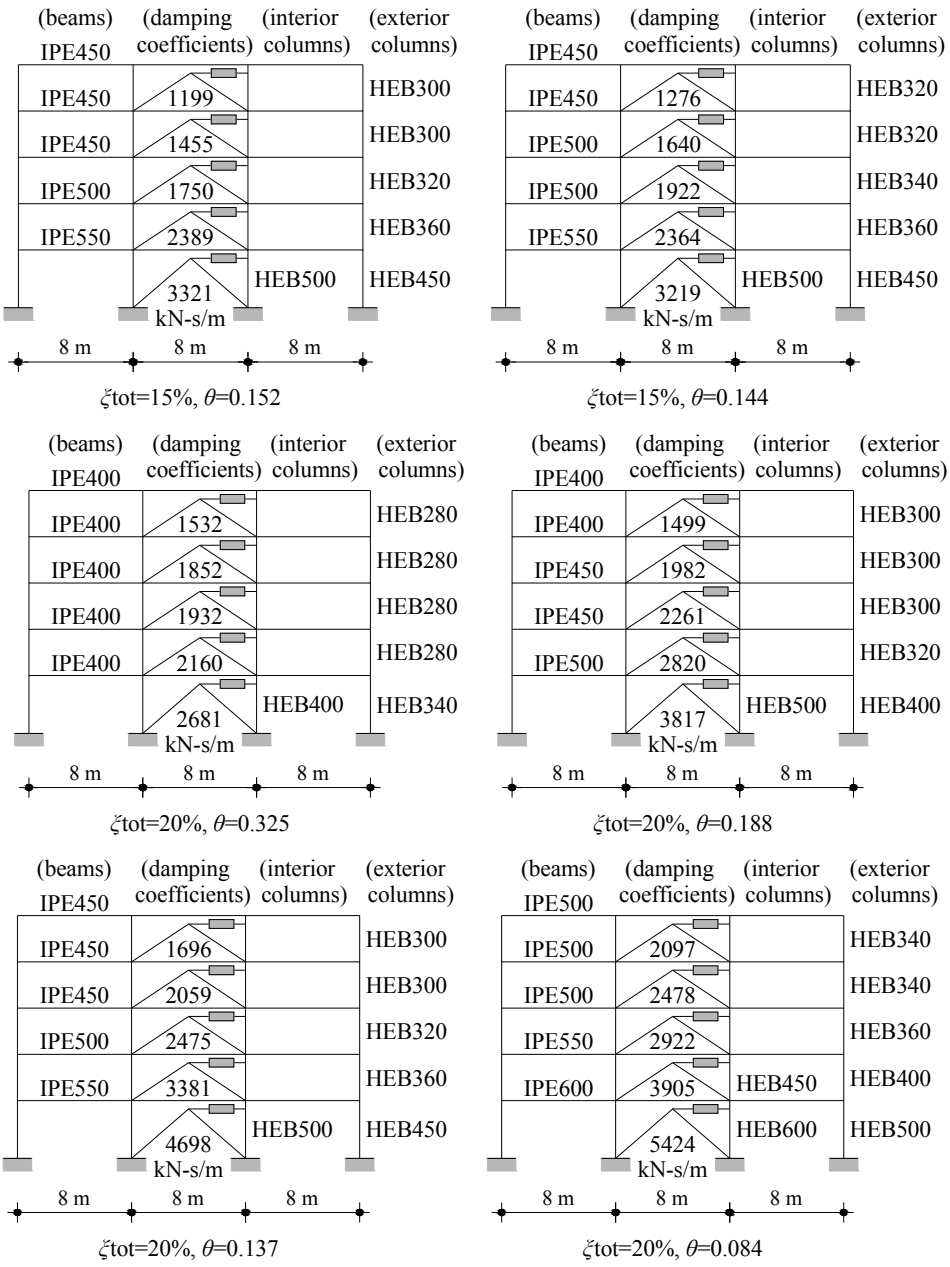

Figure D.2 Elevation view and beam/column cross-sections of the 5-storey steel MRFs with viscous dampers. The damping coefficients of the viscous dampers are also provided. The interior column cross-sections of the MRFs with viscous dampers are the same with the exterior apart from the indicated

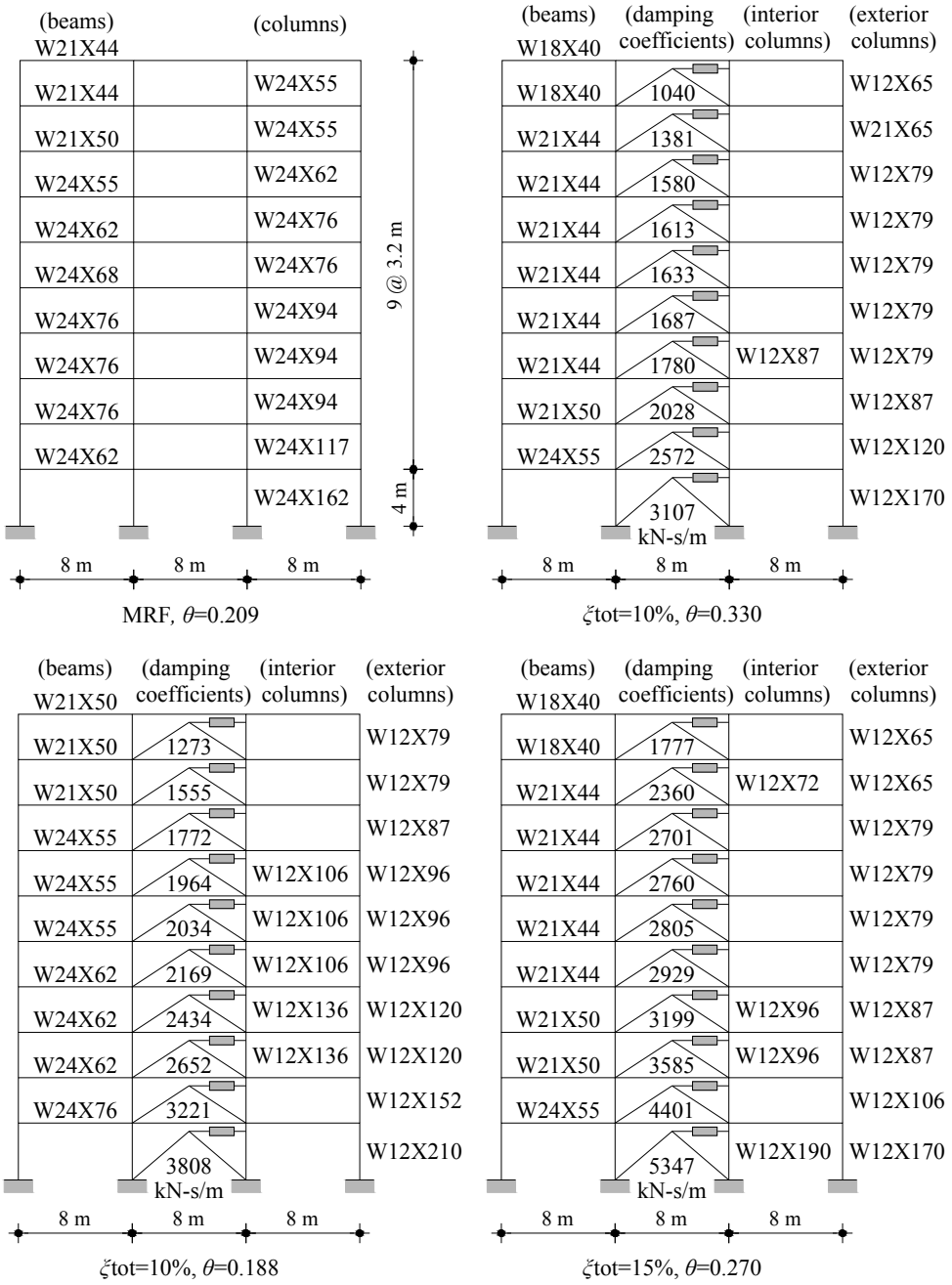

Figure D.3 Elevation view and beam/column cross-sections of the 10-storey steel MRF and the MRFs with viscous dampers. The damping coefficients of the viscous dampers are also provided. The interior column cross-sections of the MRFs with viscous dampers are the same with the exterior apart from the indicated

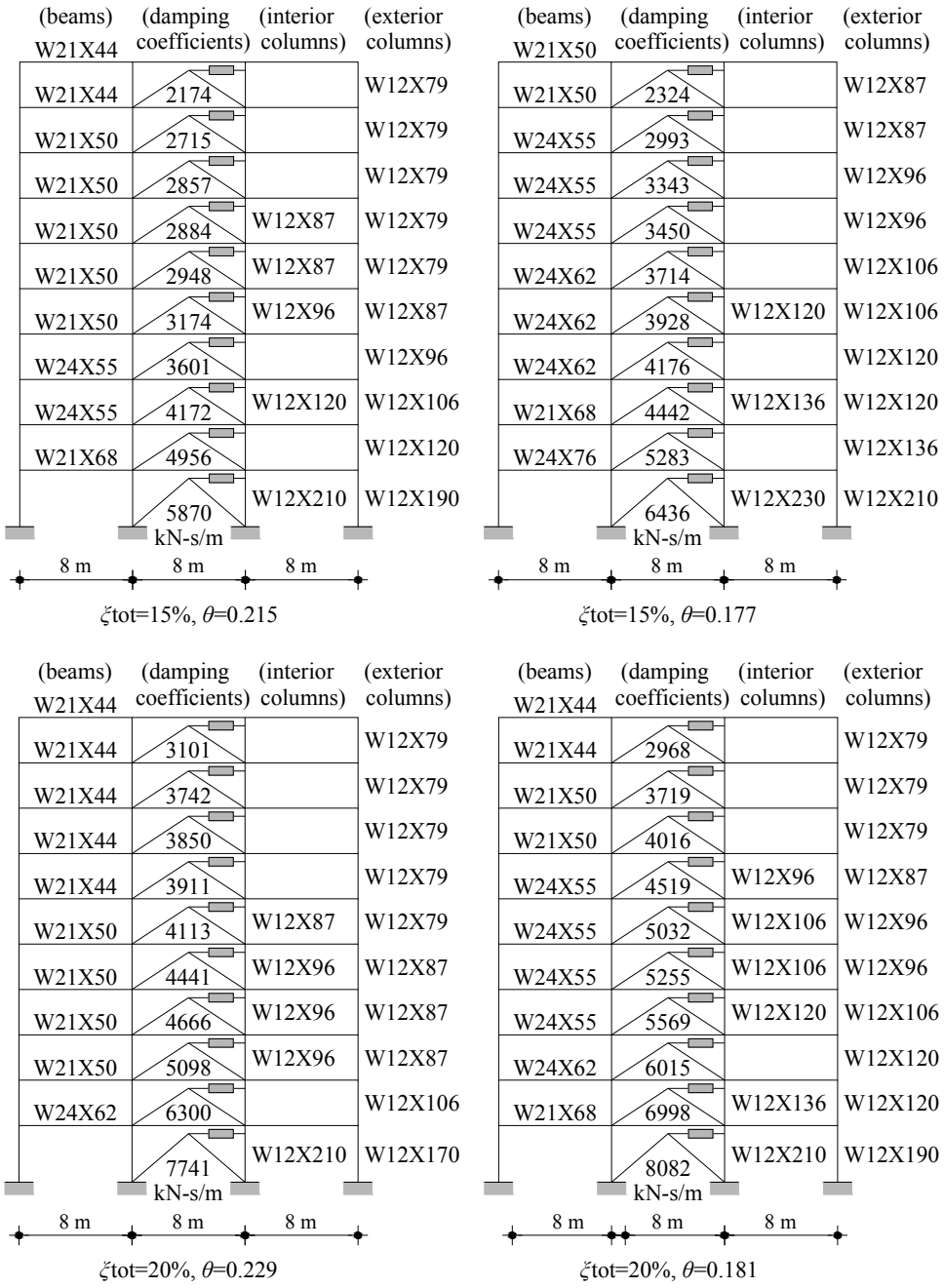

Figure D.4 Elevation view and beam/column cross-sections of the 10-storey steel MRFs with viscous dampers. The damping coefficients of the viscous dampers are also provided. The interior column cross-sections of the MRFs with viscous dampers are the same with the exterior apart from the indicated

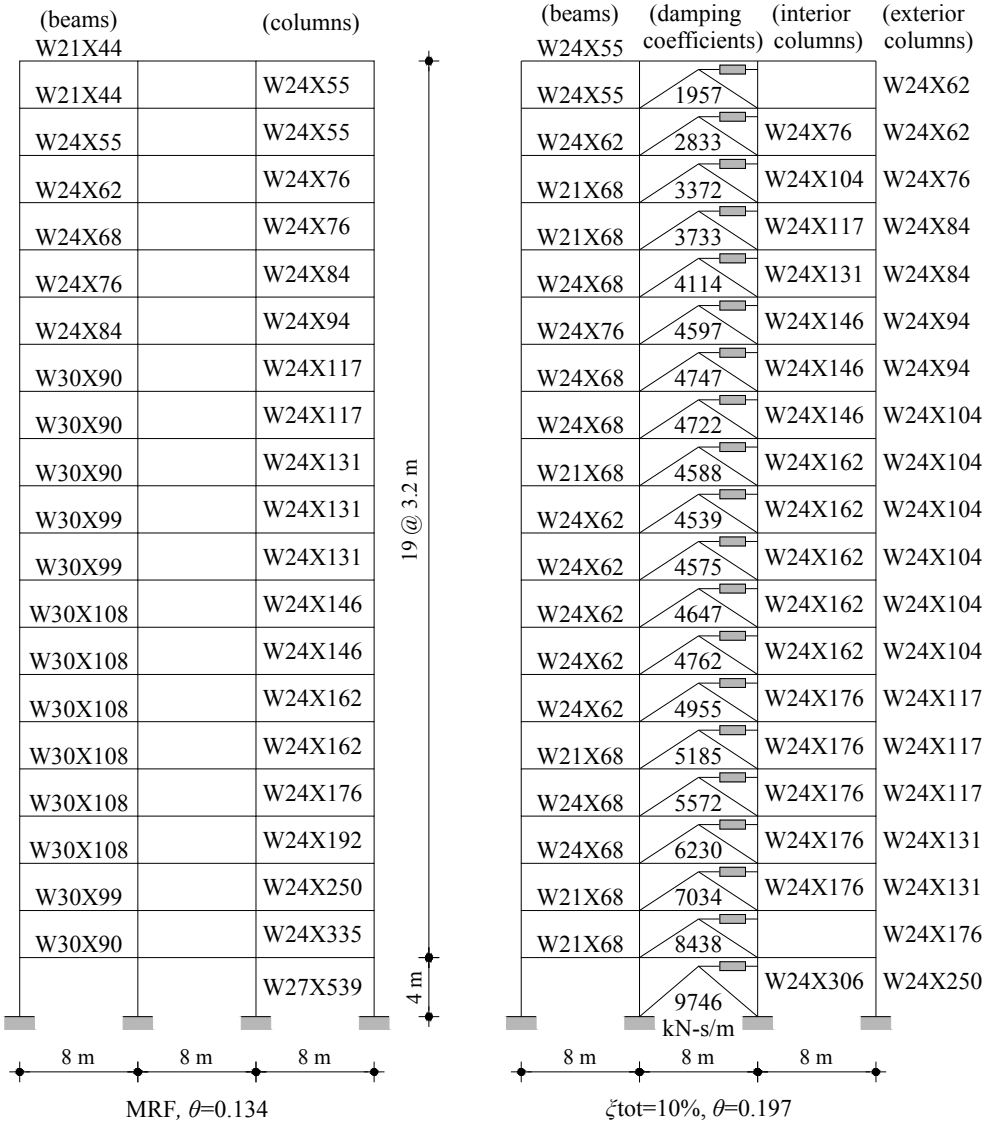

Figure D.5 Elevation view and beam/column cross-sections of the 20-storey steel MRF and the MRF with viscous dampers. The damping coefficients of the viscous dampers are also provided. The interior column cross-sections of the MRFs with viscous dampers are the same with the exterior apart from the indicated

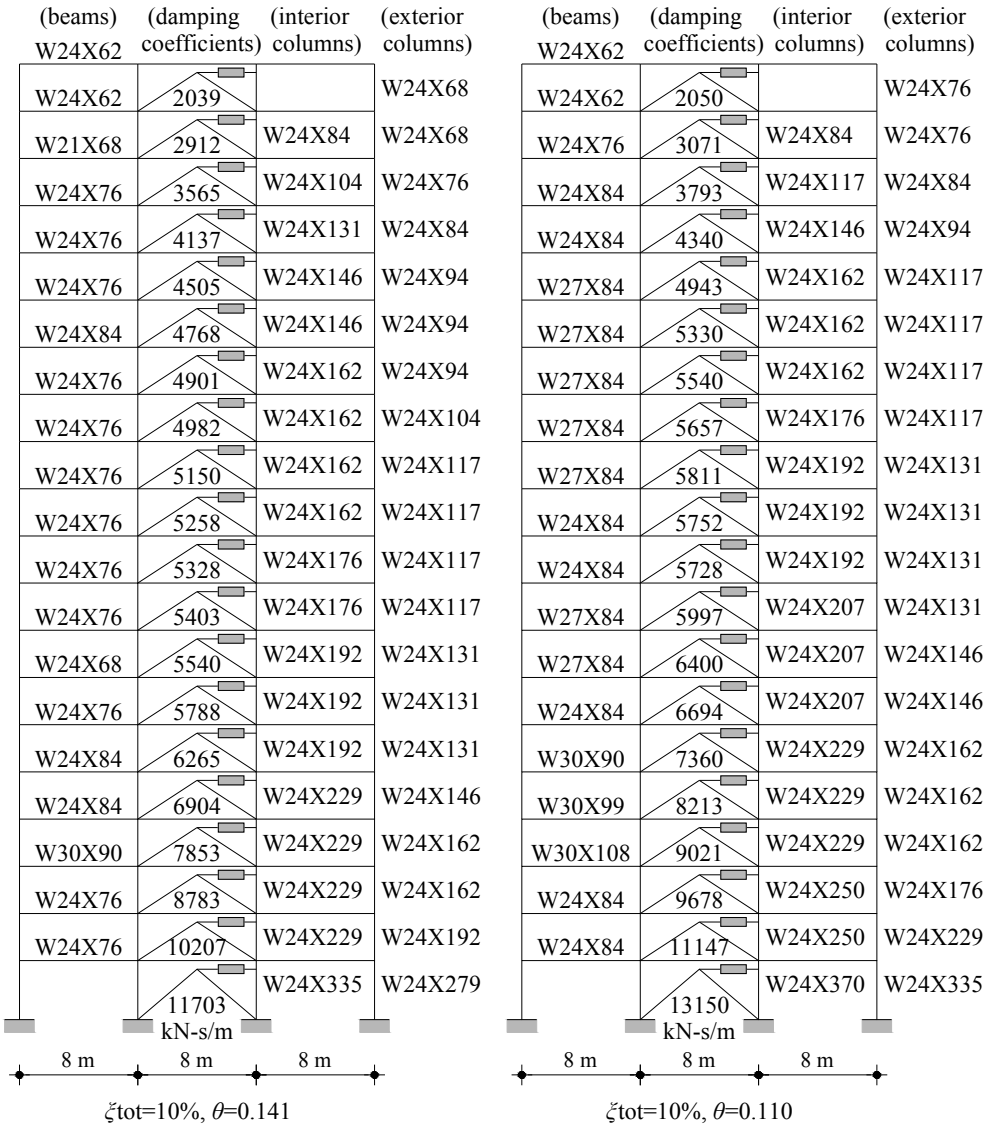

Figure D.6 Elevation view and beam/column cross-sections of the 20-storey steel MRFs with viscous dampers. The damping coefficients of the viscous dampers are also provided. The interior column cross-sections of the MRFs with viscous dampers are the same with the exterior apart from the indicated

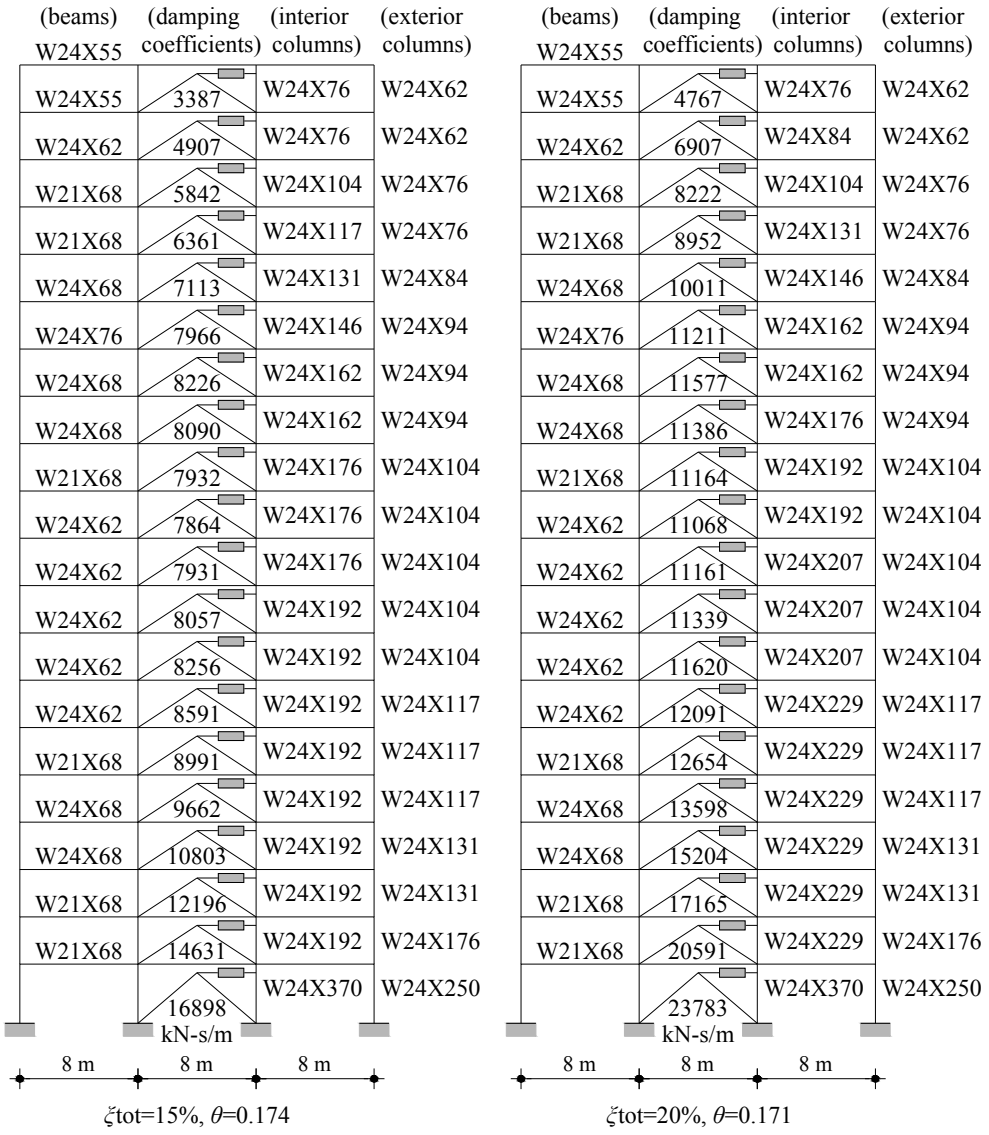

Figure D.7 Elevation view and beam/column cross-sections of the 10-storey steel MRFs with viscous dampers. The damping coefficients of the viscous dampers are also provided. The interior column cross-sections of the MRFs with viscous dampers are the same with the exterior apart from the indicated

Table D.1 *IDR* and θ (5-storey, ξ_{tot}=10%, θ=0.154, q=2.20)

Storey	d_e (m)	d_r (m)	*IDR*	P_{tot} (kN)	V_{tot} (kN)	θ
1	0.022	0.048	1.19%	11005.23	1355.17	0.097
2	0.048	0.057	1.79%	8785.93	1019.67	0.154
3	0.073	0.056	1.76%	6583.82	977.88	0.118
4	0.098	0.054	1.69%	4384.67	730.91	0.101
5	0.117	0.041	1.29%	2192.33	615.94	0.046

Table D.2 *IDR* and θ (5-storey, ξ_{tot}=10%, θ=0.112, q=1.95)

Storey	d_e (m)	d_r (m)	*IDR*	P_{tot} (kN)	V_{tot} (kN)	θ
1	0.019	0.038	0.95%	11013.16	1563.19	0.067
2	0.045	0.050	1.55%	8787.58	1216.69	0.112
3	0.073	0.055	1.72%	6582.15	1078.29	0.105
4	0.101	0.055	1.71%	4384.67	859.86	0.087
5	0.123	0.043	1.34%	2192.33	725.80	0.040

Table D.3 *IDR* and θ (5-storey, ξ_{tot}=10%, θ=0.111, q=1.95)

Storey	d_e (m)	d_r (m)	*IDR*	P_{tot} (kN)	V_{tot} (kN)	θ
1	0.020	0.039	0.98%	11021.49	1609.40	0.067
2	0.046	0.051	1.60%	8795.91	1257.61	0.111
3	0.075	0.056	1.74%	6590.47	1080.84	0.106
4	0.100	0.049	1.54%	4392.99	898.24	0.075
5	0.118	0.034	1.06%	2196.50	739.42	0.032

Table D.4 *IDR* and θ (5-storey, ξ_{tot}=15%, θ=0.175, q=2.07)

Storey	d_e (m)	d_r (m)	*IDR*	P_{tot} (kN)	V_{tot} (kN)	θ
1	0.022	0.045	1.13%	10984.46	1127.27	0.110
2	0.048	0.054	1.68%	8769.79	840.42	0.175
3	0.075	0.057	1.79%	6569.35	764.43	0.154
4	0.102	0.055	1.71%	4377.02	597.23	0.125
5	0.123	0.043	1.36%	2188.51	519.45	0.057

Table D.5 *IDR* and θ (5-storey, ξ_{tot}=15%, θ=0.165, q=1.95)

Storey	d_e (m)	d_r (m)	*IDR*	P_{tot} (kN)	V_{tot} (kN)	θ
1	0.024	0.047	1.17%	10989.75	1238.58	0.104
2	0.053	0.056	1.74%	8775.07	925.65	0.165
3	0.083	0.058	1.79%	6574.63	823.88	0.146
4	0.109	0.051	1.61%	4382.30	662.58	0.106
5	0.127	0.036	1.13%	2191.15	576.37	0.043

Table D.6 *IDR* and θ (5-storey, ξ_{tot}=15%, θ=0.152, q=1.95)

Storey	d_e (m)	d_r (m)	*IDR*	P_{tot} (kN)	V_{tot} (kN)	θ
1	0.020	0.040	0.99%	10994.36	1244.40	0.087
2	0.046	0.052	1.63%	8775.07	938.00	0.152
3	0.075	0.059	1.79%	6574.63	811.96	0.148
4	0.101	0.053	1.65%	4382.30	668.96	0.108
5	0.120	0.037	1.17%	2191.15	587.29	0.044

Table D.7 *IDR* and θ (5-storey, ξ_{tot}=15%, θ=0.144, q=1.90)

Storey	d_e (m)	d_r (m)	*IDR*	P_{tot} (kN)	V_{tot} (kN)	θ
1	0.021	0.041	1.02%	11000.89	1358.61	0.083
2	0.049	0.053	1.66%	8781.60	1011.03	0.144
3	0.078	0.054	1.68%	6581.16	920.43	0.120
4	0.102	0.047	1.46%	4384.66	731.42	0.088
5	0.121	0.035	1.09%	2192.33	604.33	0.040

Table D.8 *IDR* and θ (5-storey, ξ_{tot}=20%, θ=0.325, q=2.00)

Storey	d_e (m)	d_r (m)	*IDR*	P_{tot} (kN)	V_{tot} (kN)	θ
1	0.024	0.048	1.20%	10954.62	783.30	0.168
2	0.053	0.057	1.79%	8749.89	483.13	0.325
3	0.079	0.052	1.63%	6560.20	483.85	0.222
4	0.099	0.040	1.25%	4373.47	393.62	0.139
5	0.113	0.028	0.89%	2186.73	375.05	0.052

Table D.9 *IDR* and θ (5-storey, ξ_{tot}=20%, θ=0.188, q=1.85)

Storey	d_e (m)	d_r (m)	*IDR*	P_{tot} (kN)	V_{tot} (kN)	θ
1	0.021	0.038	0.95%	10978.19	1118.24	0.093
2	0.049	0.053	1.67%	8763.45	780.32	0.188
3	0.080	0.056	1.74%	6568.17	709.60	0.161
4	0.105	0.047	1.48%	4377.02	581.32	0.111
5	0.125	0.037	1.14%	2188.51	502.16	0.050

Table D.10 *IDR* and θ (5-storey, ξ_{tot}=20%, θ=0.137, q=1.80)

Storey	d_e (m)	d_r (m)	*IDR*	P_{tot} (kN)	V_{tot} (kN)	θ
1	0.020	0.036	0.89%	10994.36	1244.40	0.079
2	0.046	0.047	1.47%	8775.07	938.00	0.137
3	0.075	0.053	1.65%	6574.63	811.96	0.133
4	0.101	0.047	1.48%	4382.30	668.96	0.097
5	0.120	0.034	1.05%	2191.15	587.29	0.039

Table D.11 *IDR* and θ (5-storey, ξ_{tot}=20%, θ=0.084, q=1.55)

Storey	d_e (m)	d_r (m)	*IDR*	P_{tot} (kN)	V_{tot} (kN)	θ
1	0.019	0.029	0.74%	11023.46	1634.10	0.050
2	0.044	0.039	1.21%	8796.90	1302.28	0.082
3	0.073	0.045	1.40%	6590.47	1091.30	0.084
4	0.099	0.040	1.25%	4392.99	921.87	0.059
5	0.116	0.028	0.87%	2196.50	761.11	0.025

Table D.12 *IDR* and θ (10-storey, ξ_{tot}=10%, θ=0.330, q=1.65)

Storey	d_e (m)	d_r (m)	*IDR*	P_{tot} (kN)	V_{tot} (kN)	θ
1	0.021	0.035	0.89%	22002.38	1250.51	0.156
2	0.044	0.037	1.16%	19758.47	764.40	0.299
3	0.068	0.040	1.26%	17543.27	667.47	0.330
4	0.091	0.037	1.17%	15335.55	671.86	0.267
5	0.111	0.033	1.02%	13138.44	624.88	0.214
6	0.128	0.029	0.90%	10942.10	628.35	0.156
7	0.143	0.025	0.77%	8745.76	610.04	0.110
8	0.156	0.021	0.66%	6557.30	596.78	0.073
9	0.168	0.020	0.62%	4368.84	503.52	0.054
10	0.178	0.017	0.54%	2184.42	479.13	0.024

Table D.13 *IDR* and θ (10-storey, ξ_{tot}=10%, θ=0.188, q=1.45)

Storey	d_e (m)	d_r (m)	*IDR*	P_{tot} (kN)	V_{tot} (kN)	θ
1	0.023	0.034	0.84%	22097.94	1753.75	0.106
2	0.048	0.036	1.12%	19837.26	1179.59	0.188
3	0.074	0.038	1.18%	17611.20	1101.76	0.188
4	0.098	0.035	1.08%	15389.65	1131.95	0.147
5	0.121	0.033	1.03%	13177.96	956.93	0.142
6	0.142	0.030	0.95%	10973.67	947.42	0.110
7	0.160	0.027	0.83%	8769.39	914.45	0.080
8	0.177	0.025	0.78%	6572.98	810.68	0.064
9	0.193	0.023	0.71%	4380.97	704.10	0.044
10	0.204	0.017	0.52%	2190.49	620.00	0.018

Table D.14 *IDR* and θ (10-storey, ξ_{tot}=15%, θ=0.270, q=1.45)

Storey	d_e (m)	d_r (m)	*IDR*	P_{tot} (kN)	V_{tot} (kN)	θ
1	0.021	0.031	0.77%	22007.87	1326.59	0.127
2	0.044	0.033	1.04%	19761.65	764.09	0.270
3	0.068	0.035	1.10%	17548.34	728.13	0.264
4	0.091	0.032	1.00%	15337.77	716.08	0.215
5	0.111	0.029	0.91%	13139.08	627.61	0.191
6	0.129	0.026	0.82%	10942.74	647.42	0.138
7	0.144	0.023	0.71%	8746.40	627.07	0.098
8	0.158	0.020	0.61%	6557.94	609.95	0.066
9	0.170	0.018	0.56%	4369.48	518.90	0.047
10	0.181	0.016	0.49%	2184.42	483.96	0.022

Table D.15 *IDR* and θ (10-storey, ξ_{tot}=15%, θ=0.215, q=1.35)

Storey	d_e (m)	d_r (m)	*IDR*	P_{tot} (kN)	V_{tot} (kN)	θ
1	0.022	0.030	0.76%	22049.58	1536.66	0.109
2	0.047	0.033	1.02%	19794.15	935.96	0.215
3	0.071	0.033	1.03%	17576.44	986.87	0.183
4	0.094	0.032	0.99%	15360.05	819.16	0.186
5	0.116	0.030	0.93%	13158.50	784.17	0.156
6	0.137	0.028	0.86%	10957.78	761.76	0.124
7	0.155	0.024	0.75%	8758.65	751.62	0.087
8	0.170	0.021	0.65%	6567.40	699.38	0.061
9	0.183	0.018	0.55%	4376.92	620.31	0.039
10	0.193	0.014	0.43%	2188.46	547.44	0.017

Table D.16 *IDR* and θ (10-storey, ξ_{tot}=15%, θ=0.177, q=1.30)

Storey	d_e (m)	d_r (m)	*IDR*	P_{tot} (kN)	V_{tot} (kN)	θ
1	0.022	0.029	0.73%	22109.05	1817.15	0.089
2	0.048	0.033	1.04%	19846.03	1164.60	0.177
3	0.075	0.035	1.09%	17620.87	1147.83	0.167
4	0.099	0.032	1.00%	15399.33	1077.36	0.143
5	0.121	0.028	0.89%	13189.09	1021.99	0.114
6	0.141	0.026	0.82%	10980.16	954.13	0.095
7	0.160	0.024	0.76%	8774.92	877.83	0.076
8	0.176	0.021	0.65%	6579.47	841.86	0.051
9	0.190	0.018	0.56%	4384.02	706.30	0.035
10	0.200	0.014	0.43%	2192.01	601.56	0.016

Table D.17 *IDR* and θ (10-storey, ξ_{tot}=20%, θ=0.229, q=1.25)

Storey	d_e (m)	d_r (m)	*IDR*	P_{tot} (kN)	V_{tot} (kN)	θ
1	0.021	0.026	0.66%	22027.24	1455.56	0.100
2	0.045	0.030	0.95%	19776.26	839.77	0.223
3	0.071	0.033	1.02%	17562.95	778.56	0.229
4	0.095	0.029	0.92%	15352.38	772.50	0.182
5	0.115	0.025	0.79%	13151.66	740.32	0.140
6	0.134	0.023	0.72%	10950.94	693.10	0.114
7	0.151	0.021	0.67%	8753.83	669.85	0.087
8	0.165	0.019	0.58%	6565.38	639.67	0.060
9	0.178	0.015	0.48%	4376.92	571.05	0.037
10	0.187	0.012	0.36%	2188.46	523.90	0.015

Table D.18 *IDR* and θ (10-storey, ξ_{tot}=20%, θ=0.181, q=1.20)

Storey	d_e (m)	d_r (m)	*IDR*	P_{tot} (kN)	V_{tot} (kN)	θ
1	0.024	0.029	0.72%	22070.04	1608.88	0.098
2	0.049	0.030	0.94%	19814.61	1024.90	0.181
3	0.074	0.030	0.95%	17593.06	1039.83	0.161
4	0.098	0.028	0.87%	15375.36	950.26	0.141
5	0.118	0.025	0.78%	13168.82	870.71	0.118
6	0.137	0.022	0.70%	10964.53	875.80	0.088
7	0.155	0.021	0.66%	8760.24	793.63	0.073
8	0.172	0.021	0.64%	6567.40	722.34	0.058
9	0.187	0.018	0.55%	4376.92	645.03	0.037
10	0.198	0.013	0.42%	2188.46	562.37	0.016

Table D.19 *IDR* and θ (20-storey, ξ_{tot}=10%, θ=0.197, q=1.10)

Storey	d_e (m)	d_r (m)	*IDR*	P_{tot} (kN)	V_{tot} (kN)	θ
1	0.017	0.018	0.46%	44550.66	4011.57	0.051
2	0.036	0.021	0.64%	42239.38	1636.75	0.166
3	0.056	0.023	0.71%	39976.57	1437.35	0.197
4	0.076	0.022	0.69%	37717.84	1428.76	0.183
5	0.095	0.021	0.65%	35471.72	1298.23	0.178
6	0.113	0.019	0.61%	33227.02	1281.65	0.157
7	0.128	0.017	0.53%	30984.47	1242.44	0.132
8	0.141	0.014	0.44%	28752.17	1133.82	0.113
9	0.152	0.012	0.38%	26522.34	1158.61	0.087
10	0.162	0.011	0.33%	24292.52	1161.30	0.069
11	0.171	0.009	0.30%	22069.98	1158.01	0.056
12	0.179	0.009	0.28%	19845.31	1235.60	0.046
13	0.187	0.009	0.27%	17620.51	1246.04	0.039
14	0.195	0.009	0.27%	15407.06	1258.11	0.033
15	0.203	0.009	0.28%	13191.79	1263.26	0.029
16	0.212	0.010	0.32%	10979.26	1188.93	0.029
17	0.222	0.011	0.35%	8777.12	1127.34	0.027
18	0.233	0.011	0.36%	6576.28	1060.12	0.022
19	0.243	0.011	0.34%	4379.52	907.47	0.017
20	0.251	0.009	0.29%	2189.09	711.66	0.009

Table D.20 *IDR* and θ (20-storey, ξ_{tot}=10%, θ=0.141, q=1.10)

Storey	d_e (m)	d_r (m)	*IDR*	P_{tot} (kN)	V_{tot} (kN)	θ
1	0.016	0.018	0.45%	44687.65	4347.94	0.046
2	0.034	0.020	0.62%	42366.71	2019.04	0.131
3	0.054	0.021	0.67%	40094.65	1904.40	0.141
4	0.073	0.021	0.66%	37820.56	1915.10	0.129
5	0.092	0.021	0.64%	35561.10	1665.18	0.138
6	0.110	0.020	0.63%	33303.14	1589.16	0.132
7	0.127	0.019	0.60%	31052.82	1487.80	0.125
8	0.143	0.017	0.54%	28815.49	1445.71	0.108
9	0.158	0.016	0.49%	26575.41	1436.11	0.091
10	0.170	0.014	0.44%	24338.10	1428.63	0.075
11	0.182	0.013	0.40%	22108.08	1401.87	0.064
12	0.193	0.012	0.39%	19879.33	1440.65	0.053
13	0.204	0.012	0.37%	17650.59	1423.88	0.046
14	0.215	0.012	0.36%	15432.90	1450.79	0.039
15	0.225	0.012	0.36%	13213.39	1416.06	0.034
16	0.236	0.012	0.37%	10998.12	1367.95	0.030
17	0.247	0.012	0.37%	8790.74	1309.01	0.025
18	0.258	0.012	0.39%	6585.74	1184.16	0.021
19	0.269	0.012	0.38%	4386.83	1009.32	0.016
20	0.278	0.010	0.31%	2192.69	767.26	0.009

Table D.21 *IDR* and θ (20-storey, ξ_{tot}=10%, θ=0.111, q=1.00)

Storey	d_e (m)	d_r (m)	*IDR*	P_{tot} (kN)	V_{tot} (kN)	θ
1	0.017	0.017	0.44%	44809.70	5257.85	0.037
2	0.037	0.020	0.62%	42475.29	2559.26	0.103
3	0.058	0.021	0.66%	40195.02	2409.02	0.110
4	0.078	0.020	0.62%	37911.34	2530.38	0.093
5	0.097	0.019	0.59%	35646.64	2303.80	0.092
6	0.116	0.019	0.59%	33385.16	2030.08	0.097
7	0.135	0.019	0.58%	31125.70	1851.72	0.098
8	0.152	0.017	0.54%	28879.94	1959.77	0.079
9	0.168	0.016	0.51%	26634.17	1813.84	0.075
10	0.184	0.016	0.49%	24389.96	1727.72	0.069
11	0.198	0.014	0.45%	22154.43	1776.67	0.056
12	0.212	0.013	0.41%	19918.79	1830.67	0.045
13	0.224	0.013	0.39%	17683.14	1770.66	0.039
14	0.236	0.012	0.38%	15460.12	1760.61	0.034
15	0.249	0.012	0.38%	13238.36	1743.99	0.029
16	0.261	0.012	0.38%	11016.61	1674.83	0.025
17	0.273	0.013	0.39%	8802.86	1570.46	0.022
18	0.286	0.013	0.39%	6592.73	1453.22	0.018
19	0.298	0.012	0.39%	4389.03	1199.34	0.014
20	0.309	0.010	0.33%	2194.15	881.81	0.008

Table D.22 *IDR* and θ (20-storey, ξ_{tot}=15%, θ=0.174, q=1.00)

Storey	d_e (m)	d_r (m)	*IDR*	P_{tot} (kN)	V_{tot} (kN)	θ
1	0.015	0.015	0.39%	44579.02	4065.62	0.042
2	0.033	0.018	0.56%	42260.11	1645.95	0.143
3	0.053	0.020	0.63%	39995.83	1436.99	0.174
4	0.073	0.020	0.62%	37735.64	1412.89	0.165
5	0.092	0.019	0.59%	35488.06	1291.61	0.161
6	0.109	0.017	0.55%	33241.90	1277.06	0.142
7	0.125	0.015	0.48%	30997.88	1235.80	0.120
8	0.138	0.013	0.40%	28764.12	1138.55	0.102
9	0.149	0.011	0.35%	26531.56	1157.27	0.080
10	0.159	0.010	0.31%	24299.00	1143.99	0.065
11	0.167	0.009	0.27%	22075.20	1148.50	0.053
12	0.176	0.008	0.26%	19849.25	1223.26	0.042
13	0.184	0.008	0.25%	17623.18	1228.39	0.036
14	0.191	0.008	0.24%	15409.15	1254.34	0.030
15	0.200	0.008	0.26%	13192.39	1239.84	0.027
16	0.209	0.009	0.29%	10979.86	1179.69	0.027
17	0.219	0.010	0.32%	8777.72	1112.91	0.025
18	0.229	0.010	0.32%	6577.61	1055.34	0.020
19	0.239	0.010	0.31%	4380.86	901.87	0.015
20	0.247	0.008	0.26%	2190.43	710.50	0.008

Table D.23 *IDR* and θ (20-storey, ξ_{tot}=20%, θ=0.171, q=1.00)

Storey	d_e (m)	d_r (m)	*IDR*	P_{tot} (kN)	V_{tot} (kN)	θ
1	0.014	0.014	0.35%	44614.62	3652.93	0.043
2	0.030	0.016	0.50%	42295.71	1494.21	0.142
3	0.048	0.018	0.56%	40027.97	1309.22	0.171
4	0.066	0.018	0.55%	37764.31	1286.44	0.163
5	0.083	0.017	0.53%	35513.26	1173.85	0.159
6	0.098	0.016	0.49%	33263.64	1161.83	0.140
7	0.112	0.014	0.43%	31016.16	1128.52	0.119
8	0.124	0.012	0.37%	28778.93	1029.12	0.103
9	0.134	0.010	0.32%	26544.97	1049.23	0.081
10	0.143	0.009	0.28%	24311.02	1051.46	0.064
11	0.151	0.008	0.25%	22084.35	1036.53	0.054
12	0.159	0.008	0.24%	19856.94	1110.87	0.043
13	0.166	0.007	0.23%	17629.41	1119.32	0.036
14	0.173	0.007	0.22%	15414.11	1126.05	0.031
15	0.181	0.007	0.23%	13197.35	1131.98	0.027
16	0.189	0.008	0.26%	10983.33	1067.50	0.027
17	0.198	0.009	0.29%	8779.76	1015.23	0.025
18	0.207	0.009	0.29%	6578.35	949.49	0.020
19	0.216	0.009	0.28%	4381.59	819.62	0.015
20	0.224	0.007	0.23%	2190.43	639.55	0.008

APPENDIX E

IDA CURVES FOR STEEL MRFS IN CHAPTER 5

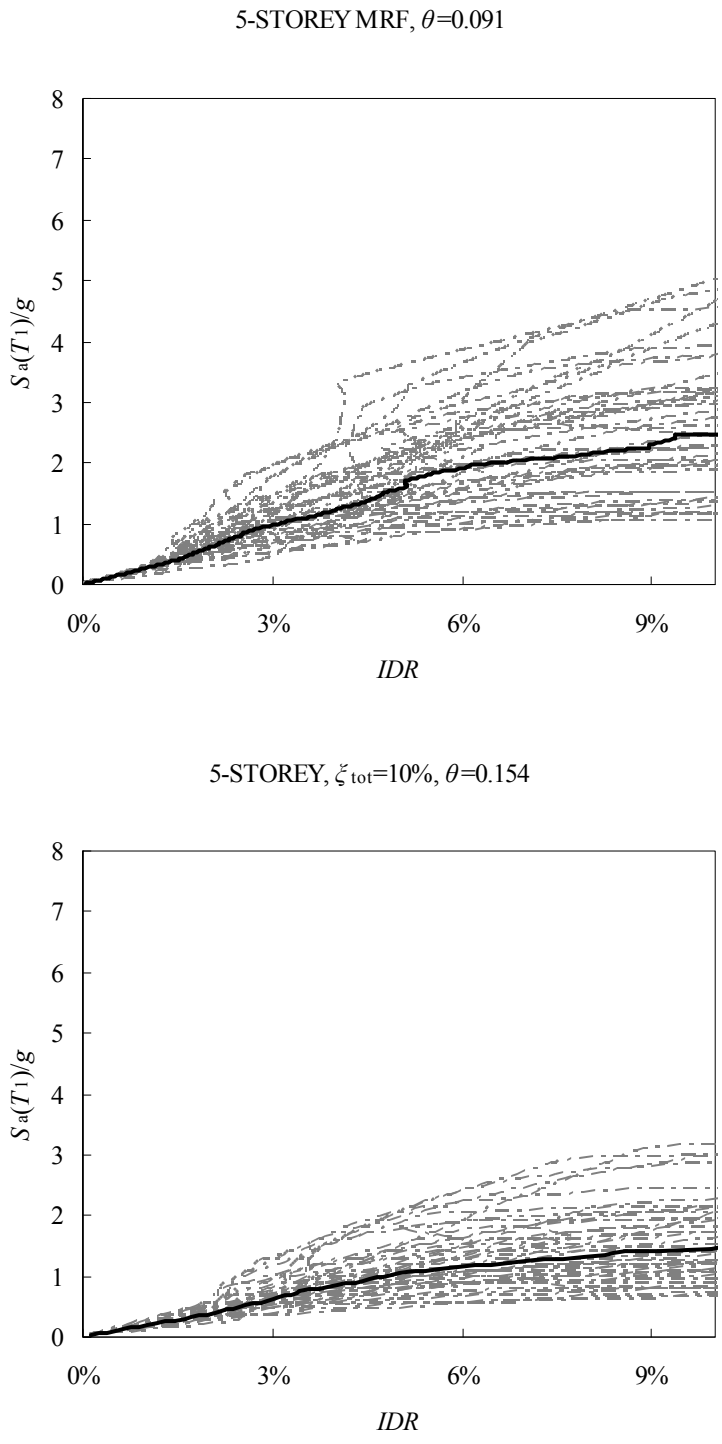

Figure E.1 IDA curves for the 5-storey steel MRF and the MRF with viscous dampers (solid line indicates median)

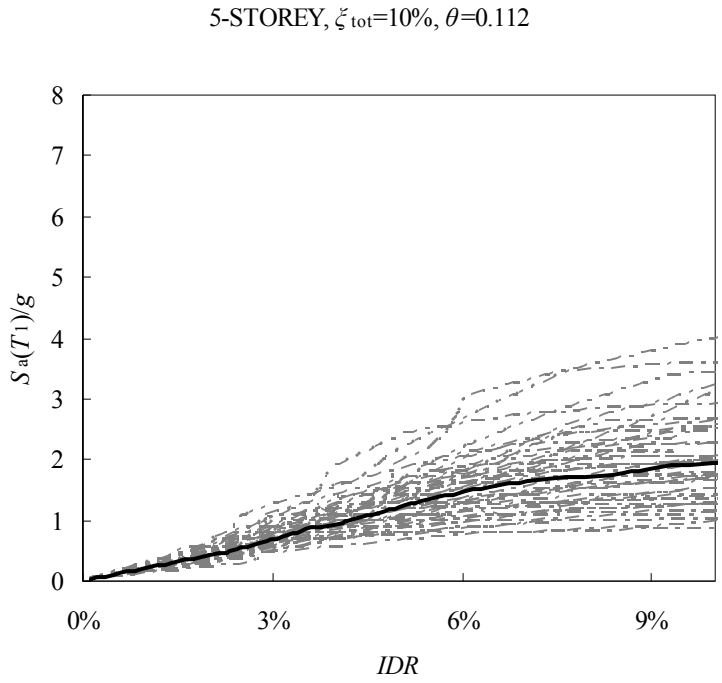

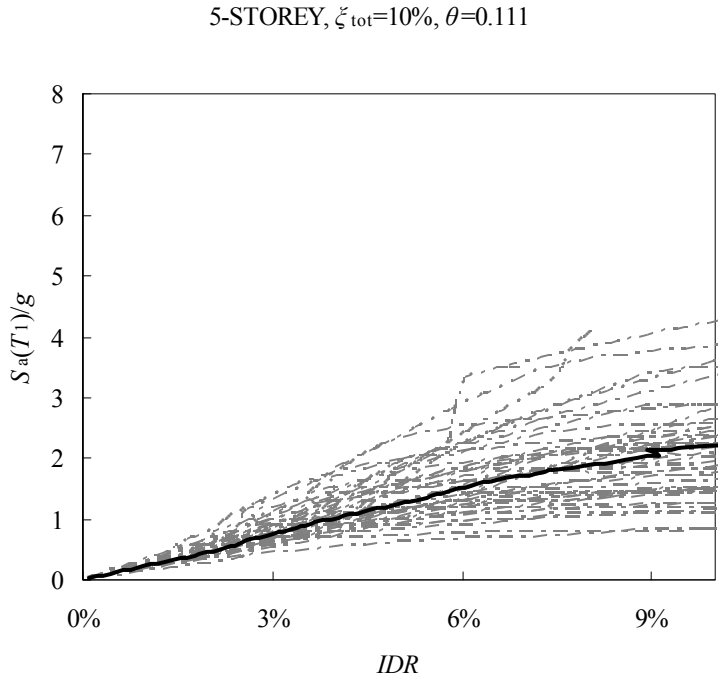

Figure E.2 IDA curves for the 5-storey steel MRFs with viscous dampers (solid line indicates median)

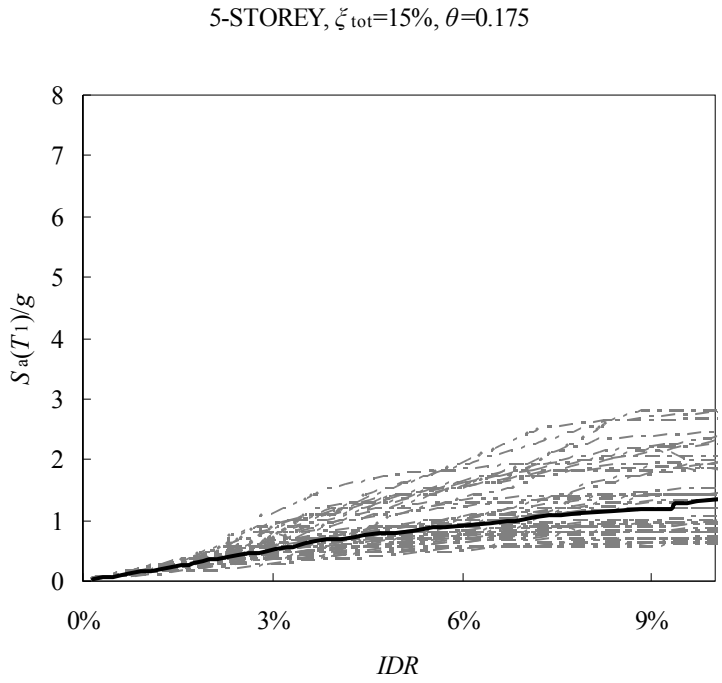

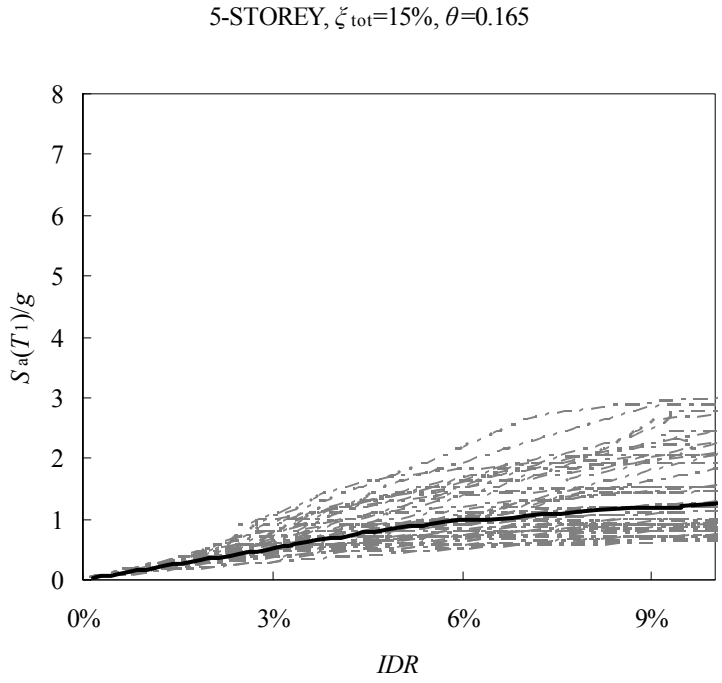

Figure E.3 IDA curves for the 5-storey steel MRFs with viscous dampers (solid line indicates median)

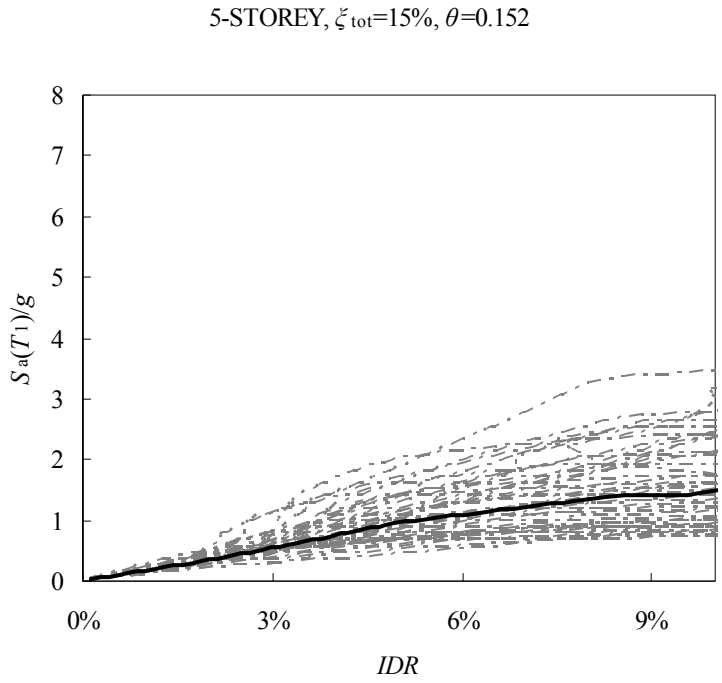

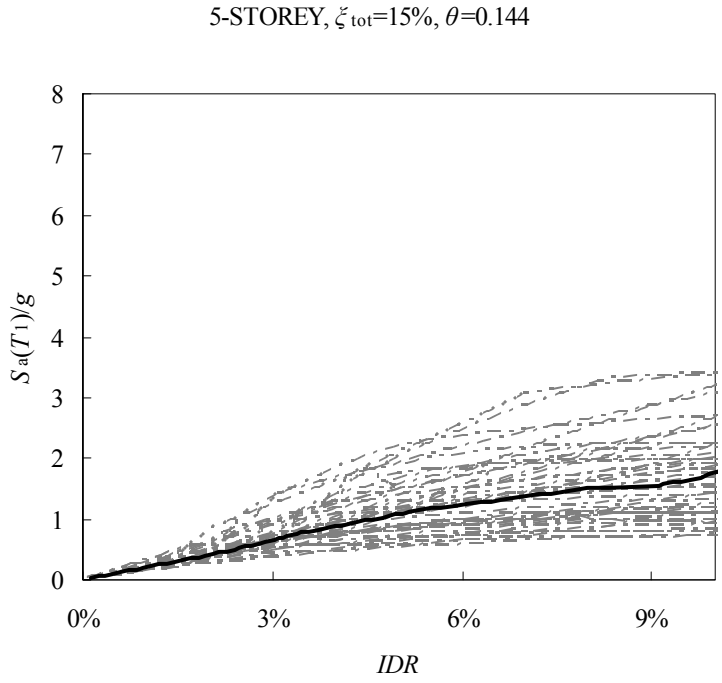

Figure E.4 IDA curves for the 5-storey steel MRFs with viscous dampers (solid line indicates median)

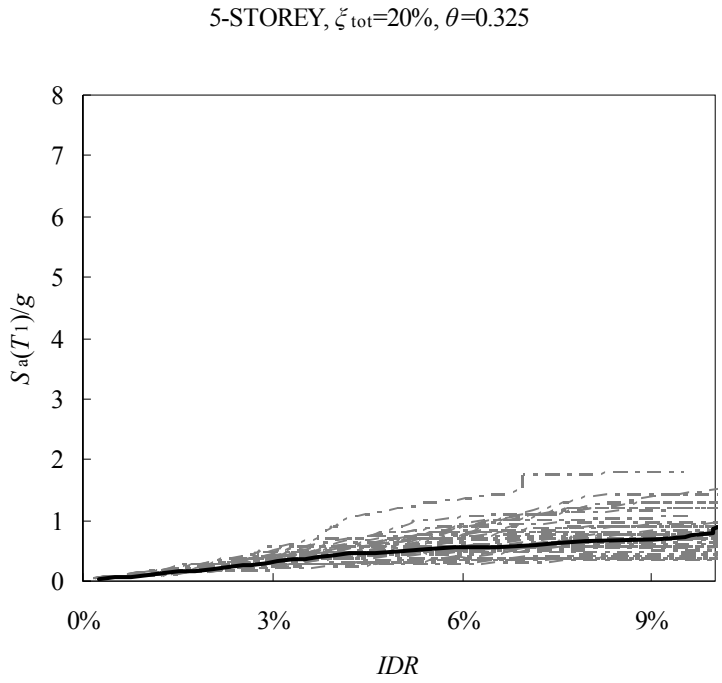

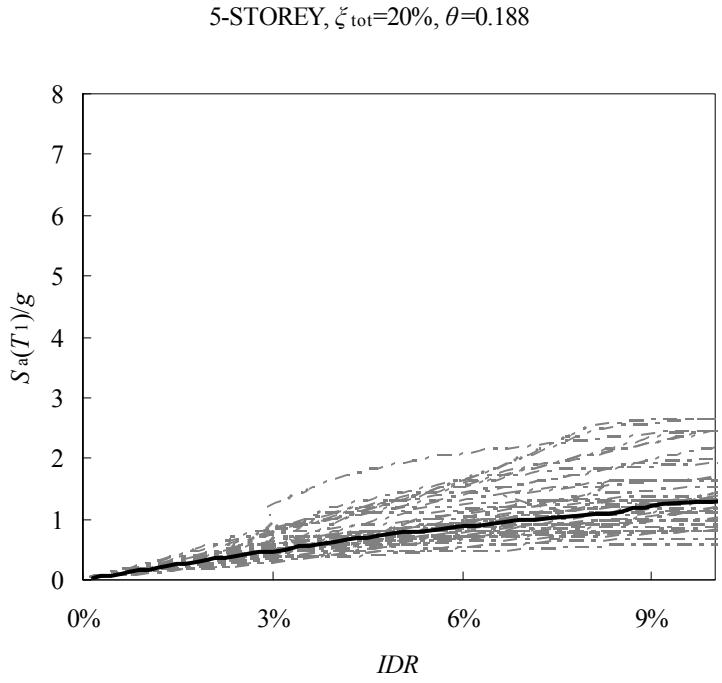

Figure E.5 IDA curves for the 5-storey steel MRFs with viscous dampers (solid line indicates median)

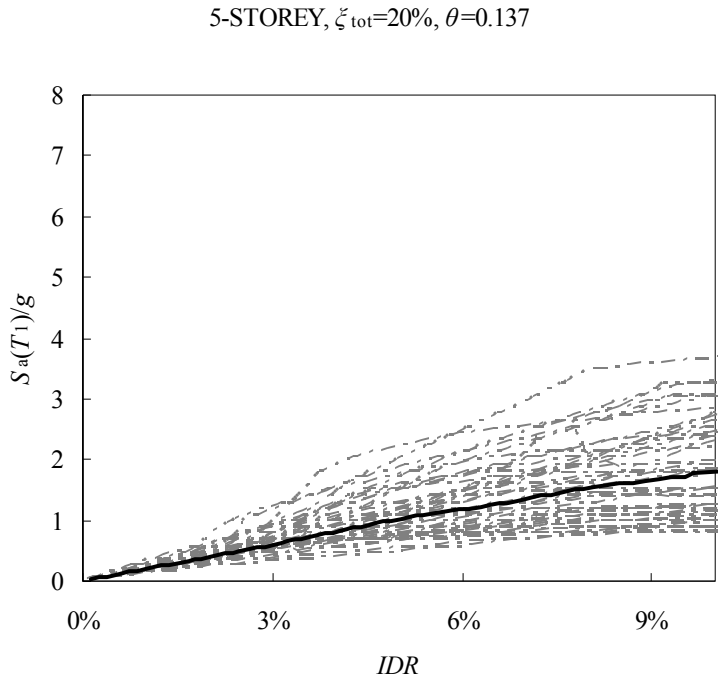

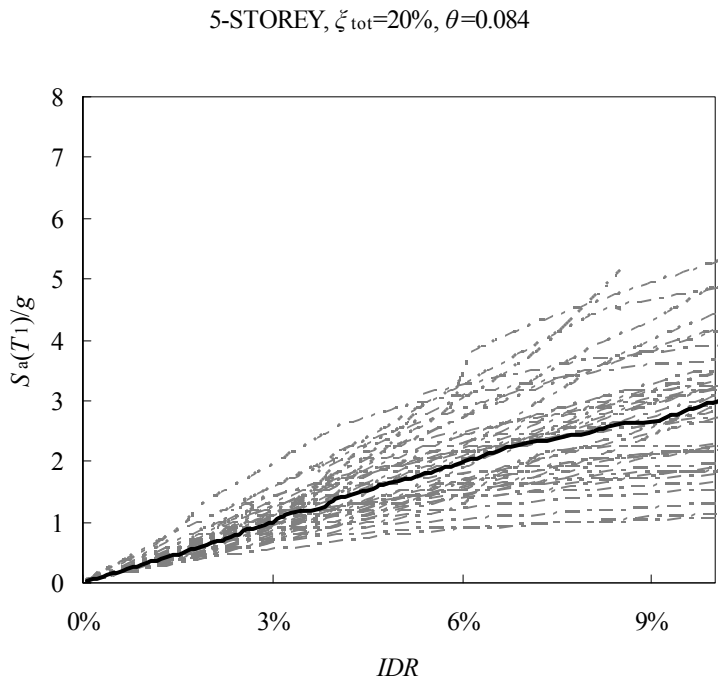

Figure E.6 IDA curves for the 5-storey steel MRFs with viscous dampers (solid line indicates median)

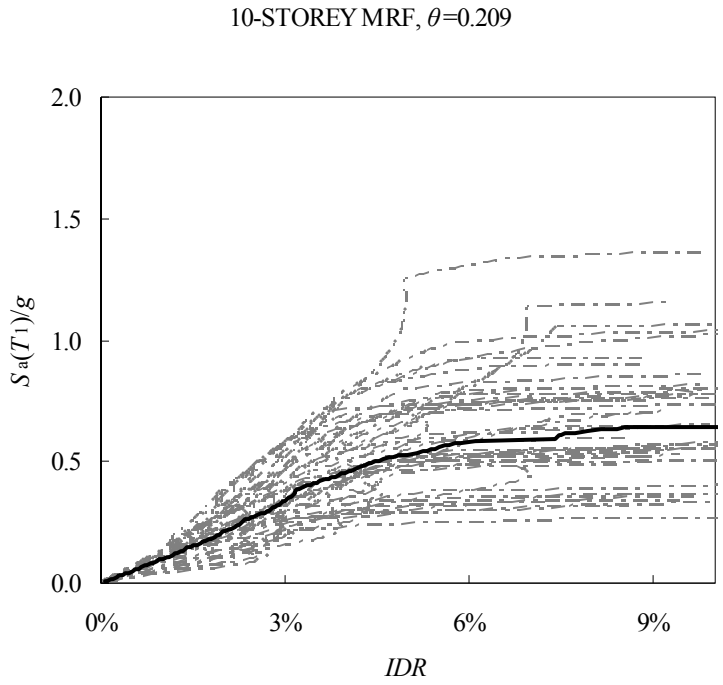

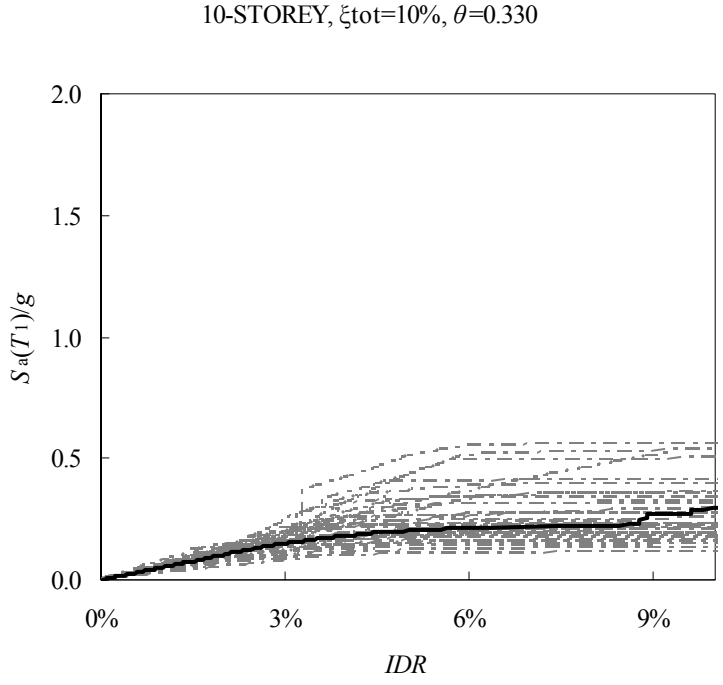

Figure E.7 IDA curves for the 10-storey steel MRF and the MRF with viscous dampers (solid line indicates median)

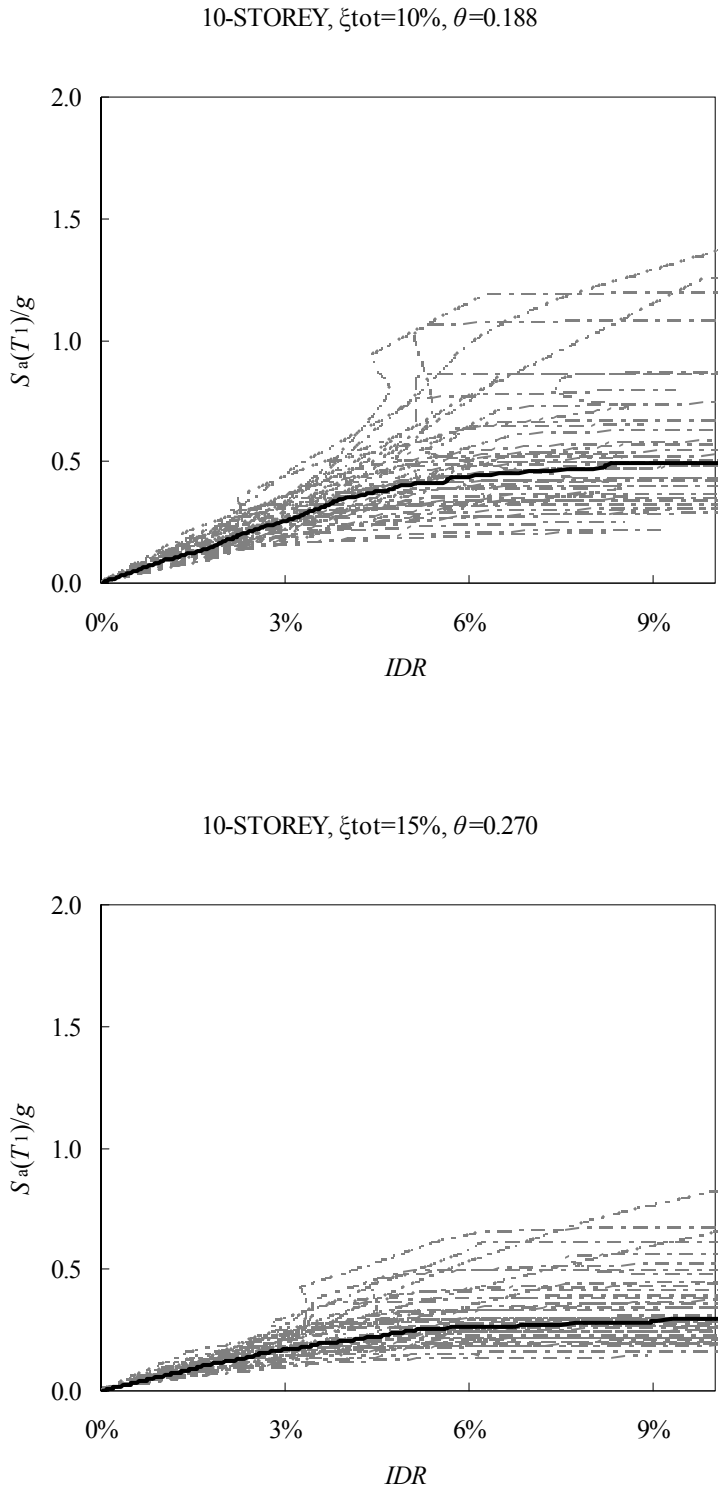

Figure E.8 IDA curves for the 10-storey steel MRFs with viscous dampers (solid line indicates median)

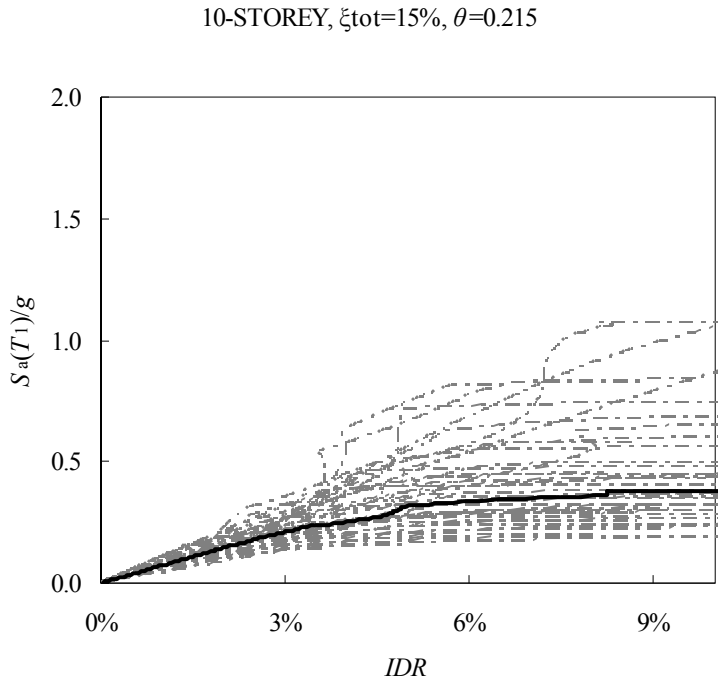

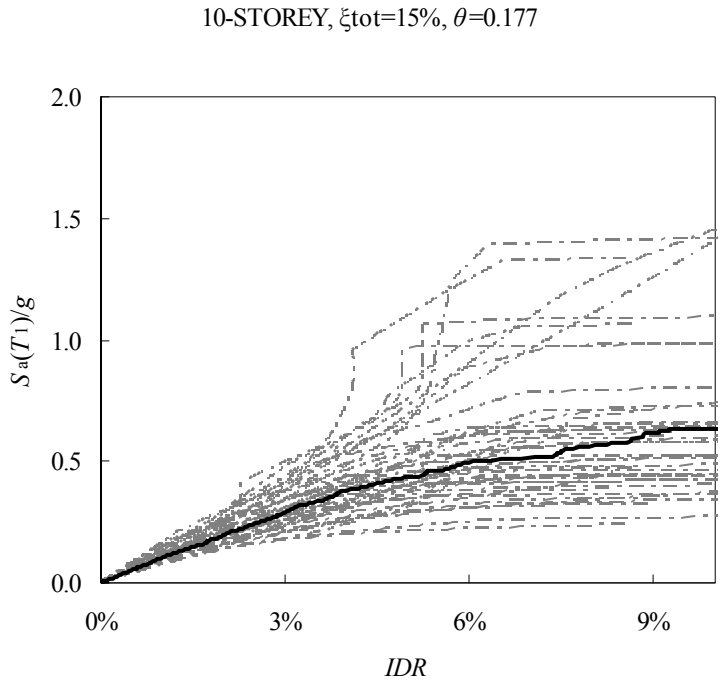

Figure E.9 IDA curves for the 10-storey steel MRFs with viscous dampers (solid line indicates median)

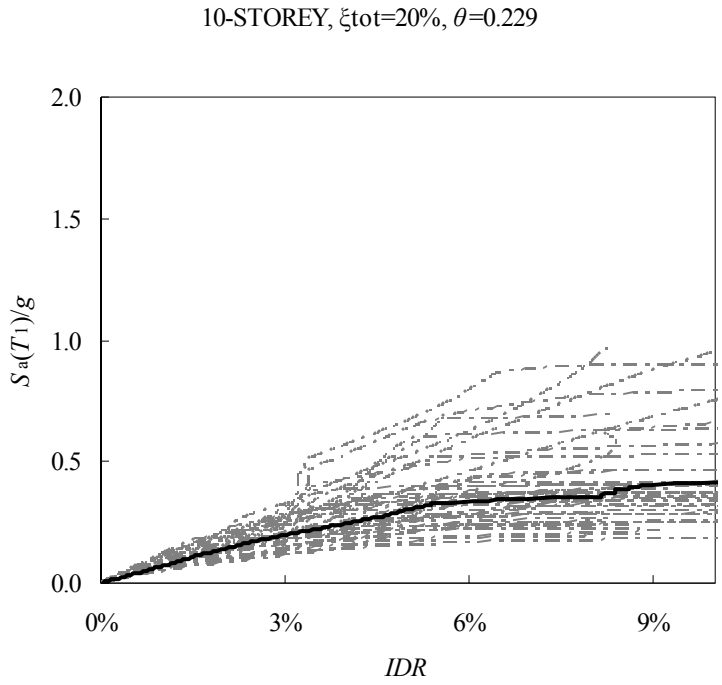

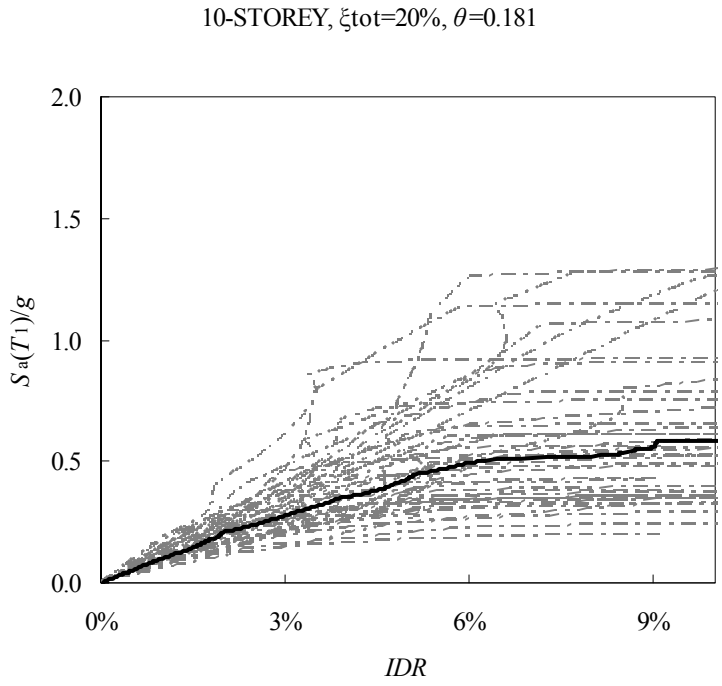

Figure E.10 IDA curves for the 10-storey steel MRFs with viscous dampers (solid line indicates median)

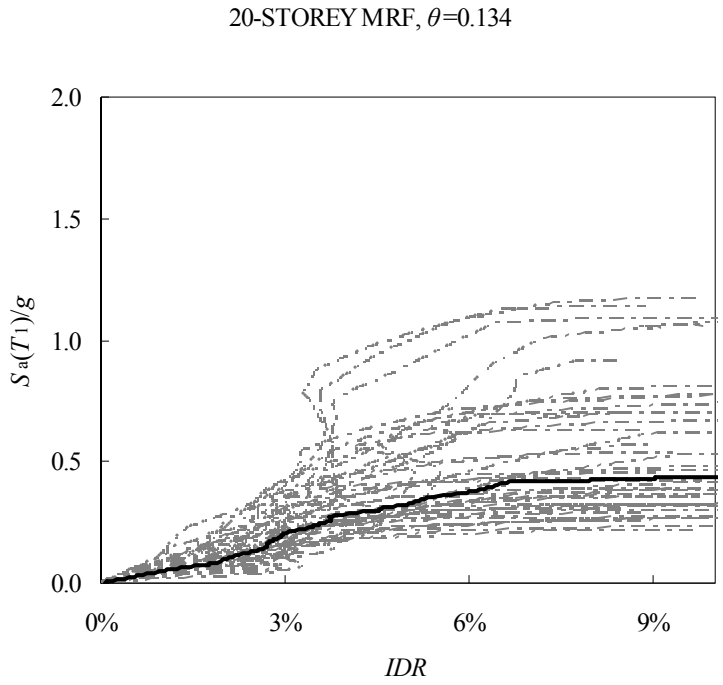

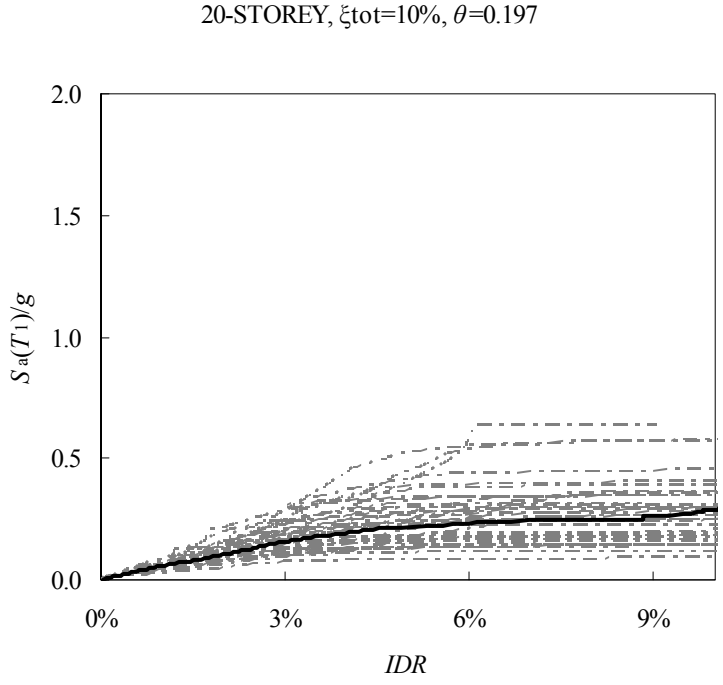

Figure E.11 IDA curves for the 20-storey steel MRF and the MRF with viscous dampers (solid line indicates median)

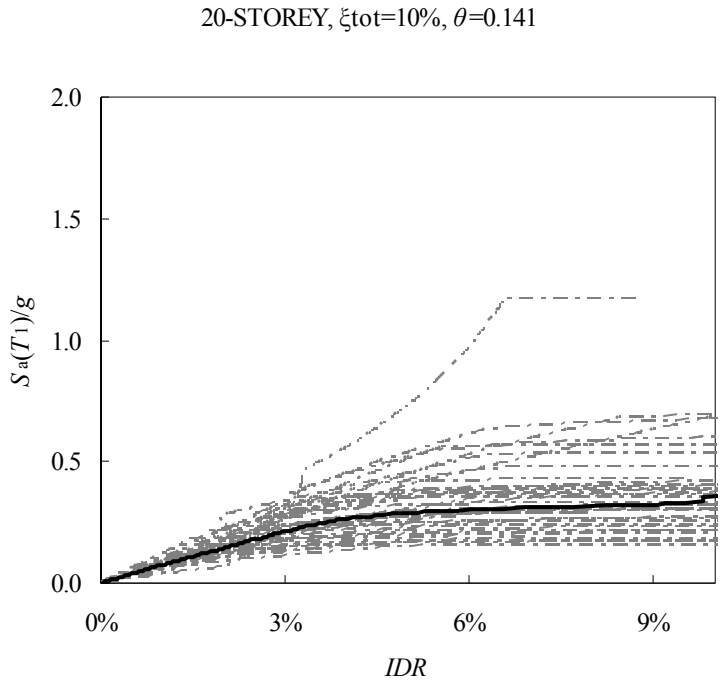

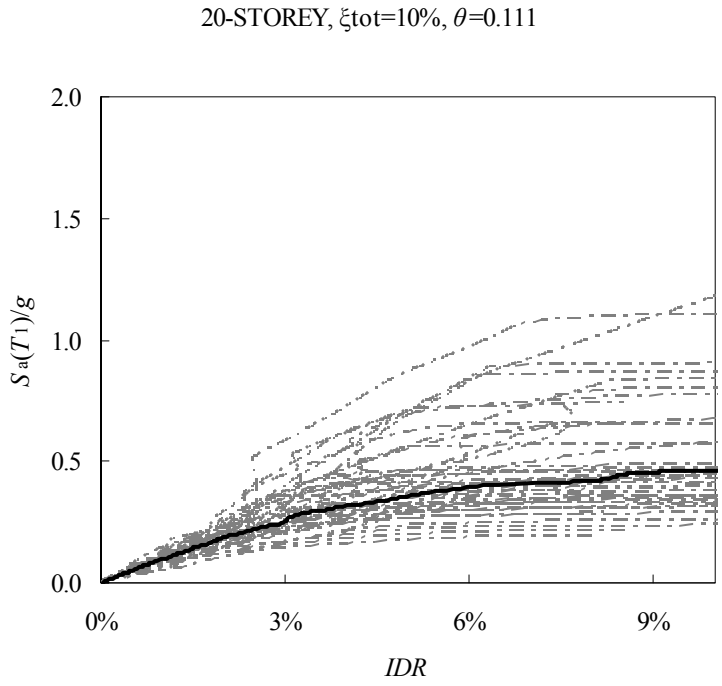

Figure E.12 IDA curves for the 20-storey steel MRFs with viscous dampers (solid line indicates median)

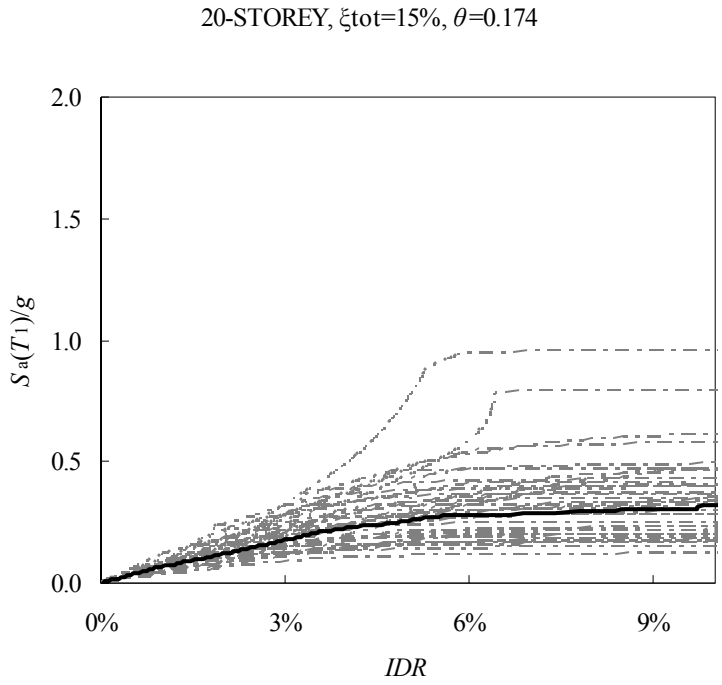

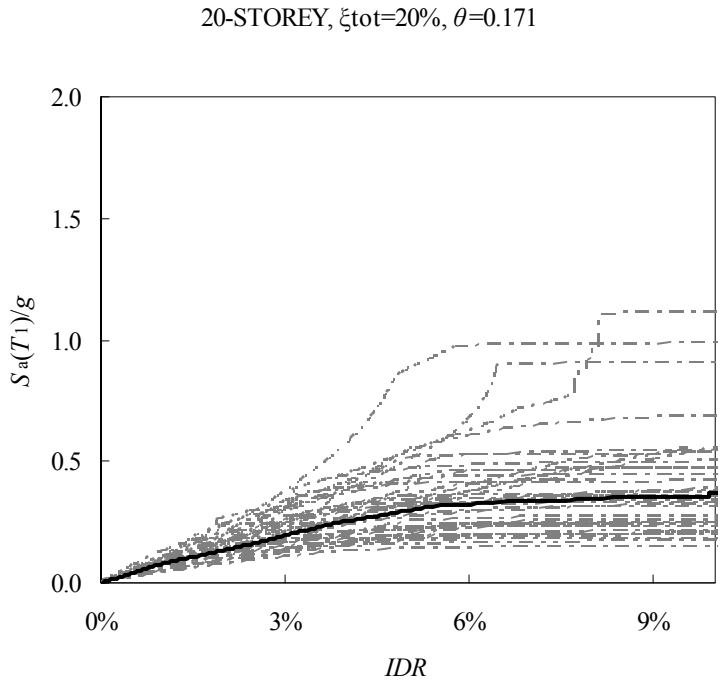

Figure E.13 IDA curves for the 20-storey steel MRFs with viscous dampers (solid line indicates median)